Molecular Simulation of Phase and Reaction Equilibria
Software and Algorithm Development

Hens, R.

DOI
10.4233/uuid:41c32a8f-2db7-4091-abb5-4d6a5e596345

Publication date
2020

Document Version
Final published version

Citation (APA)
Hens, R. (2020). *Molecular Simulation of Phase and Reaction Equilibria: Software and Algorithm Development*. [Dissertation (TU Delft), Delft University of Technology].
https://doi.org/10.4233/uuid:41c32a8f-2db7-4091-abb5-4d6a5e596345

Important note
To cite this publication, please use the final published version (if applicable).
Please check the document version above.

Molecular Simulation of Phase and Reaction Equilibria

Software and Algorithm Development

Molecular Simulation of Phase and Reaction Equilibria

Software and Algorithm Development

Proefschrift

ter verkrijging van de graad van doctor
aan de Technische Universiteit Delft,
op gezag van de Rector Magnificus prof. dr. ir. T.H.J.J. van der Hagen,
voorzitter van het College voor Promoties,
in het openbaar te verdedigen op
dinsdag 20 oktober 2020 om 15:00 uur

door

Remco HENS

Master of Science in Physics and Astronomy,
Radboud Universiteit, Nijmegen, Nederland,
geboren te Tilburg, Nederland.

Dit proefschrift is goedgekeurd door de promotor.

Samenstelling promotiecommissie:

Rector Magnificus,	voorzitter
Prof. dr. ir. T.J.H Vlugt,	Technische Universiteit Delft, promotor
Onafhankelijke leden:	
Prof. dr. S. Calero	Universidad Pablo de Olavide Sevilla, Spanje
Prof. dr. S.J. Marrink	Rijksuniversiteit Groningen
Prof. dr. ir. J.T. Padding	Technische Universiteit Delft
Prof. dr. ir. L.J. Sluys	Technische Universiteit Delft
Dr. A.V. Lyulin	Technische Universiteit Eindhoven
Overig lid:	
Dr. ir. M. Ramdin	Technische Universiteit Delft

This work was sponsored by NWO Exacte Wetenschappen (Physical Sciences) for the use of supercomputer facilities, with financial support from the Nederlandse Organisatie voor Wetenschappelijk Onderzoek (Netherlands Organization for Scientific Research, NWO). This project was funded by the VICI grant of the promotor.

Keywords: Molecular Simulation, Monte Carlo Simulation, Phase Equilibrium, Reaction Equilibrium

Printed by: Ridderprint, Alblasserdam

Cover by: R. Hens

ISBN 978-94-6366-303-8

An electronic version of this dissertation is available at
http://repository.tudelft.nl/.

Contents

1

Introduction

Knowledge of chemical potentials, partial molar properties and phase and reaction equilibria is essential for the design and operation of chemical processes [1–8], such as separation systems [9], chemisorption processes [7, 8, 10], and equilibrium and non-equilibrium reactive systems [7, 8, 10]. In the past decades, molecular simulation has become an important tool for predicting these equilibria based on the interactions between molecules: the so-called force field [11–14]. Molecular simulation offers several advantages over experiments. Systems can for example easily be studied at extreme conditions (high temperatures and pressures), or with dangerous and toxic compounds. Furthermore, molecular simulations can provide information on the molecular level leading to the understanding on how molecule interactions lead to the microscopic behavior of the system. Simulations can be used to predict properties of molecules without the need to synthesize them first (and thus save the production costs).

There are two main branches of force field-based molecular simulation: Molecular Dynamics and Monte Carlo simulations [15, 16]. In Molecular Dynamics simulation the equations of motion are numerically integrated for the system under study. The basis for Monte Carlo force field-based molecular simulations is statistical mechanics and is what we focus on in this dissertation. The key idea from statistical mechanics is that all thermodynamic properties are related to the so-called *partition function*, Q, of the system [17]. The free energy of the system for example equals:

$$F = -k_{\mathrm{B}} T \ln Q \tag{1.1}$$

where k_{B} is the Boltzmann constant and T the temperature. The chemical potential equals [17]:

$$\mu = \left(\frac{\partial F}{\partial N}\right)_{\mathrm{V,T}} = -\frac{k_{\mathrm{B}} T}{Q}\left(\frac{\partial Q}{\partial N}\right)_{\mathrm{V,T}} \tag{1.2}$$

where N is the number of particles and V is the volume of the system. Similar expressions exist for other thermodynamic properties. Therefore, if the partition

function Q is known as a function of N, V and, T, all properties of the system can be derived. For a system of N particles in a constant volume V at temperature T and potential energy $U(\mathrm{r}^N)$ (the so-called *canonical ensemble*) the partition function is [15]:

$$Q = \frac{1}{\Lambda^{3N} N!} \int_V \mathrm{d}\mathrm{r}^N \exp[-\beta U(\mathrm{r}^N)] \tag{1.3}$$

where Λ is the thermal wavelength. Apart from trivial choices for the potential energy (such as $U(\mathrm{r}^N) = 0$, corresponding to an ideal gas), this partition function can not be calculated analytically. This is the case for almost all ensembles: the partition function can never be explicitly calculated and therefore a different approach is needed. This different approach makes use of the similarity between probability theory and statistical mechanics and is in fact where the partition function originates from [17]. The average value of a variable $X(\mathrm{r}^N)$ in the canonical ensemble is equal to:

$$\langle X \rangle = \frac{\int X(\mathrm{r}^N) \mathrm{d}\mathrm{r}^N \exp[-\beta U(\mathrm{r}^N)]}{\int \mathrm{d}\mathrm{r}^N \exp[-\beta U(\mathrm{r}^N)]} \tag{1.4}$$

with corresponding probability distribution:

$$\mathcal{N}(\mathrm{r}^{\mathcal{N}}) = \frac{\exp[-\beta U(\mathrm{r}^N)]}{\int \mathrm{d}\mathrm{r}^N \exp[-\beta U(\mathrm{r}^N)]} = \frac{\frac{1}{\Lambda^{3N} N!} \exp[-\beta U(\mathrm{r}^N)]}{Q} \tag{1.5}$$

Instead of explicitly calculating the average in Eq. 1.4, in a Monte Carlo simulation, system states (r^N) will be generated according to the probability distribution in Eq. 1.5. Using the Metropolis algorithm [18], this method does not involve the calculation of the partition function Q and the calculation of averages is straightforward. The different system states in a molecular simulation are generated by so-called *trial moves*. Starting from a random system state (configuration) $\mathrm{r}^N_{\mathrm{old}}$ one can for example move one molecule (a translation move, Fig. 1.1a) or rotate a molecule (a rotation move, Fig. 1.1b) to create a new configuration $\mathrm{r}^N_{\mathrm{new}}$. The displacement (or rotation angle) can be chosen at random. The trial move will then be either accepted or rejected based on a so-called *acceptance rule* to ensure that system states are generated according to the imposed probability distribution [18]. This usually imposes detailed balance [15]. An accepted trial move implies that the next configuration is generated from the new one $\mathrm{r}^N_{\mathrm{new}}$. A rejected trial move implies that the next configuration equals the old one $\mathrm{r}^N_{\mathrm{old}}$. The translation and rotation trial moves are examples of trial moves where one particle moves but one can also use other trial moves depending on the chosen ensemble. In the *NPT* ensemble, the volume of the system is not fixed and one can for example increase/decrease the volume of the system by a random amount so that the particles in the system get further away/closer from each other (Fig. 1.1c). In open ensembles, the number of particles in the system is fluctuating, and trial moves can be used to insert or remove particles (Fig. 1.1d). Examples of open ensembles are the Gibbs Ensemble [19, 20], the Reaction Ensemble [21, 22] and the Grand-Canonical Ensemble

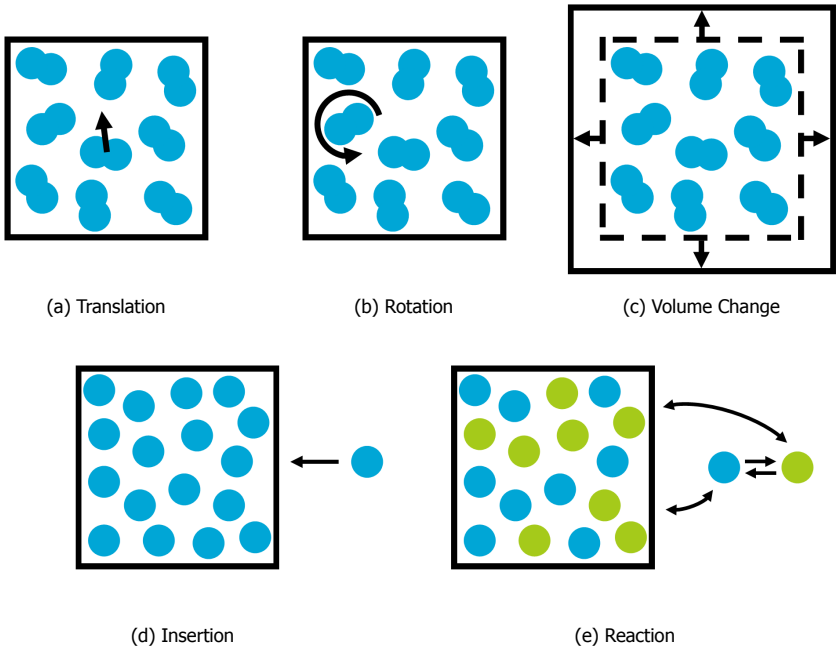

Figure 1.1: Schematic illustrations of trial moves for Monte Carlo simulations. In a translation trial move, a molecule is displaced in a random direction by a random distance. In a rotation trial move, a molecule is rotated by a random angle around a random axis. In a volume change trial move, the volume of the system is changed by a random amount. In a insertion trial move, a particle is inserted at a random position. In a reaction trial move, reactants are converted into products.

[23, 24]. In the Reaction Ensemble, the particles in the system react with each other and trial moves can be used to remove particles of one type and insert particles of a different type (Fig. 1.1e). There are many other trial moves possible, and each of them comes with its own acceptance rule to generate system states according to the probability distribution. An extensive overview of molecular simulations can be found in the books by Frenkel and Smit [15] and Allen and Tildesley [16].

As mentioned, open ensembles require trial moves for the insertion and removal of particles from the system. This is problematic for dense systems because the inserted particle will overlap with other particles in the system, leading to large energy barriers. This situation if often encountered in many molecular simulations such as vapor-liquid equilibrium simulations, adsorption in zeolites, reactions in a liquid, etc.

In this dissertation we focus on molecular simulation of phase and reaction equilibria using the Monte Carlo method. We work on the development and improvement of trial moves for efficiently generating system states and computation of thermodynamic properties and investigate methods to reduce the computational cost (CPU time) of simulations. This leads to the development of our own molecular

simulation software, Brick-CFCMC [25], that provides a solution for the inefficient insertions and removals of particles in Monte Carlo simulations.

Chapter 2 provides an introduction of the methods that are used in the simulations in this dissertation. An overview is provided of the different thermodynamic ensembles that are considered and the corresponding trial moves. We develop and improve methods to simulate reaction equilibria and calculate partial molar properties. The second half of this chapter points out features of the software that were developed in this work based on our improved methods. This software is used for the simulations in this dissertation. Chapter 3 focuses on an alternative, computationally faster, method for the calculation of electrostatic interactions (the Wolf method) in simulations of vapor-liquid equilibria of hydrogen sulfide, methanol, and carbon dioxide. In Chapter 4, we use our improved method for Monte Carlo simulations of reaction equilibria. Using this method we study the Haber-Bosch process for ammonia synthesis. In Chapter 5, we use our new method to calculate partial molar properties. Based on the results from Chapter 4, we calculate partial molar enthalpy and partial molar volume of nitrogen, hydrogen, and ammonia in the Haber-Bosch process. In Chapter 6, we study a combined phase and reaction equilibrium: the esterification of methanol with acetic acid and compute chemical potentials and activity coefficients.

2

Methods & Software

This chapter is based on the papers:

A. Poursaeidesfahani, R. Hens, A. Rahbari, M. Ramdin, D. Dubbeldam, and T. J. H. Vlugt, *Efficient Application of Continuous Fractional Component Monte Carlo in the Reaction Ensemble*, Journal of Chemical Theory and Computation, **13**, 4452-4466 (2017) [26].

R. Hens and T. J. H. Vlugt, *Molecular Simulation of Vapor-Liquid Equilibria using the Wolf Method for Electrostatic Interactions*, Journal of Chemical and Engineering Data, **63**, 1096-1102 (2018) [27].

A. Rahbari, R. Hens, I. K. Nikolaidis, A. Poursaeidesfahani, M. Ramdin, I. G. Economou, O. A. Moultos, D. Dubbeldam, and T. J. H. Vlugt, *Computation of Partial Molar Properties using Continuous Fractional Component Monte Carlo*, Molecular Physics, **116**, 3331-3344 (2018) [28].

R. Hens, A. Rahbari, S. Caro-Ortiz, N. Dawass, M. Erdős, A. Poursaeidesfahani, H. S. Salehi, A. T. Celebi, M. Ramdin, O. A. Moultos, D. Dubbeldam, and T. J. H. Vlugt *Brick-CFCMC: Open Source Software for Monte Carlo Simulations of Phase and Reaction Equilibria using the Continuous Fractional Component Method*, Journal of Chemical Information and Modeling, **60**, 2678-2682 (2020) [25].

2.1. Introduction

In this chapter, we provide an overview of the methods and software package that are used in this dissertation. We focus primarily on methods to compute partial molar properties efficiently. Partial molar properties are first order derivatives of the chemical potential [15, 29–31]. The partial molar enthalpy of component i in a multicomponent mixture equals:

$$\bar{h}_i = \left(\frac{\partial H}{\partial N_i}\right)_{N_{j\neq i},P,T} = \left(\frac{\partial \beta\mu_i}{\partial \beta}\right)_{N_i,P} \tag{2.1}$$

For convenience, we consider partial molar properties per molecule instead of per mole. In Eq. 2.1, H is the enthalpy of the system, N_i denotes the number of molecules of component i, μ_i is the chemical potential of component i, P is the imposed pressure, T is the temperature, $\beta = 1/(k_\mathrm{B}T)$, and k_B is the Boltzmann constant. The partial molar volume of component i equals:

$$\bar{v}_i = \left(\frac{\partial V}{\partial N_i}\right)_{N_{j\neq i},P,T} = \left(\frac{\partial \mu_i}{\partial P}\right)_{N_i,T} \tag{2.2}$$

in which V is the volume of the mixture. Partial molar properties are computationally difficult to calculate and are experimentally difficult to measure at extreme conditions [30–35]. At present, application of computer simulations to calculate partial molar properties is limited and more work is needed in this field [36]. In a molecular simulation, chemical potentials and partial molar properties cannot be computed directly as a function of atomic positions and/or momenta of the molecules in the system [15, 30, 31, 37, 38], and special molecular simulation techniques are required. To date, different molecular simulation techniques have been used to compute partial molar properties: (1) Numerical differentiation: in a multicomponent mixture, the partial molar properties of component i are computed directly by numerically differentiating the total property of the mixture at constant temperature and pressure with respect to the number of molecules of component i, while keeping the number of molecules of all other components constant [39–41]. This requires several independent and long simulations. Therefore, it is not well suited for multicomponent mixtures. Moreover, the accuracy of the numerical differentiation depends strongly on the uncertainty of the computed total property [30, 31]. (2) Kirkwood-Buff integrals: Schnell et al. have used Kirkwood-Buff integrals to compute the partial molar enthalpies for mixtures of gases or liquids [39, 42–47]. This method uses transformations between ensembles and it is numerically difficult to compute partial molar enthalpies. However, the computation of partial molar volumes using Kirkwood-Buff integrals is straightforward [48]. (3) Direct Method: in their pioneering work in 1987, Frenkel et al. used the Widom's Test Particle Insertion (WTPI) method [49] to compute partial molar properties of components in a single Monte Carlo simulation in the *NPT* ensemble [30, 31]. Due to the inefficiency of the WTPI method for dense systems, application of this method is rather limited [30, 50–54]. (4) Difference Method (DM): to avoid sampling issues of the WTPI

method, an alternative approach was proposed by Frenkel et al. which uses identity changes between two molecule types [30, 31]. From this, partial molar properties of binary systems could be computed. However, if the two molecules are very different in size or have very different interactions with surrounding molecules, identity changes often lead to unfavorable configurations in phase space, resulting in poor statistics. (5) From fluctuations in open ensembles and using linear regression [55, 56].

The methods for computing partial molar properties often rely on insertions and exchanges of molecules. In dense systems, this leads to overlaps, resulting in high energy barriers, Shi and Maginn [57, 58] developed the Continuous Fractional Component method. In this method, instead of inserting molecules in one Monte Carlo trial move, molecules are inserted in a gradual manner. In Sec. 2.2 we further explain and develop this method such that we can use it to obtain chemical potentials and partial molar properties directly from simulations in the *NPT* ensemble.

Furthermore, just as for other ensembles that rely on sufficient molecule insertions and removals, the CFC method is also an attractive method to use in the Gibbs Ensemble and Reaction Ensemble to obtain phase and reaction equilibria from Monte Carlo simulations. For the Gibbs Ensemble, a more efficient approach of the CFC method was introduced by Poursaeidesfahani et al. [37] and we describe this method briefly in Sec. 2.4. In Sec. 2.3, we further extend the CFC method for the Reaction Ensemble. In Sec. 2.5 we introduce the software that was used for performing all Monte Carlo simulations in this dissertation.

2.2. The CFC*NPT* Ensemble

The most commonly used method for determining the chemical potential of a component in a molecular simulation was introduced by Widom in 1963 [59, 60]. The chemical potential can be calculated using Widom's Test Particle Insertion (WTPI) method by sampling the interaction energy of a test molecule, inserted in the system at random positions with a random orientation. It is well-known that the chemical potential of component i in the conventional *NPT* ensemble of a multicomponent mixture using the WTPI method equals [15, 30, 31, 59]:

$$\mu_i = -\frac{1}{\beta} \ln \left\langle \frac{q_i V_0}{\Lambda_i^3} \cdot \frac{V}{N_i + 1} \exp\left[-\beta \Delta U_i^+\right] \right\rangle_{N_j,P,T} \tag{2.3}$$

where μ_i is the chemical potential of component i, $\beta = 1/(k_\mathrm{B}T)$, k_B is the Boltzmann constant, T is the temperature, q_i is the partition function of the isolated molecule of component i excluding the translational part, V_0 is an arbitrary reference volume (here set to 1 Å^3), Λ_i is the thermal wavelength, N_i is the number of molecules, ΔU_i^+ is the interaction between the inserted test molecule and the rest of the system, V is the volume of the system, and P is the imposed pressure. The brackets $\langle \cdots \rangle_{N_j,P,T}$ denote an ensemble average in the *NPT* ensemble in which the number of molecules of each component j is constant.

In 1987, Frenkel et al. extended the WTPI method to compute first order derivatives of the chemical potential, namely the partial molar excess enthalpy and the

partial molar volume [30, 31]. These authors have shown that the partial molar excess enthalpy of a component i in the conventional *NPT* ensemble of a multicomponent mixture using the WTPI method equals:

$$h_i^{\text{excess}} = -\frac{1}{\beta} + \frac{\left\langle (\Delta U_i^+ + U + PV)V \exp\left[-\beta \Delta U_i^+\right]\right\rangle_{N_j,P,T}}{\left\langle V \exp\left[-\beta \Delta U_i^+\right]\right\rangle_{N_j,P,T}} - \langle U + PV\rangle_{N_j,P,T} \tag{2.4}$$

where U is the total energy of the system. For an ideal gas, the partial molar excess enthalpy equals zero, since there are no interactions between ideal gas molecules. This is shown analytically in the Supporting Information of Ref. [28]. The partial molar volume of component i equals:

$$v_i = \frac{\left\langle V^2 \exp\left[-\beta \Delta U_i^+\right]\right\rangle_{N_j,P,T}}{\left\langle V \exp\left[-\beta \Delta U_i^+\right]\right\rangle_{N_j,P,T}} - \langle V\rangle_{N_j,P,T} \tag{2.5}$$

and a detailed derivation of Eqs. 2.3, 2.4 and 2.5 is provided in the Supporting Information of Ref. [28]. Although these are exact expressions, their application is rather limited because of the inefficient sampling of the WTPI method at high densities. Ensemble averages computed using the WTPI method strongly depend on the spontaneous occurrence of cavities large enough to accommodate the test molecule (i.e. the test molecule should 'fit' in the system). These spontaneous cavities occur rarely at high densities which renders the WTPI method essentially inefficient. To circumvent these sampling problems of the WTPI method, the CFC method is used to compute the ensemble averages in Eqs. 2.3, 2.4, and 2.5 without relying on test particle insertions and removals. We introduce an expanded version of the conventional *NPT* ensemble by adding a so-called *fractional* molecule to the system. The interactions of the fractional molecule are scaled by a parameter $\lambda \in [0,1]$. When $\lambda = 0$, no interactions are present which means that this molecule is treated as an ideal gas molecule. At $\lambda = 1$, the fractional molecule has the same interactions as the other molecules not being a fractional molecule, so-called *whole* molecules. This is schematically illustrated in Fig. 2.1. The partition function of the *NPT* ensemble of a multicomponent mixture of S monoatomic components expanded with a fractional molecule of component i equals [26, 37]:

$$\begin{aligned} Q_{\text{CFC}NPT} = &\beta P \left[\prod_{j=1}^{S} \frac{q_j^{N_j}}{\Lambda_j^{3N_j} N_j!}\right] \frac{1}{\Lambda_i^3} \int_0^1 \mathrm{d}\lambda_i \int \mathrm{d}V V^{N+1} \exp\left[-\beta PV\right] \\ &\times \int \mathrm{d}s^N \exp[-\beta U] \int \mathrm{d}s_i^{\text{frac}} \exp[-\beta U_i^{\text{frac}}] \end{aligned} \tag{2.6}$$

where $Q_{\text{CFC}NPT}$ is the partition function of the mixture in the Continuous Fractional Component *NPT* (CFC*NPT*) ensemble, N is the total number of whole molecules in the system, U is the interaction potential for whole molecules, and U_i^{frac} is the interaction potential between the fractional molecule of component i and the whole molecules [26, 57, 58]. $\lambda_i \in [0,1]$ is the fractional parameter for the scaling of

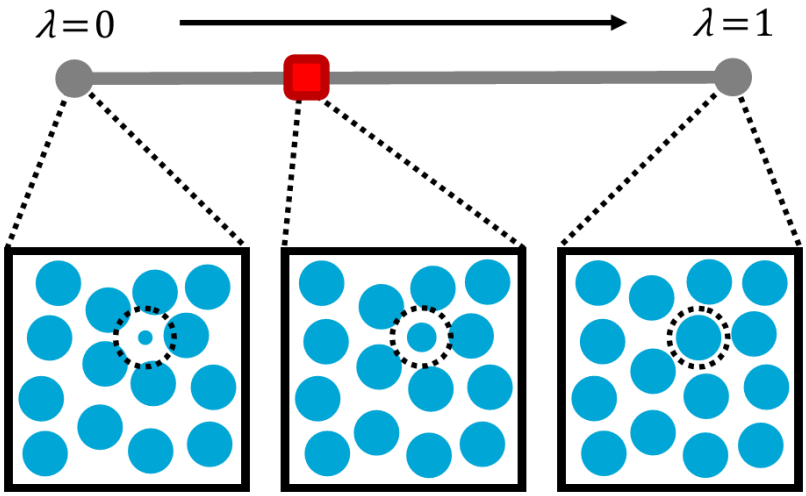

Figure 2.1: Schematic illustration of the Continuous Fractional Component method. The fractional parameter λ regulates the strength of the interactions of the fractional particle with the other particles. For $\lambda = 0$, there are no interactions and the particle acts like as in an ideal gas. At $\lambda = 1$, the interactions are the same as any other particle in the system.

interactions between the fractional molecule, of component i, and surrounding molecules. The partition function in Eq. 2.6 can be extended to mixtures of polyatomic molecules by simply multiplying it by the partition functions of the isolated molecule (excluding the translational part) of each molecule type [10, 15, 61]. This changes only the reference state of the partial molar properties and not the excess part [15, 43, 61]. The chemical potential of component i in simulations using the CFC method equals [28, 37]:

$$\mu_i = -\frac{1}{\beta}\ln\left(\frac{q_i V_0}{\Lambda_i^3}\right) + \frac{1}{\beta}\ln\left(\frac{\langle\rho_i\rangle}{\rho_0}\right) - \frac{1}{\beta}\ln\left(\frac{p\left(\lambda_i = 1\right)}{p\left(\lambda_i = 0\right)}\right) \tag{2.7}$$

where the brackets $\langle\cdots\rangle$ denote the ensemble average, ρ_i is the number density of component i, ρ_0 is an arbitrary reference number density (here set to 1 Å^{-3}), and $p\left(\lambda_i = 1\right)$ and $p\left(\lambda_i = 0\right)$ are the probabilities that the fractional parameter λ_i takes the values 1 and 0, respectively. The first term on the right-hand side of Eq. 2.7 only depends on the temperature and is denoted by μ_i°. The second term on the right-hand side depends on the number density (and is together with the first term referred to as the ideal gas contribution to the chemical potential). The third term on the right-hand side is the excess chemical potential. In the Supporting Information of Ref. [28], it is shown that Eq. 2.3 and Eq. 2.7 yield identical results.

The partial molar enthalpy of component i can be computed in the *NPT* ensemble with the CFC method using [28]:

$$h_i^{\text{excess}} = -\frac{1}{\beta} + \langle H\,(\lambda_i = 1)\rangle_{\text{CFC}NPT} - \frac{\langle H/V\,(\lambda_i = 0)\rangle_{\text{CFC}NPT}}{\langle 1/V\,(\lambda_i = 0)\rangle_{\text{CFC}NPT}} \tag{2.8}$$

where $\langle H\,(\lambda_i = 1)\rangle_{\text{CFC}NPT}$ is the average enthalpy of the system in the *NPT* ensemble with the CFC method when $\lambda_i = 1$, $\langle H/V\,(\lambda_i = 0)\rangle$ is the average of the ratio between total enthalpy and the volume of the system when $\lambda_i = 0$, and $\langle 1/V\,(\lambda_i = 0)\rangle$ is the average of the inverse volume where $\lambda_i = 0$. In the Supporting Information of Ref. [28], it is shown that Eq. 2.4 and eq. 2.8 yield identical results.

The expression for the partial molar volume of component i in the *NPT* ensemble with the CFC method equals:

$$v_i = \langle V\,(\lambda_i = 1)\rangle_{\text{CFC}NPT} - \langle 1/V\,(\lambda_i = 0)\rangle^{-1}_{\text{CFC}NPT} \tag{2.9}$$

where $\langle V\,(\lambda_i = 1)\rangle_{\text{CFC}NPT}$ is the average volume when $\lambda_i = 1$. Using Eqs. 2.7, 2.8 and 2.9, one can compute the chemical potential, partial molar excess enthalpy, and partial molar volume of a component in a single simulation without relying on the WTPI method.

2.2.1. Trial Moves

In Monte Carlo simulations in the *NPT* ensemble with the CFC method three additional trial moves are used to facilitate the gradual insertion and removal of molecules:

- Changes in λ: the fractional parameter λ is changed by a random value which results in a change of the interaction between the fractional molecule and the whole molecules. The value of λ is constraint to the interval $[0, 1]$.
- Reinsertions: the fractional molecule is removed from the system and reinserted at a random position with a random orientation. The value of λ is unchanged. This trial move has a high acceptance probability when λ is close to 0 because for these values of λ the fractional molecule does only have weak interactions.
- Identity changes: the fractional molecule is transformed into a whole molecule and a randomly selected whole molecule, of the same type, is transformed into a fractional molecule. The value of λ is unchanged. This trial move has a high acceptance probability when λ is close to 1 because for these values of λ the fractional molecule does have similar interactions to that of the whole molecules.

These trial moves, together with the conventional trial moves for thermalization such as translations, rotations and volume changes [15], allow for efficient sampling of the different system states in the *NPT* ensemble.

2.3. The Reaction Ensemble

Chemical reaction equilibria can be simulated by performing Monte Carlo simulations in the Reaction Ensemble. In the Reaction Ensemble, the number of atoms is conserved but not the number of molecule types [62]. Usually, the temperature is constant and either the pressure or volume is imposed. The Reaction Ensemble at constant pressure is more interesting for practical applications. Therefore, in this section, we discuss the partition function and acceptance rules for trial moves in the Reaction Ensemble at constant pressure. In addition to the conventional Monte Carlo trial moves, this ensemble uses trial moves that attempt to remove reactants and insert products and vice versa. Here, for simplicity, we only consider systems with a single reaction as an extension to systems with multiple reactions is straightforward [10, 15]. The partition function for the conventional Reaction Ensemble at constant pressure equals [21, 62]:

$$\begin{aligned} Q_{\mathrm{RE},P}^{\mathrm{conv}} = \beta P \sum_{N_1=0}^{\infty} \cdots \sum_{N_S=0}^{\infty} \int \mathrm{d}V \exp[-\beta P V] \\ \times \exp\left[\sum_{i=1}^{S} \left(\beta \mu_i N_i + N_i \ln \frac{V q_i}{\Lambda_i^3} - \ln N_i!\right)\right] \int \mathrm{d}s^N \exp[-\beta U] \end{aligned} \tag{2.10}$$

where $\beta = 1/(k_{\mathrm{B}}T)$, k_{B} is the Boltzmann constant, P is the pressure, S is the number of components, V is the volume of the simulation box, μ_i is the chemical potential of component i, N_i is the number of molecules of component i, q_i is the partition function (excluding the translational part) of the isolated molecule of component i, Λ_i is the thermal wavelength of component i, and U is the total potential energy.

The Reaction Ensemble is subject to the constraint that the total number of atoms of each type is constant and that chemical reactions converting reactants into products are in equilibrium. This sets limits on the values of μ_i. Sampling the different thermodynamic states in this ensemble requires: (1) sampling of the degrees of freedom of the interacting molecules (e.g. translations, rotations, and internal configurations); (2) sampling of volume fluctuations; (3) sampling of chemical reactions subject to the constraint that the total number of atoms of each component is constant, as well as that the reaction is at chemical equilibrium. In Monte Carlo simulations in the conventional Reaction Ensemble, the latter is obtained by performing reaction trial moves. The reaction trial move is an attempt to remove randomly selected molecules of the reactants and insert molecules of the products. Due to simultaneous insertion of the molecules in a single step, the efficiency of this algorithm can be low at high densities. This is also the case when Configurational-Bias Monte Carlo is used for inserting and deleting molecules [63].

2.3.1. Parallel CFC

In the Reaction Ensemble combined with the *parallel* CFC method [64], the conventional Reaction Ensemble is expanded with fractional molecules of each component participating in the reaction. The number of fractional molecules of each component is equal to its stoichiometric coefficient. Similar to the CFC*NPT* Ensemble (Sec. 2.2), interactions of the fractional molecules are scaled with a parameter λ_i. The value $\lambda_i = 0$ corresponds to no interactions with the surrounding molecules (the fractional molecule acts as an ideal gas molecule), and $\lambda_i = 1$ corresponds to full interactions with the surrounding molecules. There are two fractional parameters per reaction, one for all reactants (λ_R) and one for all products (λ_P). In the parallel CFC method, the fractional parameters for the fractional molecules of reactants and products are constrained to:

$$\lambda_\mathrm{R} + \lambda_\mathrm{P} = 1$$

This constraint results in a simultaneous gradual insertion of reactants (products) and gradual removal of products (reactants).

2.3.2. Trial Moves

In Monte Carlo simulations in the Reaction Ensemble using the parallel CFC method, trial moves are used to change the fractional parameters:

$$\lambda_{\mathrm{R,n}} = \lambda_{\mathrm{R,o}} + \Delta\lambda \text{ with } \Delta\lambda \in [-\Delta\lambda_{\max}, +\Delta\lambda_{\max}]$$

where the subscripts o and n indicate the old and new system state, respectively. Due to the constraint $\lambda_\mathrm{R} + \lambda_\mathrm{P} = 1$, the fractional parameter of the fractional molecules of products also changes according to $\lambda_{\mathrm{P,n}} = \lambda_{\mathrm{P,o}} - \Delta\lambda$. When $\lambda_{\mathrm{P,n}} > 1$ or $\lambda_{\mathrm{P,n}} < 0$, an attempt is made to perform a chemical reaction. In the case that $\lambda_{\mathrm{P,n}} > 1$ (and $\lambda_{\mathrm{R,n}} < 0$), the following procedure is executed:

- The fractional molecules of the products are transformed into whole molecules.
- The fractional molecules of the reactants are removed from the system.
- Randomly selected whole molecules of the reactants are transformed into fractional molecules.
- The fractional parameters change:

$$\lambda_{\mathrm{R,n}} \to \lambda_{\mathrm{R,n}} + 1;$$
$$\lambda_{\mathrm{P,n}} \to \lambda_{\mathrm{P,n}} - 1.$$

We refer to this as the *forward* reaction (e.g. more products are formed in the system). In the case that $\lambda_{\mathrm{R,n}} > 1$ (and $\lambda_{\mathrm{P,n}} < 0$), the exact opposite of the previously described routine is executed (reactants and products switch roles) and this is referred to as the *backward* reaction.

2.3.3. Serial CFC

Inspired by this, we introduce a different formulation for the CFC method in the Reaction Ensemble (denoted by *serial* CFC). In the Reaction Ensemble combined with the serial CFC method, either fractional molecules of the reactants or products are present in the system, in sharp contrast to the parallel version where always fractional molecules of both reactants and products are present. The partition function for the ensemble at constant pressure equals [26]:

$$
\begin{aligned}
Q_{\mathrm{RE},P}^{\mathrm{serial}} = & \beta P \sum_{N_1=0}^{\infty} \cdots \sum_{N_S=0}^{\infty} \sum_{\delta=0}^{1} \int \mathrm{d}V \exp[-\beta P V] \exp\left[-\sum_{i=1}^{S} \ln N_i!\right] \\
& \times \exp\left[\beta \sum_{i=1}^{R} \mu_i \left(N_i + \nu_i \delta\right) + \sum_{i=1}^{R} \left(N_i + \nu_i \delta\right) \ln \frac{V q_i}{\Lambda_i^3}\right] \\
& \times \exp\left[\beta \sum_{j=R+1}^{S} \mu_j \left(N_j + \nu_j (1-\delta)\right) + \sum_{j=R+1}^{S} \left(N_j + \nu_j (1-\delta)\right) \ln \frac{V q_j}{\Lambda_j^3}\right] \\
& \times \int_0^1 \mathrm{d}\lambda \int \mathrm{d}s^N \exp[-\beta U] \left(\prod_{i=1}^{R} \int \mathrm{d}s^{\mathrm{frac}} \exp[-\beta \delta U_i^{\mathrm{frac}}]\right) \\
& \times \left(\prod_{j=R+1}^{S} \int \mathrm{d}s^{\mathrm{frac}} \exp[-\beta (1-\delta) U_j^{\mathrm{frac}}]\right)
\end{aligned}
\tag{2.11}
$$

where N is the total number of whole molecules (regardless the type) and N_i is the number of whole molecules of component i. When $\delta = 1$, fractional molecules of reactants are present in the simulation box (ν_i fractional molecules for component i), and when $\delta = 0$, fractional molecules of products are present. Here, a system with a single reaction is considered. U is the total internal energy of whole molecules and U_i^{frac} is the interaction energy of fractional molecules of component i with the other molecules, including other fractional molecules. The interactions of the fractional molecules with the surroundings are such that $\lambda = 0$ means no interactions, $\lambda = 1$ means full interactions, and the value of λ is restricted to $\lambda \in [0, 1]$.

Since fractional molecules are always distinguishable from whole molecules, the term $N_i!$ only counts for indistinguishable whole molecules. The main difference between Eq. 2.11 and Eq. 2.10 is the integration over λ in Eq. 2.11. This is an immediate consequence of expanding the conventional Reaction Ensemble with fractional molecules. In the Supporting Information of Ref. [26], it is shown that for systems without intermolecular interactions (ideal gas), the partition functions of Eq. 2.11 and Eq. 2.10 are proportional. Therefore, these ensembles result in identical average numbers of molecules for each component, provided that fractional molecules are not counted when computing ensemble averages. The fact that one should not count fractional molecules when computing the average number of molecules is in line with earlier studies in the Gibbs Ensemble and in the Grand-Canonical Ensemble [65, 66].

2.3.4. Trial Moves

In Monte Carlo simulations, in addition to the conventional Monte Carlo trial moves for thermalization and volume changes, there are trial moves in the Reaction Ensemble with the serial CFC method to mimic the chemical reaction:

- Changes in λ: the value of λ is changed, for either reactants or products, depending on the value of δ. The value of λ is changed according to $\lambda_{\mathrm{n}} = \lambda_{\mathrm{o}} + \Delta\lambda$ in which $\Delta\lambda$ is a uniformly distributed random number between $-\Delta\lambda_{\max}$ and $+\Delta\lambda_{\max}$. Note that $\Delta\lambda_{\max}$ can be different for reactants and products. When the new value of λ is not in the range $\lambda \in [0, 1]$, this trial move is automatically rejected. In this trial move, the positions of all molecules, the value of δ, and the number of whole molecules and fractional molecules remain the same. By changing the value of λ, only the interactions between the fractional molecules and other molecules are changed. The acceptance rule for this trial move is:

$$\mathrm{acc}(\mathrm{o} \to \mathrm{n}) = \min\left(1, \exp\left[-\beta \Delta U\right]\right) \tag{2.12}$$

  where $\Delta U = U_{\mathrm{n}}^{\mathrm{frac}} - U_{\mathrm{o}}^{\mathrm{frac}}$ is the total energy change in the system.

- Reaction of fractional molecules: fractional molecules of reactants/products are removed and fractional molecules of products/reactants are inserted at random positions with a random orientation. In this trial move, essentially the value of δ is changed: if $\delta_{\mathrm{o}} = 1$ then $\delta_{\mathrm{n}} = 0$ and vice versa. The number of whole molecules and, the value of λ remain unchanged. This trial move mimics a chemical reaction for the fractional molecules. The acceptance rule for the forward reaction (converting reactants into products) is [26]:

$$\mathrm{acc}(\mathrm{o} \to \mathrm{n}) = \min\left(1, \prod_{i=1}^{R} \left(\frac{V q_i}{\Lambda_i^3}\right)^{-\nu_i} \prod_{j=R+1}^{S} \left(\frac{V q_j}{\Lambda_j^3}\right)^{\nu_j} \exp\left[-\beta \Delta U\right]\right) \tag{2.13}$$

  where $\Delta U = U_{\mathrm{n}}^{\mathrm{frac}} - U_{\mathrm{o}}^{\mathrm{frac}}$ is the total energy change in the system. Since the number of whole molecules remains constant during this move, the terms involving the number of whole molecules N_i are not present in Eq. 2.13. The acceptance rule for the backward reaction simply follows by swapping the labels of the reactants and products. The acceptance probability for this trial move is high when λ is close to 0. The reason for this is that fractional molecules have very limited interactions with the surrounding molecules and therefore, the term ΔU is nearly zero.

- Reaction for whole molecules: fractional molecules of reactants/products are transformed into whole molecules of reactants/products, while simultaneously, randomly selected whole molecules of products/reactants are transformed into fractional molecules of products/reactants. In this trial move, the positions of all molecules and the value of λ remain unchanged. The value of δ is changed as follows: if $\delta_{\mathrm{o}} = 1$ then $\delta_{\mathrm{n}} = 0$ and vice versa (i.e. the direction of the reaction depends on the value of δ for the old configuration). In the forward reaction, whole molecules of reactants are transformed

into fractional molecules, and fractional molecules of products are turned into whole molecules. Essentially, the number of whole molecules of reactants is reduced and the number of whole molecules of products is increased, according to their stoichiometric coefficients. Trial moves are automatically rejected when there are not enough whole molecules to turn into fractional molecules. The acceptance rule for this trial move is [26]:

$$\mathrm{acc}(\mathrm{o} \rightarrow \mathrm{n}) = \min\left[1, \prod_{i=1}^{R} \frac{N_i!}{(N_i - \nu_i)!} \prod_{j=R+1}^{S} \frac{N_j!}{(N_j + \nu_j)!} \exp\left[-\beta \Delta U\right]\right] \quad (2.14)$$

where $\Delta U = U_{\mathrm{n}} + U_{\mathrm{n}}^{\mathrm{frac}} - U_{\mathrm{o}} - U_{\mathrm{o}}^{\mathrm{frac}}$ is the total energy change in the system including the interactions of fractional molecules. The acceptance rule for the reverse reaction simply follows by swapping the labels. Since the total number of whole and fractional molecules for each component remains constant, partition functions of the isolated molecule are not present in Eq. 2.14. This trial move has a high acceptance probability when the value of λ is close to 1. The reason for this is that fractional molecules have almost the same interactions as whole molecules and therefore, the term ΔU is nearly zero.

A detailed description of these trial moves and the derivation of the acceptance rules is provided in the Supporting Information of Ref. [26]. From here on, for the Reaction Ensemble, when we refer to the CFC method we refer to the serial CFC method (unless stated differently).

2.3.5. Chemical Potential and Fugacity Coefficient

In the Reaction Ensemble combined with the CFC method, chemical potentials can be computed without additional simulations. The sum of chemical potentials of the reactants is equal to:

$$\sum_{i=1}^{R} \nu_i \mu_i = -\frac{1}{\beta} \ln \left\langle \prod_{i=1}^{R} \left(\frac{q_i}{\Lambda_i^3 \rho_i} \right)^{\nu_i} \right\rangle - \frac{1}{\beta} \ln \left(\frac{p(\lambda = 1, \delta = 1)}{p(\lambda = 0, \delta = 1)} \right) \quad (2.15)$$

A similar expression holds for the sum of the chemical potentials of the products. Eq. 2.15 allows for an independent check of reaction equilibria without any additional calculations (such as test molecules). The chemical potential of component i for a non-ideal gas equals [61, 62]:

$$\mu_i = \frac{1}{\beta} \ln \frac{\beta P_0 \Lambda_i^3}{q_i} + \frac{1}{\beta} \ln \frac{y_i P \varphi_i}{P_0} \quad (2.16)$$

where φ_i and y_i are the fugacity coefficient and mole fraction of component i, respectively. P_0 is the reference pressure (1 bar) and P is the pressure of the mixture. The first term on the right-hand side of Eq. 2.16 is the standard reference chemical potential (μ_i^0). Therefore, we have:

$$\sum_{i=1}^{R} \nu_i \mu_i = \frac{1}{\beta} \ln \left(\prod_{i=1}^{R} \left[\frac{\beta \Lambda_i^3 y_i P \varphi_i}{q_i} \right]^{\nu_i} \right) \tag{2.17}$$

Combining this with Eq. 2.15 immediately leads to:

$$\prod_{i=1}^{R} \varphi_i^{-\nu_i} = \frac{p(\lambda = 1, \delta = 1)}{p(\lambda = 0, \delta = 1)} \prod_{i=1}^{R} \left(\frac{\beta y_i P}{\rho_i} \right)^{\nu_i} \tag{2.18}$$

A similar expression holds for the products (where $\delta = 0$).

To compute the chemical potential of individual components, one should couple the interactions of different components in a smart way. The two limiting cases are well defined: at $\lambda = 0$, fractional molecules of reactants (or products) do not interact, and at $\lambda = 1$, fractional molecules of reactants have full interactions with the surrounding molecules. However, for intermediate values of λ one has a choice. One can choose different paths to scale the interactions of fractional molecules from no interactions to full interactions. The interactions can be scaled atom by atom, or molecule by molecule, or in any other way. By scaling the interactions of the fractional molecules of only one of the components from no interactions to full interactions when the value of λ is changed from 0 to λ_{k}, one can write (for reactants):

$$\nu_i \mu_i = -\frac{1}{\beta} \ln \left\langle \left(\frac{q_i}{\Lambda_i^3 \rho_i} \right)^{\nu_i} \right\rangle - \frac{1}{\beta} \ln \left(\frac{p(\lambda = \lambda_{\mathrm{k}}, \delta = 1)}{p(\lambda = 0, \delta = 1)} \right) \tag{2.19}$$

The first term on the right-hand side accounts for the ideal gas contribution and the second term on the right-hand side is the excess chemical potential (due to interactions with surrounding molecules). Similar to Eq. 2.19, one can write for φ_i:

$$\varphi_i^{-\nu_i} = \frac{p(\lambda = \lambda_{\mathrm{k}}, \delta = 1)}{p(\lambda = 0, \delta = 1)} \left(\frac{\beta y_i P}{\rho_i} \right)^{\nu_i} \tag{2.20}$$

When $\nu_i > 1$ and interactions of fractional molecules are scaled sequentially (one by one), fractional molecules that have interactions with surrounding molecules later (at higher values of λ) experience the effect of the fractional molecules which were inserted earlier (at lower values of λ). For sufficiently large system sizes this will not affect the calculated chemical potentials. However, for small system sizes there may be minor differences between the chemical potential of molecules that are inserted at lower values of λ and those inserted at at higher values of λ. Although these differences are expected to be small, one should be aware of them.

2.4. The Gibbs Ensemble

The Gibbs Ensemble can be used for the simulation of phase equilibria such as vapor-liquid coexistence. In this section we focus on the use of Gibbs Ensemble for obtaining vapor-liquid equilibria. In the Gibbs Ensemble two simulations boxes are used: one for the liquid phase and one for the vapor phase. A simulation in this ensemble involves displacements and rotations of molecules, volume changes of the boxes, and molecule transfers between the boxes. In the Gibbs Ensemble combined with the CFC method, one extra molecule per molecule type is added to the system: the fractional molecule. Interactions of the fractional molecules are scaled by the fractional parameter λ in a similar way as described in Sec. 2.2 and 2.3. In the Gibbs Ensemble, the fractional molecule can be in either of the simulation boxes.

2.4.1. Trial Moves

In Monte Carlo simulations, in addition to the conventional Monte Carlo trial moves for thermalization and volume changes, there are trial moves in the Gibbs Ensemble combined with the CFC method to facilitate molecule transfer between the boxes:

- Changes in λ: the fractional parameter λ is changed by a random value which results in a change of the interaction between the fractional molecule and the whole molecules. The value of λ is constraint to the interval $[0, 1]$.
- Swapping the fractional: the fractional molecule is transferred from one simulation box to the other. The value of λ remains unchanged. This trial move has a high acceptance probability for λ close to 0 [37].
- Identity changes: the fractional molecule transforms into a whole molecule and a molecule in the other simulation box transforms into a fractional molecule. This trial move has a high acceptance probability for λ close to 1 [37].

For the acceptance rules regarding the trial moves that facilitate these molecule transfers we refer to Ref. [37]. The Gibbs Ensemble combined with the CFC method is more efficient than the conventional Gibbs Ensemble because of higher acceptance probabilities for the molecule transfer. It has been shown that the presence of a fractional molecule has a negligible effect on the thermodynamic properties of the system [65].

2.4.2. Chemical Potential

Chemical potentials in the Gibbs Ensemble can be calculated by simply applying Eq. 2.7 for each simulation box [37]. For convenience, in this work, μ_i° (the first term on the right-hand side of Eq. 2.7) will be omitted in results from simulations in the Gibbs Ensemble since it only shifts the chemical potential by a constant value.

2.5. Brick-CFCMC

In the previous sections we discussed the CFC method for Monte Carlo simulations in different ensembles. In this section we introduce a new molecular simulation code, Brick-CFCMC (hereafter referred to as Brick), for performing these simulations. Important features of Brick are: (1) molecule exchanges are facilitated by the use of fractional molecules [57], which significantly improves insertion and deletion of molecules and allows for direct calculation of chemical potentials [37] (and their derivatives [28]); (2) flexibility of molecules is taken into account by bond-bending, torsion, and intramolecular non-bonded interactions; (3) intermolecular and intramolecular interactions are described by a combination of Lennard-Jones and electrostatic interactions; (4) both the Ewald method [67] and Wolf method [68] can be used for handling electrostatic interactions; (5) smart Monte Carlo trial moves [16, 69], that enable the collective displacement or rotation of molecules, can be used for enhanced sampling of different system states. Single- and multicomponent systems can be used. Brick is open source and can be downloaded from `https://gitlab.com/ETh_TU_Delft/Brick-CFCMC`. For many systems, it was verified to produce the same results as the RASPA software package [70, 71]. In this section we point out some features of Brick.

2.5.1. Ensembles

The following ensembles are available for performing simulations: (1) the *NVT* and *NPT* ensembles, with and without the CFC method; (2) the Gibbs Ensemble [20, 37], for simulations of phase equilibria, at constant total volume or at constant pressure; (3) the Reaction Ensemble [21, 26, 62, 64], for simulations of reaction equilibria, at constant volume or at constant pressure; (4) the Grand-Canonical Ensemble [57], at constant volume or at constant pressure. The latter is also referred to as the Osmotic Ensemble and is only meaningful for multicomponent systems in which one extensive variable is fixed [72]. In Brick, it is possible to combine ensembles. For example, one can combine the Gibbs Ensemble with the Reaction Ensemble to simulate a vapor-liquid system in which a reaction takes place. This is demonstrated with an example in Chapter 6.

2.5.2. Efficient Selection of Trial Moves

As mentioned in Secs. 2.2.1, 2.3.4 and 2.4.1, some trial moves that were introduced with the CFC method have a high acceptance probability for λ close to 0 while others have a high acceptance probability for λ close to 1. We can use this fact to make use of those trial moves even more efficient. For example, consider the CFC*NPT* Ensemble. We can combine the reinsertion and identity change trial moves into one single *hybrid* trial move by defining two points, $\lambda_{\mathrm{h},0}$ and $\lambda_{\mathrm{h},1}$, that determine what to do when the hybrid trial move is selected:

- If $\lambda < \lambda_{\mathrm{h},0}$ the reinsertion trial move is performed.
- If $\lambda > \lambda_{\mathrm{h},1}$ the identity change trial move is performed.
- Otherwise, nothing happens: the trial move is rejected.

Note that $\lambda_{\mathrm{h},0} < \lambda_{\mathrm{h},1}$. In this approach with the hybrid trial move, the CFC trial moves are selected when they have a high acceptance probability. Since the value of λ remains constant during either of these trial moves, the probabilities for selecting the trial moves also remain constant. Therefore, the condition of detailed balance is obeyed. For the Reaction Ensemble and Gibbs Ensemble similar hybrid trial moves can be constructed [26].

2.5.3. Weight Functions

With the CFC method, the fractional parameter λ introduces additional degrees of freedom to the system. To make simulations efficient, this parameter should be used to add a bias to the system such that the observed probability distribution of λ during the simulation is flat. Depending on the chosen ensemble combined with the CFC method the weight function has the following purpose:

- *NVT*/*NPT*: the weight function is one-dimensional and only depends on λ: $W = W(\lambda)$. It aims for equally probable values of λ.

- Gibbs Ensemble: the weight function is two-dimensional and depends on λ and the simulation box (i) the fractional molecule is in: $W = W(\lambda, i)$. It aims for equally probable values of λ and makes the fractional molecule equally likely to be found in one of the simulation boxes (50% in simulation box 1 an 50% in simulation box 2).

- Reaction Ensemble: the weight function is two-dimensional and depends on λ and the reaction step (fractional molecules are reactants: $\delta = 0$ or fractional molecules are products: $\delta = 1$): $W = W(\lambda, \delta)$. It aims for equally probable values of λ and makes the fractional molecule equally likely to be found in one of the reaction states (reactant or product).

By removing the bias, the Boltzmann averages can be computed using:

$$\langle X \rangle_{\mathrm{Boltzmann}} = \frac{\langle X \exp\left[-W\right] \rangle_{\mathrm{biased}}}{\langle \exp\left[-W\right] \rangle_{\mathrm{biased}}} \tag{2.21}$$

We would like to point out that the difference between the biased average and Boltzmann average is often negligible [26, 37, 73]. In a system with more than one fractional molecule the weight functions are independent [73] i.e.:

$$W(\lambda_1, \lambda_2, ..., \lambda_n) = \sum_{i=1}^{n} W(\lambda_i). \tag{2.22}$$

In Brick, the weight function can be obtained via the Wang-Landau algorithm [74] or an iterative scheme where the probability distribution is (repeatedly) used to improve the weight function.

2.5.4. Lennard-Jones Interactions

The Lennard-Jones (LJ) potential has the functional form:

$$U_{\mathrm{LJ}}\left(r_{ij}\right) = 4\varepsilon_{ij}\left[\left(\frac{\sigma_{ij}}{r_{ij}}\right)^{12} - \left(\frac{\sigma_{ij}}{r_{ij}}\right)^{6}\right] \tag{2.23}$$

where ε_{ij} and σ_{ij} are the Lennard-Jones parameters between sites i and j. There are two commonly used methods for dealing with the truncation of the potential. One of them is shifting the potential to 0 at the cutoff radius R_{c}:

$$U_{\mathrm{LJ}}^{\mathrm{shifted}}\left(r_{ij}\right) = \begin{cases} U_{\mathrm{LJ}}\left(r_{ij}\right) - U_{\mathrm{LJ}}\left(R_{\mathrm{c}}\right) & r_{ij} \leq R_{\mathrm{c}} \\ 0 & r_{ij} > R_{\mathrm{c}} \end{cases} \tag{2.24}$$

Another option is adding an average energy to the system that accounts for the interactions of the molecules beyond the cutoff radius. This term can be calculated analytically and is referred to as the analytic tail correction. It equals [16]:

$$U_{\mathrm{LJ}}^{\mathrm{tailcorrection}} = \frac{1}{2}\sum_{i,j}\frac{16\pi N_i N_j \varepsilon_{ij}}{V}\left(\frac{\sigma_{ij}^{12}}{9R_{\mathrm{c}}^{9}} - \frac{\sigma_{ij}^{6}}{3R_{\mathrm{c}}^{3}}\right) \tag{2.25}$$

where the sum ranges over all atom types in the system, N_i is the number of atoms of type i (excluding the fractional molecules), and V is the volume of the simulation box. The factor $\frac{1}{2}$ corrects for counting interactions twice. In Brick, either of these methods can be used to account for the truncation of the Lennard-Jones potential.

2.5.5. Electrostatic Interactions

The electrostatic potential has the functional form:

$$U_{\mathrm{electrostatic}}\left(r_{ij}\right) = \frac{1}{4\pi\varepsilon_0}\frac{q_i q_j}{r_{ij}} \tag{2.26}$$

where ε_0 is the permittivity of space, q_i and q_j are charges, and r_{ij} is the distance between them. In the remainder of this chapter we omit the factor $1/4\pi\varepsilon_0$ from our notation. The electrostatic interaction is a long-ranged interaction and requires more care when truncated than the Lennard-Jones interactions. In Brick, for handling electrostatic interactions it is possible to choose for the Ewald method [67], the Wolf method [68], or the damped-shifted version of the Wolf method by Fennell and Gezelter [75].

Ewald Method

The most commonly used method to calculate electrostatic interactions is the Ewald method [67, 76]. This method splits the electrostatic interactions in a short-range and long-range part and uses a Fourier Transform on the long-range part.

$$U_{\text{electrostatic}}^{\text{Ewald}} = \frac{1}{2}\sum_{i=1}^{N_\text{m}}\sum_{a=1}^{N_\text{a}^i}\sum_{\substack{j=1\\ j\neq i\\ r_{iajb}<R_\text{c}}}^{N_\text{m}}\sum_{b=1}^{N_\text{a}^j} q_{ia}q_{jb}\frac{\text{erfc}\left(\alpha r_{iajb}\right)}{r_{iajb}} \tag{2.27}$$

$$+\frac{1}{2}\sum_{i=1}^{N_\text{m}}\sum_{a=1}^{N_\text{a}^i}\sum_{\substack{b=1\\ b\neq a\\ r_{iaib}<R_\text{c}}}^{N_\text{a}^j} q_{ia}q_{ib}\frac{\text{erfc}\left(\alpha r_{iaib}\right)}{r_{iaib}} \tag{2.28}$$

$$-\frac{1}{2}\sum_{i=1}^{N_\text{m}}\sum_{a=1}^{N_\text{a}^i}\sum_{b=1}^{N_\text{a}^j} q_{ia}q_{ib}\frac{1}{r_{iaib}} \tag{2.29}$$

$$+\frac{1}{2V}\sum_{\vec{k}\neq\vec{0}}\frac{4\pi}{k^2}\left|\sum_{i=1}^{N_\text{m}}\sum_{a=1}^{N_\text{a}^i} q_{ia}\exp\left[i\vec{k}\cdot\vec{r}_{ia}\right]\right|^2\exp\left[-\frac{k^2}{4\alpha^2}\right] \tag{2.30}$$

$$-\frac{\alpha}{\sqrt{\pi}}\sum_{i=1}^{N_\text{m}}\sum_{a=1}^{N_\text{a}^i} q_{ia}^2 \tag{2.31}$$

where N_m is the number of molecules, N_a^i is the number of atoms in molecule i, q_{ia} is the partial charge of atom a in molecule i, $\text{erfc}(x)$ is the complementary error function, α is a damping parameter, $r_{iajb} = \left|\vec{r_{ia}} - \vec{r_{jb}}\right|$ is the distance between atom a in molecule i and atom b in molecule j, and R_c is the cutoff radius. Term 2.27 is the damped electrostatic potential for the short-ranged interactions. Terms 2.28 and 2.29 are corrections for intramolecular interactions (since they are calculated separately) and are referred to as the *exclusion* terms. One could say that term 2.28 completes the sum over all atoms in the simulation box and term 2.29 substracts all intramolecular interactions to obtain the proper intermolecular interactions. The sum in term 2.30 ranges over vectors $\vec{k} = \frac{2\pi}{L}(n_x, n_y, n_z)$ with $L = V^{\frac{1}{3}}$ (the length of one side of the simulation box) and integers $n_x, n_y, n_z \in \mathbb{N}$. Since this is a converging sum we can truncate it at a certain maximum vector k_max (or n_max such that $n_x, n_y, n_z \leq n_\text{max}$). The Fourier Transform (term 2.30) makes the Ewald method a computationally expensive method but can be optimized by storing the values of the double sum [77]. Term 2.31 is the self interaction. Since the Ewald method involves the calculation of a Fourier Transform it is computationally expensive.

Wolf Method

The Wolf method [68] is an alternative method to calculate electrostatic interactions, which works particularly well for dense systems (e.g. liquids). The Wolf method uses the following expression to calculate electrostatic interactions:

$$U_{\text{electrostatic}}^{\text{Wolf}} = \frac{1}{2}\sum_{i=1}^{N_\text{m}}\sum_{a=1}^{N_\text{a}^i}\sum_{\substack{j=1\\ j\neq i}}^{N_\text{m}}\sum_{b=1}^{N_\text{a}^j}\underset{r_{iajb}<R_\text{c}}{}q_{ia}q_{jb}\left(\frac{\operatorname{erfc}\left(\alpha r_{iajb}\right)}{r_{iajb}} - \frac{\operatorname{erfc}\left(\alpha R_\text{c}\right)}{R_\text{c}}\right) \tag{2.32}$$

$$+\frac{1}{2}\sum_{i=1}^{N_\text{m}}\sum_{a=1}^{N_\text{a}^i}\sum_{\substack{b=1\\ b\neq a}}^{N_\text{a}^j}\underset{r_{iaib}<R_\text{c}}{}q_{ia}q_{ib}\left(\frac{\operatorname{erfc}\left(\alpha r_{iaib}\right)}{r_{iaib}} - \frac{\operatorname{erfc}\left(\alpha R_\text{c}\right)}{R_\text{c}}\right) \tag{2.33}$$

$$-\frac{1}{2}\sum_{i=1}^{N_\text{m}}\sum_{a=1}^{N_\text{a}^i}\sum_{b=1}^{N_\text{a}^j}q_{ia}q_{ib}\frac{1}{r_{iaib}} \tag{2.34}$$

$$-\left(\frac{\operatorname{erfc}\left(\alpha R_\text{c}\right)}{2R_\text{c}} + \frac{\alpha}{\sqrt{\pi}}\right)\sum_{i=1}^{N_\text{m}}\sum_{a=1}^{N_\text{a}^i}q_{ia}^2 \tag{2.35}$$

where the variables and parameters have the same meaning as for the Ewald method. It should be kept in mind that typically the values for the damping parameters α are different for the Ewald and Wolf method (Chapter 3). Term 2.32 is the damped and shifted electrostatic potential. Terms 2.33 and 2.34 are corrections for intramolecular interactions (since they are calculated separately) and are referred to as the exclusion terms. One could say that term 2.33 completes the sum over all atoms in the simulation box and term 2.34 substracts all intramolecular interactions to obtain the proper intermolecular interactions. Term 2.35 is the self interaction. Although the electrostatic interactions can be accurately calculated using the Wolf method, for some systems artificial structuring around the cutoff distance is a potential issue [78]. A modification of the Wolf method by Fenell and Gezelter [75] solves this issue.

Modified Wolf Method (Fenell and Gezelter)

Fenell and Gezelter modified the Wolf method such that the electrostatic force at the cutoff is continuous. For this reason it is sometimes also being referred to as the Damped Shifted Force (DSF) potential. This method uses the following expression to calculate electrostatic interactions:

$$U_{\text{electrostatic}}^{\text{Fennell-Gezelter}} = \frac{1}{2}\sum_{i=1}^{N_\text{m}}\sum_{a=1}^{N_\text{a}^i}\sum_{\substack{j=1\\ j\neq i\\ r_{iajb}<R_\text{c}}}^{N_\text{m}}\sum_{b=1}^{N_\text{a}^j} q_{ia}q_{jb}\left[\frac{\operatorname{erfc}\left(\alpha r_{iajb}\right)}{r_{iajb}} - \frac{\operatorname{erfc}\left(\alpha R_\text{c}\right)}{R_\text{c}}\right.$$

$$\left. + \left(\frac{\operatorname{erfc}\left(\alpha R_\text{c}\right)}{R_\text{c}^2} + \frac{2\alpha}{\sqrt{\pi}}\frac{\exp\left[-\alpha^2 R_\text{c}^2\right]}{R_\text{c}}\right)\left(r_{iajb} - R_\text{c}\right)\right] \tag{2.36}$$

$$+ \frac{1}{2}\sum_{i=1}^{N_\text{m}}\sum_{a=1}^{N_\text{a}^i}\sum_{\substack{b=1\\ b\neq a\\ r_{iaib}<R_\text{c}}}^{N_\text{a}^j} q_{ia}q_{ib}\left(\frac{\operatorname{erfc}\left(\alpha r_{iaib}\right)}{r_{iaib}} - \frac{\operatorname{erfc}\left(\alpha R_\text{c}\right)}{R_\text{c}}\right) \tag{2.37}$$

$$- \frac{1}{2}\sum_{i=1}^{N_\text{m}}\sum_{a=1}^{N_\text{a}^i}\sum_{b=1}^{N_\text{a}^j} q_{ia}q_{ib}\frac{1}{r_{iaib}} \tag{2.38}$$

$$- \left(\frac{\operatorname{erfc}\left(\alpha R_\text{c}\right)}{2R_\text{c}} + \frac{\alpha}{\sqrt{\pi}}\right)\sum_{i=1}^{N_\text{m}}\sum_{a=1}^{N_\text{a}^i} q_{ia}^2 \tag{2.39}$$

Term 2.36 is the damped and shifted electrostatic potential. Terms 2.37 and 2.38 are corrections for intramolecular interactions (since they are calculated separately) and are referred to as the exclusion terms. One could say that term 2.37 completes the sum over all atoms in the simulation box and term 2.38 substracts all intramolecular interactions to obtain the proper intermolecular interactions. Term 2.39 is the self interaction.

2.5.6. Scaling of Interactions

The fractional parameter λ is used to scale interactions of the fractional molecules in the system. When $\lambda = 0$, the fractional molecule has no interactions with its surroundings. For $\lambda = 1$, the interactions of the fractional molecule are the same as a whole molecule. Between these two state points, a path can be chosen how to "switch on" the interactions from $\lambda = 0$ to $\lambda = 1$.

It turns out to be more efficient to scale the Lennard-Jones interactions and electrostatic interactions separately, using λ_{LJ} and λ_{EL}, respectively. We use the following procedure. Starting from $\lambda = 0$, with increasing λ we only increase the Lennard-Jones interactions of the fractional molecule i.e. increase λ_{LJ} and keep $\lambda_{\mathrm{EL}} = 0$. Then, at a certain chosen value of λ, which we refer to as λ_{s}, we reach $\lambda_{\mathrm{LJ}} = 1$. From that point (till $\lambda = 1$) we start increasing the electrostatic interactions of the fractional molecule i.e. increase λ_{EL} and keep $\lambda_{\mathrm{LJ}} = 1$. This way we gradually increase first the Lennard-Jones interactions, which prevents singularities in the electrostatic potential, and then the electrostatic interactions. It turns out to be more efficient in simulations than scaling both interactions at the same time [79].

For fractional molecules the Lennard-Jones interactions are scaled as [80]:

$$U_{\mathrm{LJ}}(r, \lambda_{\mathrm{LJ}}) = 4\lambda\varepsilon\left[\frac{1}{\left(\alpha_{\mathrm{LJ}}(1-\lambda_{\mathrm{LJ}})^{b} + \left(\frac{r}{\sigma}\right)^{c}\right)^{\frac{12}{c}}} - \frac{1}{\left(\alpha_{\mathrm{LJ}}(1-\lambda_{\mathrm{LJ}})^{b} + \left(\frac{r}{\sigma}\right)^{c}\right)^{\frac{6}{c}}}\right] \tag{2.40}$$

where typical values for α_{LJ}, b and c are 0.5, 1, and 6 respectively. Other values can be used to minimize the variance of the energy if required. The term $\alpha_{\mathrm{LJ}}(1-\lambda_{\mathrm{LJ}})^{b}$ prevents singularities for small values of r. Shifting this potential at the cutoff is straightforward. For tail corrections the substitution $N_i \rightarrow N_i + \lambda_{\mathrm{LJ}}$ is applied to Eq. 2.25 [26, 27].

The electrostatic interactions for fractional molecules are scaled similar to the Lennard-Jones interactions. This is achieved by substituting $r_{iajb} \rightarrow r_{iajb} + \alpha_{\mathrm{EL}}(1-\lambda_{\mathrm{EL}})$ (which prevents singularities at small distances) and $q_{ia} \rightarrow \lambda_{\mathrm{EL}} q_{ia}$ where we typically chose $\alpha_{\mathrm{EL}} = 0.01$ Å.

2.5.7. Intramolecular Interactions

Intramolecular Lennard-Jones interactions are calculated directly from Eq. 2.23 without truncating the interactions. Similarly, the intramolecular electrostatic interactions are calculated directly from the electrostatic potential without truncation:

$$U_{\mathrm{electrostatic}}^{\mathrm{intramolecular}} = \gamma_{ij}\frac{q_i q j}{r_{ij}} \tag{2.41}$$

where γ_{ij} is a scaling factor for the intramolecular electrostatic interactions between atoms i and j in a molecule that is required by some force fields.

2.5.8. Smart Monte Carlo

Typical translation trial moves in Monte Carlo simulations attempt to translate one molecule in a random direction by a random distance. One can optimize the efficiency of these trial moves by using the force on the particles. Instead of displacing one molecule at random, in Smart Monte Carlo simulations [16] all molecules are translated at the same time where the direction and distance are determined by the force and a random contribution [69]. This results in a faster equilibration of the system. This method is similar to the hybrid Monte Carlo method [81] that combines Monte Carlo and Molecular Dynamics. The Smart Monte Carlo translation move in Brick-CFCMC follows the following procedure [16]:

1. Random vectors u_i are generated, where the vector components are drawn from a normal distribution with the mean equal to 0 and the variance equal to 1.

2. The 'effective kinetic energy' is calculated:

$$\kappa = \sum_{i=1}^{N} \frac{1}{2} m_i \mathrm{u}_i^2$$

   where m_i is the mass of molecule i.

3. Each particle in the system is assigned a velocity

$$\mathrm{v}_{i,\mathrm{old}} = \sqrt{\frac{3Nk_\mathrm{B}T}{2\kappa}} \cdot \mathrm{u}_i$$

   where the factor $\sqrt{\frac{3Nk_\mathrm{B}T}{2\kappa}}$ guarantees that the kinetic energy of the system is equal to $\frac{3}{2}Nk_\mathrm{B}T$ (according to the equipartition theorem).

4. The forces F_i acting on each molecule are calculated.

5. Velocities are updated:

$$\mathrm{v}_i = \mathrm{v}_{i,\mathrm{old}} + \frac{\mathrm{F}_i}{2m_i}\Delta t$$

6. Positions are updated:

$$\mathrm{r}_{i,\mathrm{new}} = \mathrm{r}_{i,\mathrm{old}} + \mathrm{v}_i \Delta t$$

7. The forces F_i are recalculated (based on the new positions $\mathrm{r}_{i,\mathrm{new}}$).

8. Velocities are updated again (with the recalculated forces):

$$\mathrm{v}_{i,\mathrm{new}} = \mathrm{v}_i + \frac{\mathrm{F}_i}{2m_i}\Delta t$$

9. The trial move is accepted or rejected according to the acceptance rule:

$$\mathrm{acc}(\mathrm{o} \to \mathrm{n}) = \min\left(1, \exp[-\beta(\Delta U + \Delta K)]\right)$$

where ΔU is the difference in potential energy between the new and old configuration:

$$\Delta U = U(\mathrm{r}^N_{\mathrm{new}}) - U(\mathrm{r}^N_{\mathrm{old}})$$

and ΔK is the difference in kinetic energy:

$$\Delta K = \sum_{i=1}^{N} \frac{1}{2} m_i (\mathrm{v}^2_{i,\mathrm{new}} - \mathrm{v}^2_{i,\mathrm{old}})$$

In this routine, the velocity Verlet algorithm [82] is used to calculate the velocities and positions of the particles. This algorithm is time reversible and area-preserving (symplectic) [83]. The time step Δt can be adjusted to optimize the efficiency. Choosing a small time step results in small displacements and a high acceptance probability of this trial move. However, small displacements are not that useful for equilibrating the system. Choosing a large time step results in large displacements and small acceptance probabilities. One has to tune Δt for efficiency. In Fig. 2.2 the average accepted displacement and acceptance ratio as a function of the time step is shown for the Smart Monte Carlo translation trial move in a system of Lennard-Jones particles. Similarly, Smart Monte Carlo rotation trial moves can be performed using time reversible and symplectic integrators for rigid body dynamics [84].

Instead of performing Smart Monte Carlo for a single MD timestep, one can also consider taking N timesteps, i.e. repeating step 4 to step 8, similar to the Hybrid Monte Carlo approach [15]. Taking multiple timesteps has the advantage that the ballistic motion of the system is followed better, leading to larger displacements in phase space. However, taking N too large leads to larger computational requirements and lower acceptance probabilities (especialy for large timesteps). As an example, in Figure 2.3 we show the mean square displacement, $\langle r^2 \rangle$, as a function of the number of force evaluations for different values of N with $\Delta t = 0.03$ in a system of Lennard-Jones particles. For comparison, the case $\Delta t = 0.001$, corresponding to a trajectory in Molecular Dynamics is also included. When the number of timesteps is too large, the energy drift becomes such that the trajectories are mostly rejected. For example, for $\Delta t = 0.03$ and $N = 25$, we find that only about 9% of the trajectories are accepted. For the results shown in Fig. 2.3, the optimum seems to be around $N = 10$ with an average acceptance probability of about 25%. In principle, optimal values for N and Δt vary for each system.

2.5.9. Other Features of Brick-CFCMC

Other features of Brick are the calculation of partition function of isolated molecules from spectroscopic data [85] or QM simulations (e.g. Gaussian [86]), required for simulations in the Reaction Ensemble, calculation of fugacities in multicomponent systems using the Peng-Robinson Equation of State [87], calculation of radial distribution functions, creating snapshots of the system, and using Widom's test-particle insertion method [28, 59].

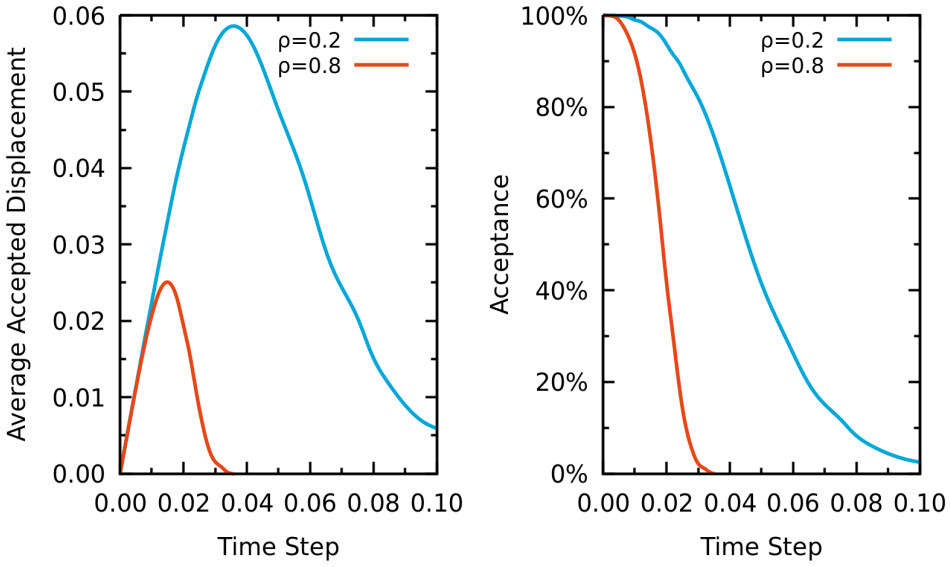

Figure 2.2: Acceptance probability and average accepted displacement of the Smart Monte Carlo translation trial move as a function of the time step in a system of Lennard-Jones particles with number densities: $\rho = 0.2$ (blue line) and $\rho = 0.8$ (red line). The temperature is set to 2.0 (reduced units). The optimal choices for Δt are around 0.04 and 0.015 (reduced units), for $\rho = 0.2$ and $\rho = 0.8$, respectively.

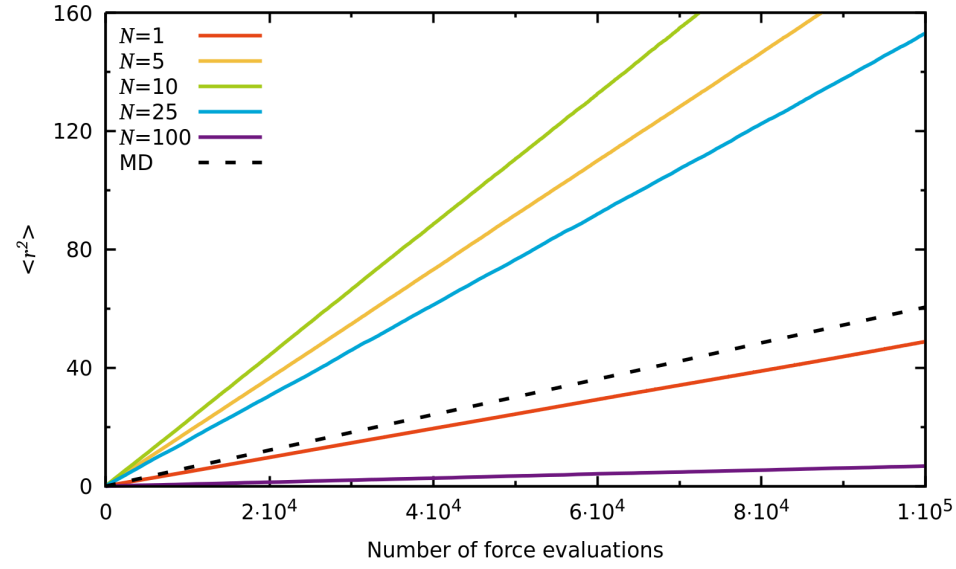

Figure 2.3: Mean square displacement $\langle r^2 \rangle$ as a function of the number of force evaluations for the Smart translation trial move in a system of Lennard-Jones particles with number density $\rho = 0.6$ and $T = 1.0$ (reduced units). Different colored lines correspond to a different number of timesteps N with $\Delta t = 0.03$. The black dashed line corresponds to the trajectory in Molecular Dynamics ($\Delta t = 0.001$).

3

Vapor-Liquid Equilibria in the Gibbs Ensemble

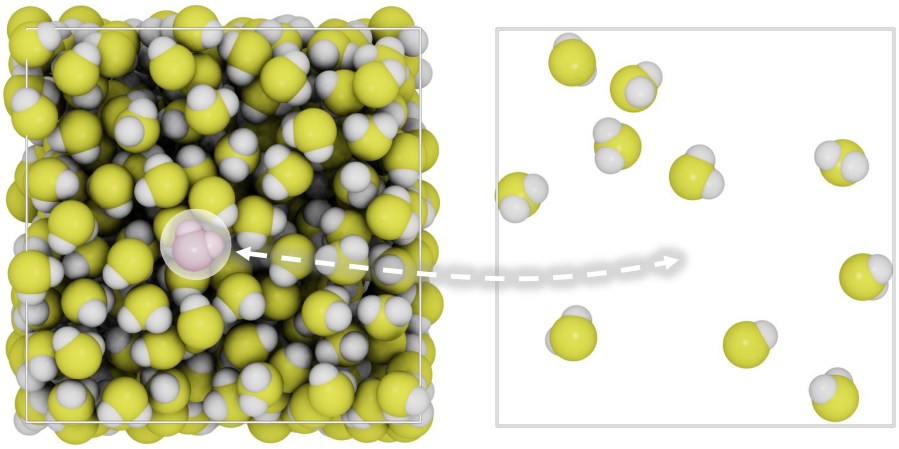

Schematic illustration of hydrogen sulfide in the Gibbs Ensemble: one liquid phase, one vapor phase and one fractional molecule that transfers between the simulation boxes to obtain vapor-liquid equilibrium.

This chapter is based on the paper:

R. Hens and T. J. H. Vlugt, *Molecular Simulation of Vapor-Liquid Equilibria using the Wolf Method for Electrostatic Interactions*, Journal of Chemical and Engineering Data, **63**, 1096-1102 (2018) [27].

3.1. Introduction

Vapor-liquid equilibria (VLE) are of great interest in chemical industry, in particular for separation processes [41, 88]. As an alternative to experiments, molecular simulation is a useful tool for obtaining VLE data, especially for multicomponent systems [20, 89, 90]. Molecular simulation critically relies on a force field and the geometry of the molecules as input. The force field describes the interactions between atoms and molecules. The past decades, there have been many simulation studies on VLE using force fields that employ a combination of a Lennard-Jones interaction potential (LJ) and an electrostatic interaction potential [11–14, 91] (Sec. 2.5.4 and Sec. 2.5.5). Different methods and force fields for describing interactions exist, such as density functional theory [92, 93] and polarizable force fields [94–96]. The LJ potential is rather short-ranged and calculating the energy is therefore straightforward i.e. by truncating the LJ potential and using analytic tail corrections [16]. However, the electrostatic potential is long-ranged and one has to take extra care when calculating this energy contribution because of periodic boundary conditions and the interaction of the molecule with its mirror images. The Ewald summation [67] is a commonly used method for calculating electrostatics. It calculates the electrostatic energy by dividing the potential in a short-range potential that can be calculated directly, and a long-range potential which requires a Fourier transform of the charge density. The Ewald summation is accurate for a wide variety of systems and the electrostatic energy is well defined [67, 76]. A disadvantage of the Ewald summation and its variants is that it is computationally expensive because a Fourier transform is involved [97, 98]. Other methods for dealing with electrostatics exist such as the reaction field method [99, 100], the particle-particle and particle-mesh algorithm [101] (a variant to the Ewald summation), and the Wolf method [68, 75]. In this chapter we focus on the latter. The past few years, the Wolf method has become quite popular for simulating dense fluids due its simplicity and efficiency [75]. The Wolf method makes use of the (strong) screening of electrostatic interactions in dense systems. All interactions are pairwise and there is no Fourier transform of the charge density involved. Calculations involve two parameters: the damping parameter α and the cutoff radius R_c. Unlike the Ewald method, there is no clear criterion for choosing these parameters. The effectivity of the Wolf method has already been demonstrated in many applications [58, 102–105]. Those simulations take place in dense liquids where there is a strong screening of the electrostatic interactions. From earlier studies, we also know that the Wolf method is not very efficient in zeolites because of less effective screening due to voids in the zeolite topology [77]. As a consequence, a larger cutoff radius for electrostatic interactions is needed in this case, making the Wolf method less efficient than one would expect. It is also unclear if and how the Wolf method influences VLE. Here, we will investigate the accuracy of the Wolf method in simulating VLE for simple compounds: hydrogen sulfide, methanol, and carbon dioxide. These compounds were chosen because of their relevance in industry and applications and because accurate force fields are available to describe these compounds. Monte Carlo simulations are performed in the Gibbs Ensemble using the Continuous Fractional Component (CFC) method (Sec. 2.4). Simulations in the Gibbs Ensemble make it possible to choose

the parameters for the Wolf method (α and R_c) in both simulation boxes (vapor and liquid) independently of each other. This is important because the Wolf method is based on the screening of charges which is dependent on the density of the system.

This chapter is organized as follows. First, in Sec. 3.2 the simulation details such as the input and force fields are discussed. Also the procedure on how to choose the optimal Wolf parameters is explained. Second, in Sec. 3.3 the simulation results for density, chemical potential, vapor pressure and critical properties are reported. Sec. 3.4 concludes this chapter with concluding remarks about the efficiency and accuracy of the Wolf method in VLE simulations.

3.2. Simulation Details

Monte Carlo simulations are performed in the Gibbs Ensemble using the CFC method as described in Sec. 2.4 to obtain vapor-liquid equilibria of three different pure compounds: hydrogen sulfide, methanol, and carbon dioxide. Although the multiple histogram reweighting method [106, 107] is a very efficient method for obtaining VLE, Monte Carlo simulations in the Gibbs Ensemble are suitable for obtaining VLE with a relatively small amount of molecules not too close to the critical point and small finite-size effects [108]. Electrostatic interactions will be calculated using the Wolf Method as described in Sec. 2.5.5. The force field parameters [89, 109, 110] used to describe the interaction between molecules are listed in Table A.1 of the Appendix and Lorentz-Berthelot mixing rules are used [16]. All molecules are treated as rigid and the bond lengths and angles are listed in Table A.2 of the Appendix. Periodic boundary conditions are used.

A Monte Carlo cycle in the simulations consist of N_{tot} Monte Carlo steps, where N_{tot} is the total number of molecules in the complete system. In each Monte Carlo step, a trial move is selected at random with the following fixed probabilities: 35% translations, 30% rotations, 1% volume changes, 17% λ changes, 8.5% swaps of the fractional molecule, and 8.5% identity changes of the fractional molecule. (Note that here we do not make use of the hybrid trial move described in Sec. 2.5.2.) Ensemble averages are updated after every cycle.

Each simulation starts with $5{\cdot}10^3$ cycles for equilibrating, where only translation and rotation moves are performed. Next, there are $5{\cdot}10^4$ cycles for initializing and further equilibrating of the system, now using all available trial moves. In this stage, the weight function $W(\lambda, i)$ is being constructed using the Wang-Landau algorithm [74]. During the initializing and equilibrating phases, the maximum displacement, rotation, and volume change are modified to achieve an acceptance ratio of 50% for those trial moves. Finally, there are $5{\cdot}10^4$ production cycles where ensemble averages are taken and the λ-probability distribution is sampled for which 100 bins are used for storage.

Multiple simulations are performed for different compounds and different Wolf parameters at different temperatures. For all simulations, a cutoff radius of 14 Å for LJ interaction is used in both simulation boxes with analytic tail corrections. The Wolf parameters (α and R_c) are chosen for each simulation as follows. First, a short *NVT* simulation is run at a density close to equilibrium (estimated from literature [109, 111, 112]) above the critical temperature (so that no phase separation occurs

Table 3.1: Values of the Wolf parameters R_c and α for different sets.

Set	Wolf Parameters
1	Optimal (as described in Sec. 3.2).
2	$\alpha = 0.12$ Å^{-1} and $R_c = 14$ Å (16 Å for CO_2) in both simulation boxes.
3	$\alpha = 0.10$ Å^{-1} in both boxes and the same R_c as in the optimal set.
4	$\alpha = 0.06$ Å^{-1} in both boxes and the same R_c as in the optimal set.

in the simulation box). Second, for the final configuration of this *NVT* simulation the electrostatic energy is calculated with the Ewald Method as well as for many different Wolf parameters. A plot comparing the electrostatic energy calculated with the Ewald method (which we consider as the exact solution) and the Wolf method for different parameters is made. Fig. 3.1 and Fig. 3.2 show typical differences in the electrostatic energy for the liquid and vapor phase of methanol, respectively. Fig. 3.1 also clearly shows the effect of a damping parameter that is too small: for $\alpha \to 0$ and large R_c the lack of screening in the cutoff spheres results in large energy differences between the Wolf method and Ewald method. From those plots, the optimal values for α and R_c can be determined i.e. the parameters that give an accurate result compared to the Ewald method, choosing R_c as small as possible (because a smaller cutoff is computationally favorable). We will refer to this values as the optimal parameter set. It is possible to take multiple configurations and use the averages of the energy differences to obtain the parameter sets. However, it turns out to be sufficient to take only a single configuration as can be seen for example in Fig. 3.1 where, for α large enough, the energy differences for different R_c converge. We also verified that the optimal parameter set is the same as when we would have taken a configuration from a Gibbs Ensemble simulation after equilibrating and following the same procedure.

Choosing the best values for α and R_c can be quite some work we also run simulations for different (easier) choices of the parameters to show the dependence of the results on the values of the Wolf parameters. The different parameter sets are listed in Table 3.1. The first set is the optimal set, obtained from the procedure described above. The second set is chosen because it should give accurate results in the liquid phase of each compound (according to the optimal set). The third set is chosen with a slightly smaller α such that it should be more accurate for the gas phase and is a value in the range that is typically chosen [75, 77, 102]. The fourth set is chosen such that it should be even more accurate for the gas phase. In the optimal parameter set for very low densities an α of 0 is found with a very large cutoff radius. This corresponds to calculating the electrostatic energy directly, ignoring any interaction between a molecule and its mirror images.

Each simulation starts with different initial configurations (how the molecules are distributed over the two simulation boxes and the size of the simulation boxes). In the Supporting Information of Ref. [27], the initial configuration can be found as well as the optimal Wolf parameter sets for each system.

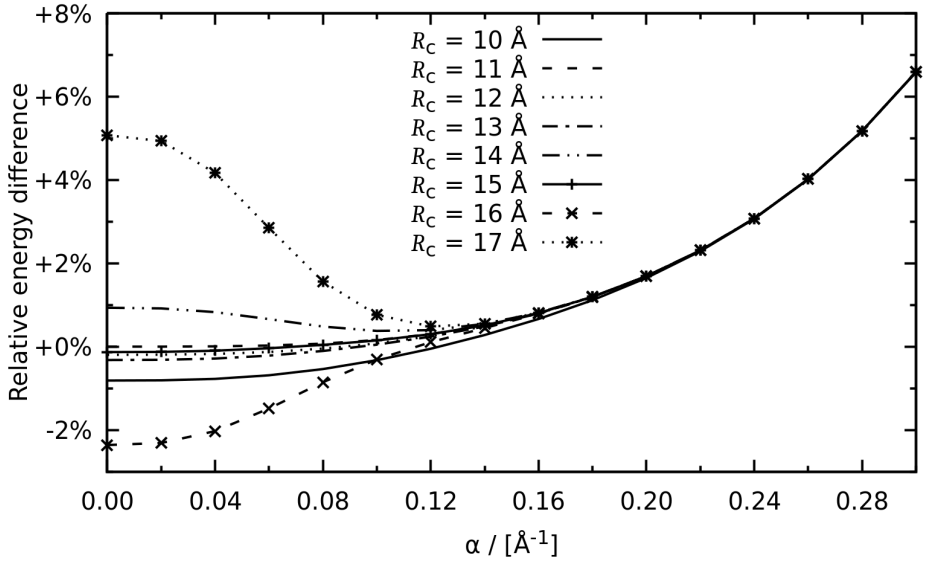

Figure 3.1: Relative difference in electrostatic energy between the Wolf method and Ewald summation for different values of R_c as a function of α. The parameters for the Ewald summation are chosen such that a relative precision of 10^{-6} is achieved. The energy is calculated for methanol at a (typical liquid) density of 692 kg/m^3 at 600 K. The optimal value of α is in the range from 0.10 Å^{-1} to 0.14 Å^{-1}.

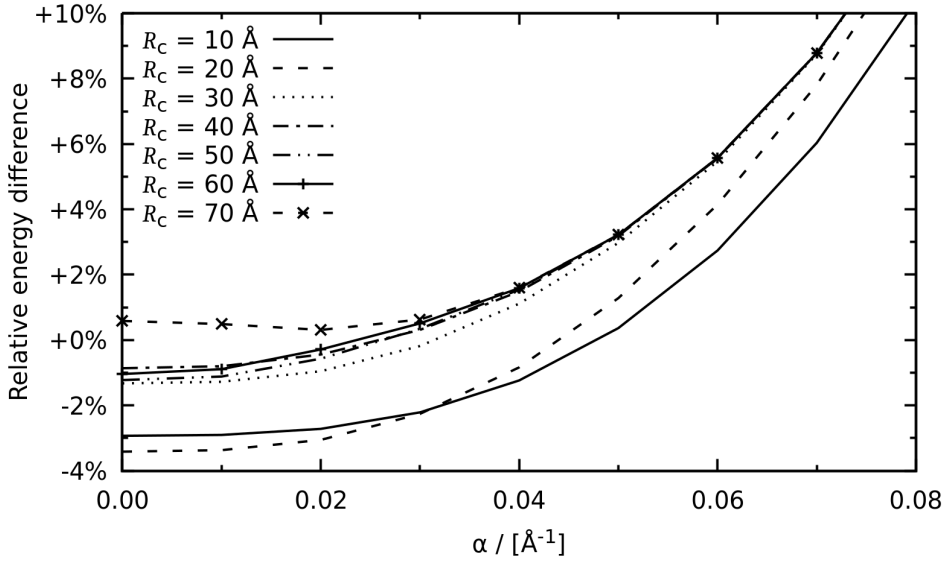

Figure 3.2: Relative difference in electrostatic energy between the Wolf method and Ewald summation for different values of R_c as a function of α. The parameters for the Ewald summation are chosen such that a relative precision of 10^{-6} is achieved. The energy is calculated for methanol at a (typical gas) density of 2.66 kg/m^3 at 600 K. The optimal value of α is in the range from 0 to 0.03 Å^{-1}.

After obtaining the densities at equilibrium, critical properties and the saturated vapor pressures P_{vap} are determined. The critical properties (density ρ_{c}, and temperature T_{c}) are calculated from the VLE-curves using the method described by Dinpajooh and co-workers [108] and in the book by Frenkel and Smit [15]:

$$\frac{\rho_{\mathrm{l}} + \rho_{\mathrm{v}}}{2} = \rho_{\mathrm{c}} + A(T - T_{\mathrm{c}}) \tag{3.1}$$

$$\rho_{\mathrm{l}} - \rho_{\mathrm{v}} = B(T - T_{\mathrm{c}})^{0.32} \tag{3.2}$$

where ρ_{l} and ρ_{v} are the liquid and vapor density, respectively, and A and B are fitting parameters. The saturated vapor pressures P_{vap} are determined in the following way. We estimate the coexistence pressure (from the ideal gas law) and set up multiple conventional *NPT* simulations at different pressures P in a range around the estimated one. From each simulation we calculate the density and from those results a (P, ρ)-diagram can be constructed. P_{vap} can then be determined (by interpolating) at the equilibrium vapor density ρ_{v}. Alternatively, one could compute the pressure at ρ_{v} in a simulation in the *NVT* ensemble.

3.3. Results

The densities at different temperatures can be found in Fig. 3.3 for hydrogen sulfide, Fig. 3.4 for methanol, and Fig. 3.5 for carbon dioxide. Our simulation results are in excellent agreement with the comparing data (simulations using the Ewald method) for almost all Wolf parameter sets. Only at high densities, the density deviates a bit for the set where $\alpha = 0.06$ Å^{-1} in both simulation boxes. This is caused by the fact that at high density there is a large effective screening of charges. This means that either a larger value of α should be used (see also Fig. 3.1). Closer to the critical temperatures small deviations in the results are found.

The chemicals potential of hydrogen sulfide, methanol, and carbon dioxide can be found in Fig. 3.6, Fig. 3.7, and Fig. 3.8 respectively as calculated from Eq. 2.7 (excluding μ_i°). From this data it can immediately be seen that the vapor and liquid are in chemical equilibrium because the chemical potential is equal in both simulation boxes. For methanol there is a tiny difference between the computed chemical potentials in the liquid and the gas phase, but this is still within the error bars. Furthermore, for methanol at $T = 180$ K and $T = 230$ K, no chemical potential could be calculated directly because of the very low density of the gas phase. Although it would be possible to calculate the chemical potential for the gas phase directly by considering it as an ideal gas, we do not do that here because of the large error bars for the density.

Critical temperatures and densities are determined from the VLE-curves. The obtained critical points of hydrogen sulfide, methanol, and carbon dioxide are listed in Table 3.2. For hydrogen sulfide and carbon dioxide acceptable critical points are obtained. Only for the Wolf parameter set with $\alpha = 0.06$ Å^{-1} in both boxes a larger deviation is found. This can again be explained by the fact that this parameter set fails to give an accurate description of the VLE (Fig. 3.5). For methanol, the critical temperatures are higher than expected and the error bars are relatively high

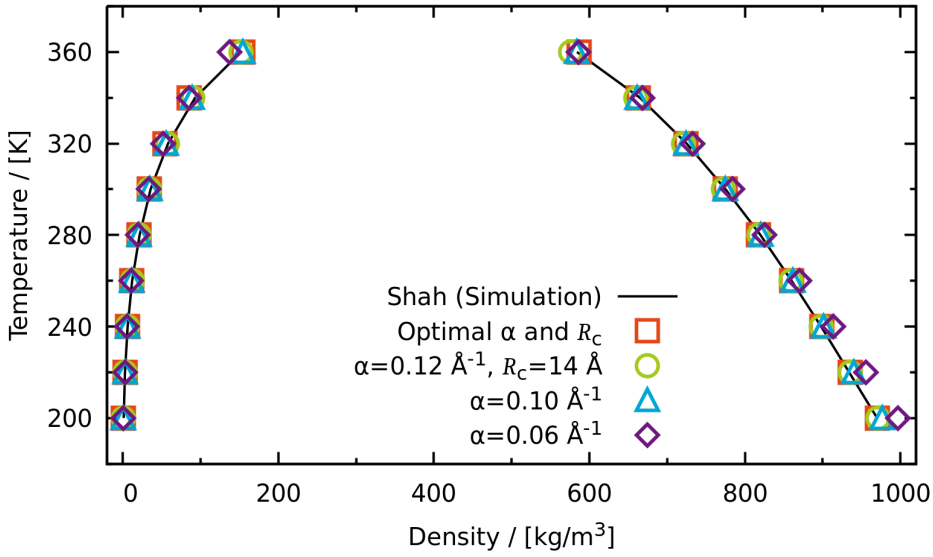

Figure 3.3: Density-temperature plot for the vapor-liquid equilibrium of hydrogen sulfide. Different symbols indicate different parameters for the Wolf method, compared to simulation results from Shah et al. [109] using the Ewald summation (solid line).

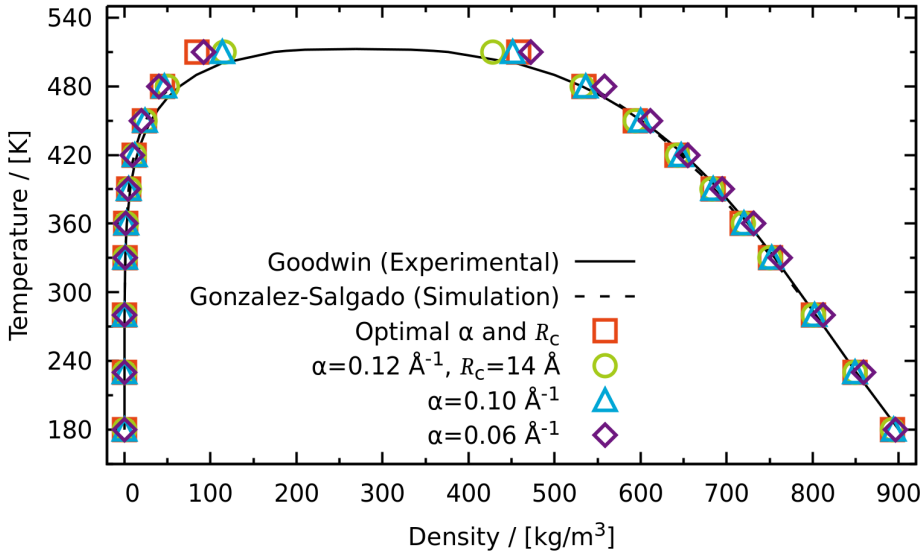

Figure 3.4: Density-temperature plot for the vapor-liquid equilibrium of methanol. Different symbols indicate different parameters for the Wolf method, compared to experimental results from Goodwin [111] (solid line) and simulations from Gonzalez-Salgado et al. [110] using the Ewald summation (dashed line).

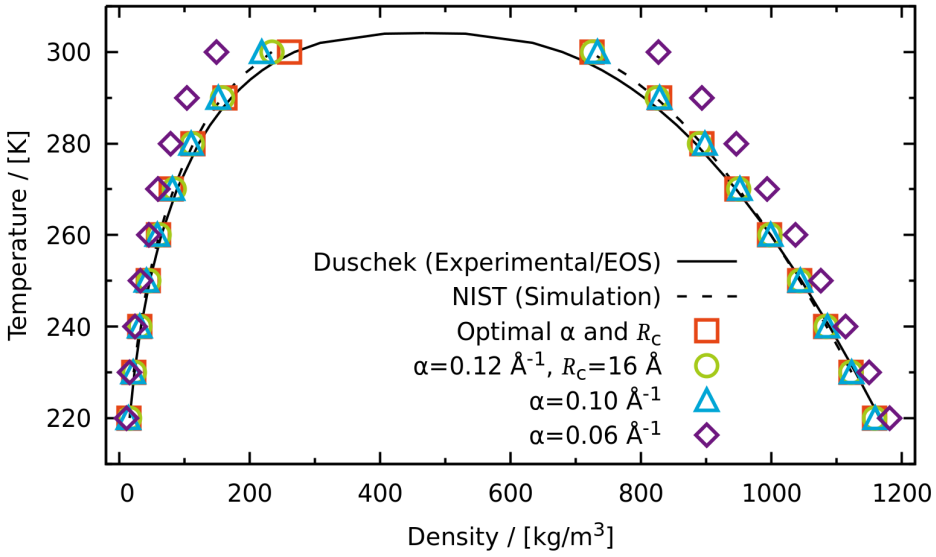

Figure 3.5: Density-temperature plot for the vapor-liquid equilibrium of carbon dioxide. Different symbols indicate different parameters for the Wolf method, compared to experimental results and equation of state from Duschek et al. [113] (solid line) and simulations from the NIST database [112] using the Ewald summation (dashed line).

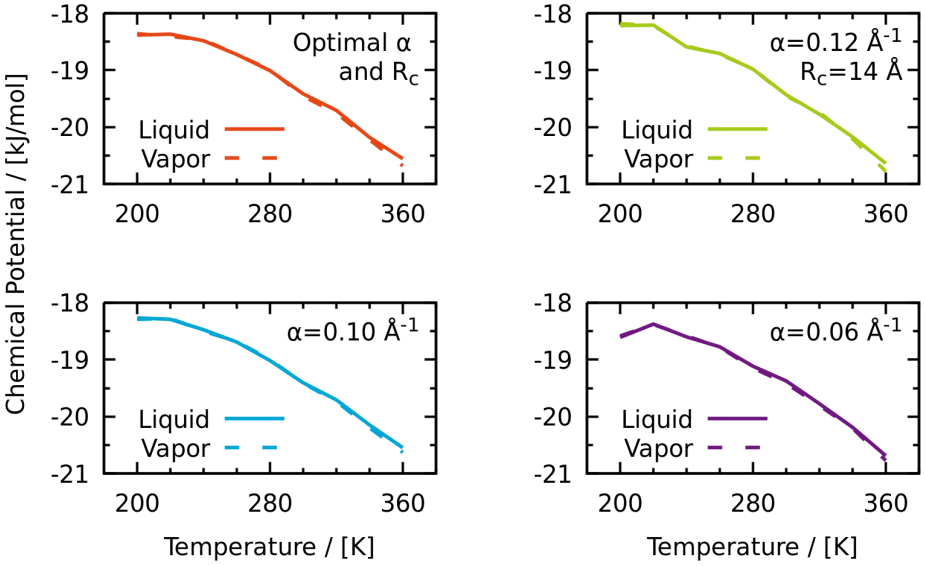

Figure 3.6: Chemical potential as a function of temperature of hydrogen sulfide. Values are computed using Eq. 2.7 (excluding μ_i°).

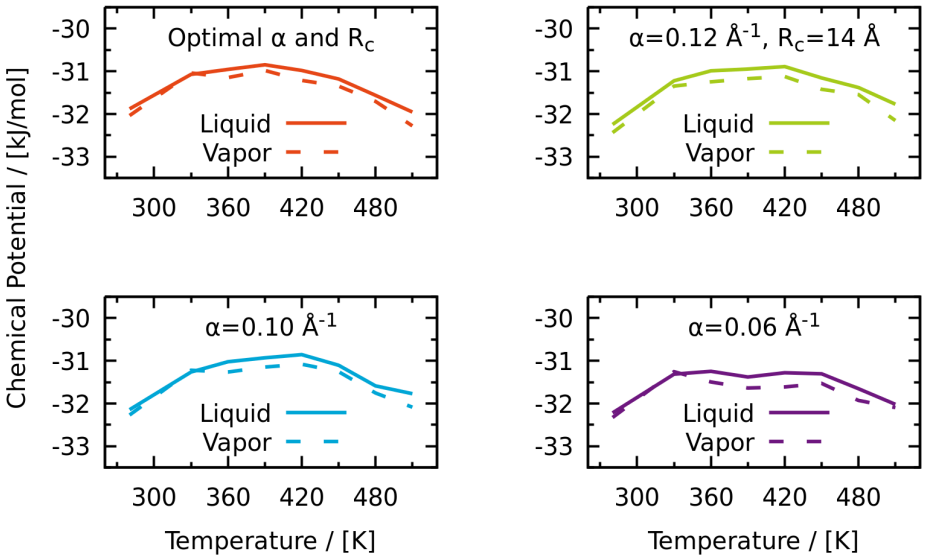

Figure 3.7: Chemical potential as a function of temperature of methanol. Values are computed using Eq. 2.7 (excluding μ_i°).

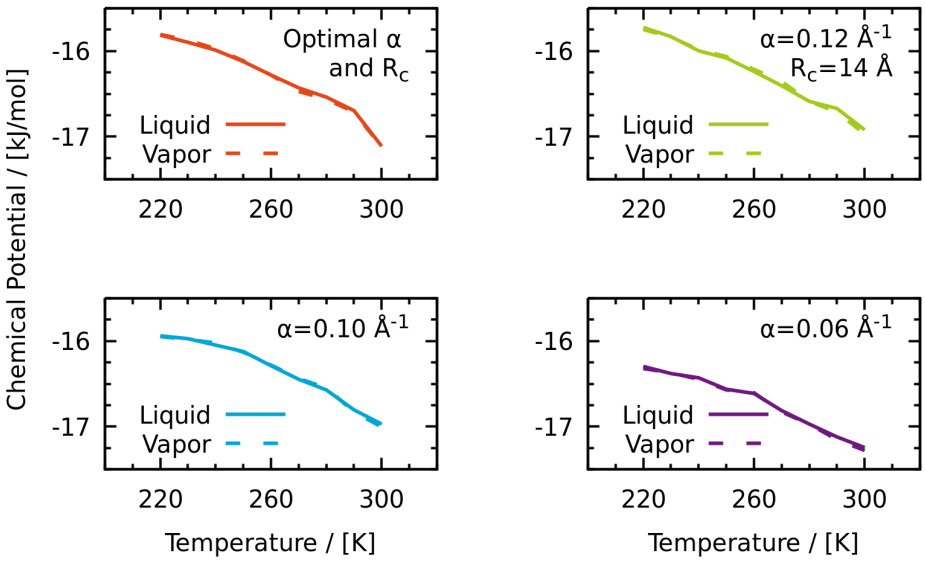

Figure 3.8: Chemical potential as a function of temperature of carbon dioxide. Values are computed using Eq. 2.7 (excluding μ_i°).

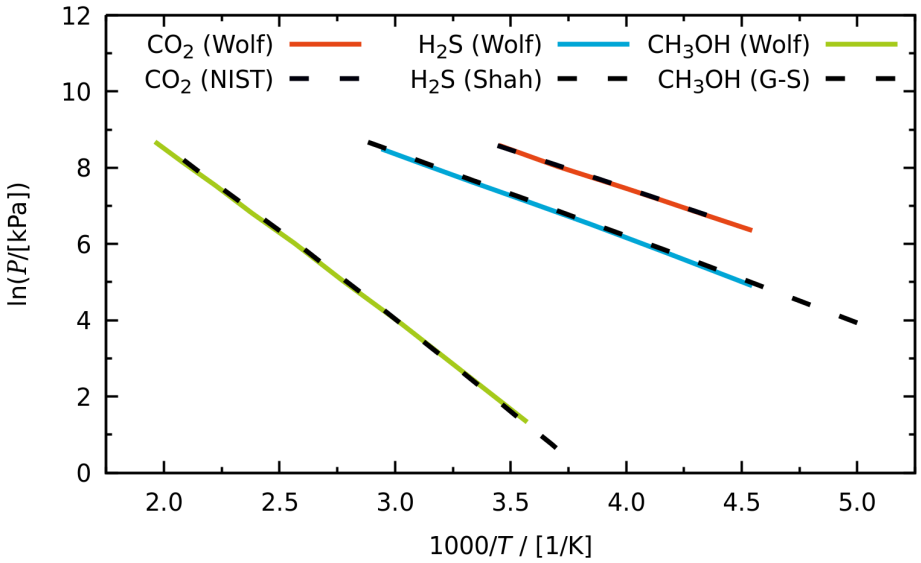

Figure 3.9: Clausius-Clapeyron plots of the saturated vapor pressure as a function of the inverse temperature. The solid lines show the results obtained from *NPT* simulations using the Wolf method for electrostatic interactions with the optimal parameters, different colors indicate the different compounds. Dashed lines show simulation data from the NIST database [112], Shah et al. [109], and Gonzalez-Salgado et al. [110].

compared to that for hydrogen sulfide and carbon dioxide. This is most likely caused by the difference in the shape of the VLE curve, compared to that of hydrogen sulfide and carbon dioxide, and the method used to extract the critical point.

Finally, from *NPT* simulations, the vapor pressures at equilibrium are determined. Only the optimal Wolf parameter sets were used. A Clausius-Clapeyron plot (Fig. 3.9) summarizes the resulting vapor pressures. We were not able to determine the vapor pressure from a *NPT* simulation at $T = 200$ K because no density corresponding to ρ_v was obtained. Also, at $T = 360$ K we were not able to obtain the pressure because the temperature is close to the critical point. For the same reason we were not able to obtain the vapor pressure for carbon dioxide at $T = 300$ K. From the slopes of the line in Fig. 3.9, the enthalpy of vaporization H_vap can be determined. Values of the enthalpy of vaporization and experimental results are reported in Table 3.3 for comparison. The computed values are in good agreement with experimental available data.

The optimal set of Wolf parameters produces results in agreement with data from literature and can therefore be considered as an accurate alternative to the Ewald method. Also note that the other parameter sets produce acceptable results as well, especially Set 2. This is most likely caused by the fact that it is more important to describe interactions in the liquid phase more accurately than it is in the vapor phase (which is close to behaving like an ideal gas). This is a useful result if one does not have data available for determining the optimal parameters

Table 3.2: Critical temperatures T_c and critical densities ρ_c for different compounds and different Wolf parameter sets. Critical properties are determined from the VLE curves with the method described by Dinpajooh and co-workers [108]. Parameter set 1 is the optimal parameter set (chosen such that results are similar to that the Ewald method). Parameter set 2 has α = 0.12 Å^{-1} and R_c = 14 Å (16 Å for CO_2) in both simulation boxes. Parameter set 3 has α = 0.10 Å^{-1} in both boxes and the same R_c as in the optimal set. Parameter set 4 has α = 0.06 Å^{-1} in both boxes and the same R_c as in the optimal set. The last rows shows reference (simulation and experimental) data for hydrogen sulfide [109, 114], methanol [110, 112], and carbon dioxide [89, 115]. Critical properties are determined using data in the following temperature ranges: hydrogen sulfide from 260 K to 320 K, methanol from 360 K to 480 K, and carbon dioxide from 220 K to 280 K. The numbers between brackets denote the uncertainty in the last digit.

	H_2S		CH_3OH		CO_2	
Parameter set	T_c/[K]	ρ_c/[kg/m^3]	T_c/[K]	ρ_c/[kg/m^3]	T_c/[K]	ρ_c/[kg/m^3]
1	377(4)	345(8)	536(16)	257(14)	307(2)	463(10)
2	374(5)	346(10)	533(19)	261(13)	307(3)	463(7)
3	375(2)	347(5)	537(21)	260(19)	308(2)	464(10)
4	378(8)	347(17)	546(10)	262(6)	320(3)	457(5)
Ref. (Sim)	374.5(6)	361(2)	521.5	272	306.2	464.9
Ref. (Exp)	373.4(2)	347(4)	513(1)	273(3)	304.18(2)	468(1)

Table 3.3: ΔH_{vap} for different compounds computed using the Clausius-Clapeyron relation (see also Fig. 3.9) compared to experimental results. The numbers between brackets denote the uncertainty in the last digit

	ΔH_{vap}/[kJ/mol]	
Compound	Simulation	Experimental
Hydrogen sulfide	18.5(2)	18.6 [116]
Methanol	37.9(3)	37.9 [117]
Carbon dioxide	16.8(2)	16.5 [118]

α and R_{c} but still wants to perform simulations using the Wolf method. Simulations using the Wolf method are found to be at least twice as fast in terms of CPU time compared to the Ewald method.

3.4. Conclusions

In this chapter, we studied the applicability of the Wolf method for electrostatic interactions in Monte Carlo simulations. By performing simulations in the Gibbs Ensemble with the CFC method, we were able to obtain accurate densities, chemical potentials, critical points and vapor pressures at vapor-liquid equilibrium for different compounds and different Wolf parameter sets. We have shown that the damping parameter α in the liquid phase should be chosen larger than α in the vapor phase, corresponding to a more effective screening of charges in the liquid phase. The cutoff radius R_{c} can be chosen smaller in the liquid phase than R_{c} in the gas phase, because of the higher value of α in the liquid. Moreover, we demonstrated that a simple estimation of the Wolf parameters can already produce accurate results for the vapor-liquid equilibrium.

4

Chemical Reaction Equilibria in the Reaction Ensemble

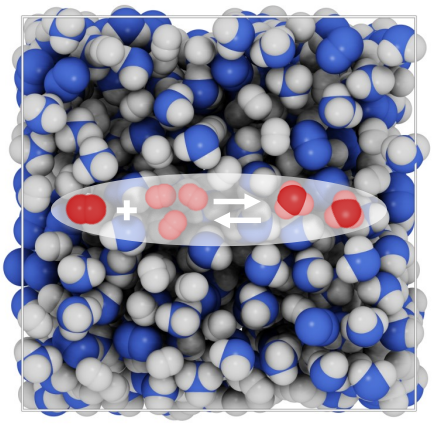

Schematic illustration of the Haber-Bosch process in the Reaction Ensemble. Fractional molecules of N_2, H_2 and NH_3 are used to facilitate the reaction and obtain the reaction equilibrium.

This chapter is based on the paper:

A. Poursaeidesfahani, R. Hens, A. Rahbari, M. Ramdin, D. Dubbeldam, and T. J. H. Vlugt, *Efficient Application of Continuous Fractional Component Monte Carlo in the Reaction Ensemble*, Journal of Chemical Theory and Computation, **13**, 4452-4466 (2017) [26].

4.1. Introduction

Substantial efforts have been made by scientists and engineers to study chemical reactions in non-ideal environments [10, 119, 120]. An optimal design and operation of many chemical processes relies on accurate information regarding reaction equilibria [62]. Reaction equilibria vary as the operating conditions of a reactor change. As a result, an approach is required which can provide information regarding chemical equilibria for a wide range of operating conditions. In an ideal gas, chemical equilibria are determined by the difference between the standard Gibbs free energies of formation of reactants and products [61]. Due to interactions of the reacting molecules with surrounding molecules, the chemical equilibrium may significantly differ from the ideal gas situation as the medium formed by the surrounding molecules may stabilize reactant and product molecules differently [62]. It is not always possible to measure reaction equilibria experimentally. The main reasons for this are: (1) extreme conditions may not be accessible experimentally; (2) kinetic limitation may prohibit reaching chemical equilibrium on accessible timescales; (3) large-scale experimental screening of solvents for chemical reactions may not be feasible. Therefore, there is a demand for theoretical methods that can accurately predict reaction equilibria. Molecular simulation is a natural tool for this as interactions between atoms and molecules are explicitly taken into account. One can perform Molecular Dynamics with a force field that can handle chemical reactions, e.g. DFT-based [121], Car-Parrinello [122, 123], or ReaxFf based Molecular Dynamics [124, 125]. The main disadvantage of these approaches is that reactions may not occur within the limited timescale of Molecular Dynamics simulations. Therefore, advanced simulation techniques such as metadynamics [126–128] or transition path sampling [129–137] may be required. These types of simulation techniques are not considered further in this chapter.

One of the most commonly used approaches in molecular simulation is to simulate the reaction equilibria in the Reaction Ensemble [10, 21, 22, 62, 63, 138–140]. In this approach, the chemical reaction is carried out by Monte Carlo trial moves. Beside thermalization, trial moves are carried out in which reactants are removed and products are inserted in the system, in such a way that an equilibrium distribution of reactants and products is obtained. The mechanism and the transition state of the reaction are not considered as this approach is purely thermodynamic and reaction kinetics are not taken into account. As a result, the efficiency of this simulation technique is not affected by the height of the activation energy barrier of the reaction. The Reaction Ensemble requires the partition functions of isolated molecules of all reactant and product molecules, a list of all possible chemical reactions in the system, and an appropriate force field describing interactions between molecules [62]. The partition functions of the isolated molecule can be obtained from Quantum Mechanics [61, 63, 141] or standard thermochemical tables such as the JANAF tables [142]. Computing partition functions of isolated molecules using quantum packages is well-established [141]. However, due to lack of experimental data, it is not always straightforward to obtain partition functions from QM software, especially for large molecules or ions [143, 144]. A detailed review of Monte Carlo simulations in the Reaction Ensemble can be found in Ref. [62].

Just as other ensembles that rely on sufficient molecule insertions and removals (e.g. the Gibbs Ensemble and Grand-Canonical Ensemble) [15], simulations in the Reaction Ensemble struggle when insertions and removals of molecules are difficult (systems at low temperatures and high densities). During the past few years, significant progress has been made in Monte Carlo techniques for the insertion and deletion of molecules. There are two types of solutions to overcome low acceptance probabilities for molecule insertions and removals in the Reaction Ensemble: methods such as Configurational-Bias Monte Carlo or related methods [63, 140, 145–152] that try to insert molecules in a single Monte Carlo trial move, and methods based on the idea of expanded ensembles [153–155] such as the Continuous Fractional Component method first developed by Shi and Maginn [57, 58]. The main advantage of the latter approach is that instead of inserting molecules in a single trial move, molecules are inserted gradually, so that the surroundings can easily adapt to the inserted/deleted molecules. This is particularly important at high densities [66]. Therefore, the CFC method does not rely on the spontaneous occurrence of cavities in the system that are large enough to accommodate a large molecule. The CFC method is frequently used for simulations that suffer from low acceptance probability of molecule insertions and removals [10, 64, 66, 72, 156–163]. Applications of this approach include: computation of the loading and enthalpy of adsorption of guest molecules in porous materials near the saturation loading [66, 150], reaction equilibria of complex systems [10], and solubilities of small molecules in ionic liquids [57, 58, 156–158, 164–166]. More details on the challenges of Monte Carlo simulations in open ensembles can be found in Refs. [70, 71, 167].

As mentioned in Sec. 2.3, the combination of the CFC method with the Reaction Ensemble was first proposed by Rosch and Maginn [64] (from now on referred to as *parallel* CFC). Balaji et al. used the parallel CFC method to compute the equilibrium concentrations of the different species in CO_2/monoethanolamine solutions for different CO_2 loadings [10]. In this method, fractional molecules of products are gradually changed into whole product molecules, while the fractional molecules of reactants are gradually removed, and vice versa. A key ingredient of parallel CFC is that the fractional molecules of both reactants and products are always present in the system (Sec. 2.3.1). This version of the Reaction Ensemble improves the acceptance probability of molecule insertions and removals significantly compared to the conventional algorithm [64]. However, it does not allow for direct calculation of chemical potentials and it is not possible to directly check if the reaction reached an equilibrium. Additional free energy calculations are needed to compute the chemical potentials of reactants and products. The fractional molecules of reactants and products have to adapt to their surroundings simultaneously, which reduces the efficiency of the algorithm.

Inspired by this, we introduce a new formulation for the CFC method in the Reaction Ensemble (denoted by *serial* CFC) [26]. The crucial difference with parallel CFC is that either fractional molecules of reactants or products are present in the system (Sec. 2.3.3). The chemical potentials of reactants/products are directly obtained without using Widom's test particle insertion method (or similar). Therefore, one can directly check for the condition of chemical equilibrium. This new formula-

tion, as well as the conventional and parallel CFC method, have been described in Sec. 2.3.

This chapter is organized as follows. In Sec. 4.2 the simulation details and the systems under study are described. In Sec. 4.3, the performance of the serial CFC method is compared to conventional Reaction Ensemble and parallel CFC for Lennard-Jones particles. The applicability of the serial CFC method is also demonstrated for the ammonia synthesis reaction at various temperatures and pressures. Compared to the parallel CFC method, the serial CFC method is more efficient, computationally cheaper and allows for the computation of chemical potentials of all components without any additional calculations or simulations. The main findings are summarized in Sec. 4.4.

4.2. Simulation Details

As a proof of principle for the serial CFC method, simulations are performed for different systems of Lennard-Jones particles. Furthermore, the ammonia synthesis reaction is considered at various pressures (100 bar to 1000 bar) and temperatures (573 K to 873 K) as a practically important application.

For different systems of Lennard-Jones particles, simulations are performed at constant pressure and temperature using the conventional Reaction Ensemble, the parallel CFC method [64], and the serial CFC method. For these simulations, all properties are defined in reduced units. The interactions are truncated and shifted at 2.5σ. The temperature is set to $T = 2$ (reduced units), and simulations always start with 400 particles of type A. The maximum molecule displacements and maximum volume changes are set to achieve 50% acceptance for these trial moves. In each Monte Carlo step, a trial move is selected at random with the following probabilities: 49.5% translation, 1% volume changes, and 49.5% reaction trial moves.

For the ammonia synthesis reaction, simulations are performed at constant pressure and temperature using the serial CFC method. All simulations start with a random configuration of 120 N_2 molecules, 360 H_2 molecules, and 0 NH_3 molecules. Fractional molecules are added to this system. All molecules are treated as rigid and interactions are described by a combination of Lennard-Jones and electrostatic interactions. Force field parameters for N_2, H_2, and NH_3 are taken from literature [89, 168, 169] and are listed in Tables A.3 and A.4 of the Appendix. The Wolf method is used to compute electrostatic interactions [68]. The partition functions of the isolated molecule for this system are listed in Table 4.1. In each Monte Carlo step, a trial move is selected at random with the following probabilities: 33% translations, 33% rotations, 1% volume changes, and 33% reaction trial moves. For the ammonia synthesis reaction, the switching point for interactions, λ_s (see Sec. 2.5.6), is set to 0.9.

For all simulations using the parallel or serial CFC method, the weight function (Sec. 2.5.3) is determined using the Wang-Landau algorithm [74]. For the serial CFC method, the weight function $W(\lambda, \delta)$ is determined such that the observed two-dimensional probability distribution $p(\lambda, \delta)$ is flat where δ indicates whether the fractional molecule(s) is/are reactants of products. 200 bins are used to store the probability distribution of λ for reactants and products. All simulations are started

Table 4.1: Partition functions of isolated molecules (excluding the translational part) divided by the thermal wavelength, q/Λ^3, at different temperatures taken from Ref. [61]. Reported values of q/Λ^3 are in Å^{-3}.

T/[K]	N_2	H_2	NH_3
573	$2.60 \cdot 10^{90}$	$6.46 \cdot 10^{40}$	$1.50 \cdot 10^{110}$
673	$6.89 \cdot 10^{77}$	$1.28 \cdot 10^{35}$	$5.42 \cdot 10^{94}$
773	$3.44 \cdot 10^{68}$	$8.28 \cdot 10^{30}$	$2.12 \cdot 10^{83}$
873	$2.42 \cdot 10^{61}$	$5.08 \cdot 10^{27}$	$3.65 \cdot 10^{74}$

with $2 \cdot 10^5$ Monte Carlo cycles to equilibrate the system, followed by $1 \cdot 10^6$ cycles for production (obtaining averages). The number of Monte Carlo steps per cycle equals the total number of molecules initially in the system. As described in Sec. 2.3, in the conventional Reaction Ensemble and the Reaction Ensemble combined with the parallel CFC method, there is only one type of reaction trial move. In contrast, the serial CFC method requires three types of trial moves for facilitating molecule transfers of which 50% will be changes in λ, and 50% for the hybrid reaction trial moves (Sec. 2.5.2). With the serial CFC method, the chemical potentials are computed from Eq. 2.15. The contribution of fractional molecules are excluded in the computation of ensemble averages such as the density [65].
Comparison of the efficiency of the three methods, requires a fair definition pf the efficiency. Here, the efficiency for all three methods is defined as the number of accepted trial moves (either forward or backward reaction) resulting in a change in the number of whole molecules due to the reaction, divided by the total number of reaction trial moves. For the parallel CFC method, this means: the number of accepted λ trial moves that result in $\lambda > 1$ or $\lambda < 0$, divided by the total number of λ trial moves (Sec. 2.3.2). For the serial CFC method, this means: the number of accepted reaction trial moves for whole molecules divided by the total number of all reaction trial moves, including changing the value of λ, reaction for fractional molecules, and reaction for whole molecules (Sec. 2.3.4). It should be noted that reaction trial moves for the serial CFC method are computationally cheaper than for the parallel CFC method. This is due to the reduction in the number of fractional molecules and therefore a reduction in the number of interacting molecules. Simulations performed using the serial CFC method require less CPU time compared to similar simulations when the parallel CFC method is used. The CPU time depends on the programming of the algorithms, the compiler, and CPUs performing the calculations. Here, different approaches are compared only in terms of efficiency and not CPU time. This can be considered as the worst-case scenario for the serial CFC method.

4.3. Results

To insure correct implementation of the serial CFC method, the equilibrium composition is computed and compared for the three methods for different reactions in

Table 4.2: Interaction parameters (Lennard-Jones) and dimensionless partition functions (q/Λ^3) for different particle types. Note that there are several particle types with exactly the same interaction parameters. This was done to show the effect of (in)distinguishability of the particles in the reactions.

Particle type	σ	ϵ	q/Λ^3
A	1.0	1.0	0.002
B	1.0	1.0	0.002
C	1.1	0.9	0.002
D	1.0	1.0	0.02
E	1.1	0.9	0.02
F	1.0	1.0	0.02

a system of Lennard-Jones particles. The Lennard-Jones parameters and partition functions for the particles used in this study are listed in Table 4.2. The equilibrium composition obtained with different methods at reduced pressures $P = 0.3$, $P = 1.0$, $P = 3.0$ and, $P = 5.0$ are shown in Tables 4.3, 4.4, 4.5 and 4.6, respectively. Equilibrium compositions obtained for the three methods are the same for all reactions and conditions. This confirms the validity of the expressions used for the partition function and acceptance rules for the serial CFC method, and indicates that this method is implemented correctly.

The efficiencies of the three methods for different reactions are also shown in Tables 4.3, 4.4, 4.5 and 4.6. The conventional method has a very high efficiency for all reactions at the lowest pressure ($P = 0.3$). Since in this case, the density of the system is very low and therefore interactions between the particles are small, there is almost no energy penalty for the reaction trial moves and most of the attempts to perform reaction trial moves for whole particles are accepted. Therefore, the method which attempts to directly replace the reactants with reaction products and vice versa has a high efficiency. For the conventional method [21, 22], reaction trial moves for the whole particles is the only reaction trial move and this trial move has a high acceptance probability for the low pressure case. As a result, this method has high efficiencies for this case. In the parallel CFC method, many trial moves are spent diffusing through the entire λ-space and less attempts are made to perform a reaction. Therefore, this method has the lowest efficiency for the low pressure case. Already at $P = 1.0$, the efficiency of the conventional method is much lower than its efficiency at $P = 0.3$. At higher pressures ($P = 3.0$ and $P = 5.0$), the efficiency of the conventional method drops below 0.01 even for the simplest reaction (A $\rightleftharpoons$ B). When the density is high, most of the reaction trial moves in the conventional method result in an overlap between the newly inserted particles and particles that are already in the system. Therefore, this move has very low acceptance probability. In this case, the efficiency of the parallel CFC method varies between 0.06 to 0.1 while the efficiency of the serial CFC method varies between 0.1 to 0.2 depending on the reaction. Due to the efficient use of the three trial moves in the serial CFC method, it has a better performance compared to the

Table 4.3: Average number of particles and densities at equilibrium for different reactions for different methods. The efficiency is defined in Sec. 4.2. The pressure and temperature are set to $P = 0.3$ and $T = 2$, respectively (reduced units). Simulations are started with 400 particles of type A. The interaction parameters of the different particles are listed in Table 4.2. The numbers between brackets denote the uncertainty in the last digit.

Reaction	$\langle N_{\mathrm{A}} \rangle$	$\langle N_{\mathrm{Product1}} \rangle$	$\langle N_{\mathrm{Product2}} \rangle$	$\langle \rho_{\mathrm{tot}} \rangle$	Efficiency	Method
A ⇌ B	200.00(3)	200.00(3)		0.162(0)	0.40	Conventional
	199.99(7)	200.01(7)		0.161(0)	0.11	Parallel CFC
	199.98(6)	200.02(6)		0.161(0)	0.30	Serial CFC
A ⇌ C	206.62(2)	193.38(2)		0.155(0)	0.37	Conventional
	206.63(3)	193.37(2)		0.154(0)	0.098	Parallel CFC
	206.62(5)	193.38(5)		0.155(0)	0.30	Serial CFC
A ⇌ 2D	192.59(6)	414.8(2)		0.162(0)	0.26	Conventional
	192.27(6)	415.5(2)		0.161(0)	0.097	Parallel CFC
	192.36(4)	415.27(8)		0.161(0)	0.25	Serial CFC
A ⇌ 2E	202.75(5)	394.5(1)		0.153(0)	0.21	Conventional
	202.35(6)	395.3(2)		0.152(0)	0.086	Parallel CFC
	202.47(4)	395.06(8)		0.152(0)	0.25	Serial CFC
A ⇌ D + F	91.52(3)	308.48(3)	308.48(3)	0.162(0)	0.26	Conventional
	91.22(9)	308.78(9)	308.78(9)	0.161(0)	0.097	Parallel CFC
	91.33(3)	308.67(3)	308.67(3)	0.161(0)	0.25	Serial CFC
A ⇌ D + E	95.57(3)	304.43(3)	304.43(3)	0.156(0)	0.23	Conventional
	95.28(4)	304.72(4)	304.72(4)	0.155(0)	0.094	Parallel CFC
	95.39(2)	304.61(2)	304.61(2)	0.155(0)	0.25	Serial CFC

Table 4.4: Average number of particles and densities at equilibrium for different reactions for different methods. The efficiency is defined in Sec. 4.2. The pressure and temperature are set to $P = 1.0$ and $T = 2$, respectively (reduced units). Simulations are started with 400 particles of type A. The interaction parameters of the different particles are listed in Table 4.2. The numbers between brackets denote the uncertainty in the last digit.

Reaction	$\langle N_{\mathrm{A}} \rangle$	$\langle N_{\mathrm{Product1}} \rangle$	$\langle N_{\mathrm{Product2}} \rangle$	$\langle \rho_{\mathrm{tot}} \rangle$	Efficiency	Method
	200.00(4)	200.00(4)		0.433(0)	0.077	Conventional
A ⇌ B	200.0(2)	200.0(2)		0.431(0)	0.095	Parallel CFC
	200.01(8)	199.99(8)		0.432(0)	0.26	Serial CFC
	226.48(4)	173.52(4)		0.392(0)	0.068	Conventional
A ⇌ C	226.4(2)	173.6(2)		0.390(0)	0.079	Parallel CFC
	226.45(9)	173.55(9)		0.391(0)	0.26	Serial CFC
	273.05(5)	253.89(9)		0.433(0)	0.017	Conventional
A ⇌ 2D	272.8(2)	254.5(4)		0.430(0)	0.074	Parallel CFC
	272.8(2)	254.3(3)		0.431(0)	0.17	Serial CFC
	300.57(6)	198.9(2)		0.395(0)	0.011	Conventional
A ⇌ 2E	300.3(1)	199.4(2)		0.393(0)	0.059	Parallel CFC
	300.4(2)	199.3(3)		0.394(0)	0.17	Serial CFC
	177.73(5)	222.27(5)	222.27(5)	0.433(0)	0.017	Conventional
A ⇌ D + F	177.4(3)	222.6(3)	222.6(3)	0.431(0)	0.075	Parallel CFC
	177.5(2)	222.5(2)	222.5(2)	0.431(0)	0.17	Serial CFC
	197.92(7)	202.08(7)	202.08(7)	0.401(0)	0.014	Conventional
A ⇌ D + E	197.6(3)	202.4(3)	202.4(3)	0.399(0)	0.070	Parallel CFC
	197.6(2)	202.4(2)	202.4(2)	0.399(0)	0.17	Serial CFC

Table 4.5: Average number of particles and densities at equilibrium for different reactions for different methods. The efficiency is defined in Sec. 4.2. The pressure and temperature are set to $P = 3.0$ and $T = 2$, respectively (reduced units). Simulations are started with 400 particles of type A. The interaction parameters of the different particles are listed in Table 4.2. The numbers between brackets denote the uncertainty in the last digit.

Reaction	$\langle N_{\mathrm{A}} \rangle$	$\langle N_{\mathrm{Product1}} \rangle$	$\langle N_{\mathrm{Product2}} \rangle$	$\langle \rho_{\mathrm{tot}} \rangle$	Efficiency	Method
	200.1(2)	199.9(2)		0.667(0)	$7 \cdot 10^{-3}$	Conventional
A ⇌ B	199.9(4)	200.1(4)		0.665(0)	0.096	Parallel CFC
	199.9(2)	200.1(2)		0.667(0)	0.20	Serial CFC
	268.7(2)	131.3(2)		0.614(0)	$5 \cdot 10^{-3}$	Conventional
A ⇌ C	268.8(2)	131.2(2)		0.612(0)	0.076	Parallel CFC
	268.7(2)	131.3(2)		0.614(0)	0.20	Serial CFC
	345.2(2)	109.5(4)		0.667(0)	$3 \cdot 10^{-4}$	Conventional
A ⇌ 2D	345.0(3)	110.0(5)		0.665(0)	0.066	Parallel CFC
	344.8(4)	110.5(8)		0.666(0)	0.11	Serial CFC
	373.0(2)	54.0(3)		0.646(0)	$1 \cdot 10^{-4}$	Conventional
A ⇌ 2E	372.9(2)	54.1(3)		0.643(0)	0.051	Parallel CFC
	372.9(2)	54.3(4)		0.645(0)	0.11	Serial CFC
	293.5(3)	106.5(3)	106.5(3)	0.667(0)	$3 \cdot 10^{-4}$	Conventional
A ⇌ D + F	293.1(6)	106.9(6)	106.9(6)	0.665(0)	0.068	Parallel CFC
	293.3(5)	106.7(5)	106.7(5)	0.666(0)	0.11	Serial CFC
	324.2(2)	75.8(2)	75.8(2)	0.641(0)	$2 \cdot 10^{-4}$	Conventional
A ⇌ D + E	324.2(5)	75.8(5)	75.8(5)	0.638(0)	0.064	Parallel CFC
	324.1(4)	75.9(1)	75.9(1)	0.639(0)	0.11	Serial CFC

Table 4.6: Average number of particles and densities at equilibrium for different reactions for different methods. The efficiency is defined in Sec. 4.2. The pressure and temperature are set to $P = 5.0$ and $T = 2$, respectively (reduced units). Simulations are started with 400 particles of type A. The interaction parameters of the different particles are listed in Table 4.2. The numbers between brackets denote the uncertainty in the last digit.

Reaction	$\langle N_{\mathrm{A}} \rangle$	$\langle N_{\mathrm{Product1}} \rangle$	$\langle N_{\mathrm{Product2}} \rangle$	$\langle \rho_{\mathrm{tot}} \rangle$	Efficiency	Method
	199.8(3)	200.2(3)		0.766(0)	$1 \cdot 10^{-3}$	Conventional
A ⇌ B	199(1)	201(1)		0.764(0)	0.096	Parallel CFC
	200.1(4)	199.9(4)		0.766(0)	0.20	Serial CFC
	298.5(5)	101.5(5)		0.718(0)	$9 \cdot 10^{-4}$	Conventional
A ⇌ C	298.5(8)	101.5(8)		0.716(0)	0.079	Parallel CFC
	298.6(4)	101.4(4)		0.718(0)	0.20	Serial CFC
	372.5(3)	54.9(6)		0.766(0)	$3 \cdot 10^{-5}$	Conventional
A ⇌ 2D	372.1(4)	55.8(7)		0.764(0)	0.063	Parallel CFC
	372.4(2)	55.2(4)		0.765(0)	0.11	Serial CFC
	390.6(3)	18.8(5)		0.757(1)	$6 \cdot 10^{-6}$	Conventional
A ⇌ 2E	390.6(2)	18.9(3)		0.755(0)	0.048	Parallel CFC
	390.5(2)	19.0(4)		0.756(0)	0.11	Serial CFC
	345.2(5)	54.8(5)	54.8(2)	0.766(0)	$3 \cdot 10^{-5}$	Conventional
A ⇌ D + F	345.4(6)	54.6(6)	54.6(6)	0.764(0)	0.067	Parallel CFC
	345.3(6)	54.7(6)	54.7(6)	0.765(0)	0.12	Serial CFC
	368.1(6)	31.9(6)	31.9(6)	0.752(0)	$1 \cdot 10^{-5}$	Conventional
A ⇌ D + E	368.2(4)	31.8(4)	31.8(4)	0.749(1)	0.063	Parallel CFC
	368.1(5)	31.9(5)	31.9(5)	0.751(0)	0.11	Serial CFC

conventional method and parallel CFC method.

In Table 4.7, the sum of the total and excess chemical potentials times the stoichiometric coefficients are shown for the reactants and products for different pressures and reactions. These values can only be directly computed using the serial CFC method from Eq. 2.15. The data provided in Table 4.7 shows that for the reaction A ⇌ B where the reactant and products have identical interactions, the values obtained for the chemical potentials of the reactants and products are equal. Since particles of type A and B are identical (Table 4.2), this is exactly what is expected. This case is included because it is trivial and can serve as an additional check on the implementation and convergence of the simulation. It is verified that the computed excess chemical potentials are identical to those obtained from Widom's test particle insertion method in the conventional *NPT* ensemble at the same conditions (data not shown here) [15].

Reaction equilibrium implies equal chemical potentials of both reactants and products:

$$\sum_{i=1}^{R} \mu_i \nu_i = \sum_{j=R+1}^{S} \mu_j \nu_j \tag{4.1}$$

where R is the number of reactants and S the total number of components. It can be clearly seen that this condition is satisfied for all reactions at all pressures within the error bars. This indicates that simulations have reached the condition of chemical equilibrium. Moreover, one can directly compute the excess chemical potential of individual components according to Eq. 2.19.

To test the suitability of the serial CFC method in the Reaction Ensemble, simulations are performed of a practical system: the ammonia synthesis reaction (N_2+3H_2⇌2NH_3). Equilibrium compositions obtained with the serial CFC method are validated with the RASPA software [70, 71]. In Fig. 4.1, the mole fractions of ammonia at equilibrium obtained from simulations using the serial CFC method at different temperatures and pressures are compared with experimental results [170] and results using equation of state modeling (Peng-Robinson equation of state [87], for details we refer to the Supporting Information of Ref. [26]). Excellent agreement is observed between the equilibrium compositions obtained using the three different approaches. This validates the applicability of serial CFC method in the Reaction Ensemble for systems including molecules with electrostatic interactions. In Fig. 4.2, fugacity coefficients of ammonia at equilibrium obtained using the serial CFC method are compared with the results using equation of state modeling (using the Peng-Robinson equation of state) at different temperatures and pressures. It is well-known that cubic equations of state fail to provide accurate estimates for the fugacity coefficient at very high pressures [3].

Table 4.7: Chemical potentials of reactants and products for different reactions in a system of Lennard-Jones particles at different pressures obtained with the serial CFC method in the Reaction Ensemble. The temperature is set to $T = 2$ (reduced units). The interaction parameters of different particles are listed in Table 4.2. The numbers between brackets denote the uncertainty in the last digit.

Reaction	P	$\sum_{\text{reactants}} \nu_i \mu_i^{\text{excess}}$	$\sum_{\text{reactants}} \nu_i \mu_i^{\text{tot}}$	$\sum_{\text{products}} \nu_i \mu_i^{\text{excess}}$	$\sum_{\text{products}} \nu_i \mu_i^{\text{tot}}$
A ⇌ B	0.3	-0.344(9)	7.036(9)	-0.344(6)	7.036(6)
	1.0	0.07(1)	9.42(1)	0.066(6)	9.421(6)
	3.0	2.73(1)	12.95(1)	2.727(6)	12.953(6)
	5.0	5.23(1)	15.74(1)	5.23(2)	15.73(1)
A ⇌ C	0.3	-0.265(8)	7.101(8)	-0.133(6)	7.101(6)
	1.0	0.25(1)	9.66(1)	0.79(1)	9.67(1)
	3.0	2.887(6)	13.541(6)	4.32(1)	13.53(1)
	5.0	5.35(2)	16.53(2)	7.51(2)	16.52(2)
A ⇌ 2D	0.3	-0.34(1)	6.13(1)	-0.68(1)	6.12(1)
	1.0	0.07(1)	9.49(1)	0.13(1)	9.48(1)
	3.0	2.73(1)	13.79(1)	5.43(4)	13.74(2)
	5.0	5.23(2)	16.84(2)	10.45(3)	16.74(2)
A ⇌ 2E	0.3	-0.240(9)	6.253(8)	-0.205(9)	6.245(9)
	1.0	0.247(8)	9.791(7)	1.553(9)	9.772(9)
	3.0	2.81(1)	14.08(1)	8.45(3)	13.98(1)
	5.0	5.25(3)	17.02(3)	14.78(8)	16.67(6)
A ⇌ D + F	0.3	-0.340(8)	4.319(8)	-0.68(1)	4.32(1)
	1.0	0.07(1)	8.30(2)	0.13(1)	8.29(1)
	3.0	2.724(9)	13.246(6)	5.44(2)	13.213(8)
	5.0	5.23(1)	16.57(1)	10.45(4)	16.52(2)
A ⇌ D + E	0.3	-0.270(7)	4.418(7)	-0.41(1)	4.43(1)
	1.0	0.220(9)	8.578(9)	0.96(1)	8.57(1)
	3.0	2.809(9)	13.573(9)	7.04(2)	13.528(6)
	5.0	5.27(2)	16.80(2)	12.69(6)	16.69(3)

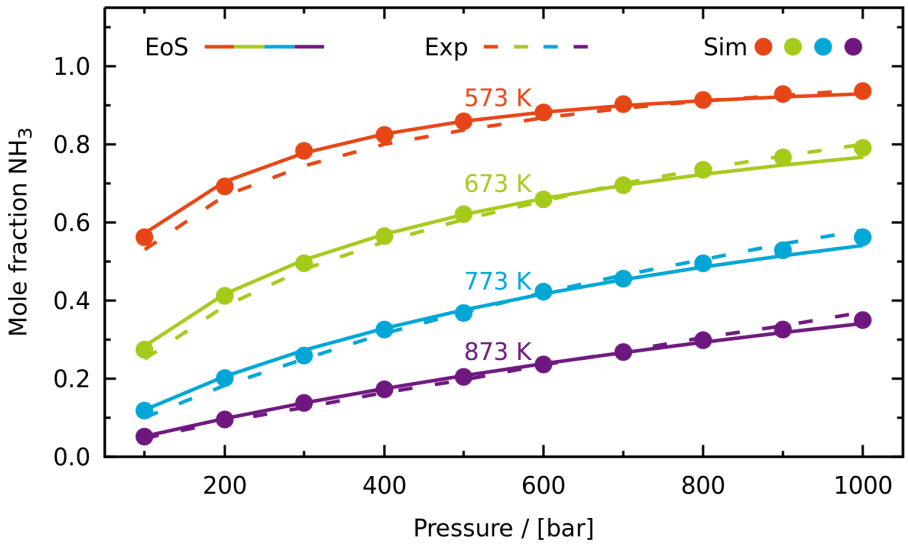

Figure 4.1: Mole fractions of ammonia at equilibrium obtained with the serial CFC method in the Reaction Ensemble as a function of pressure for different temperatures. Comparison of the Peng-Robinson Equation of State [87], experimental work [170], and simulations using the serial CFC method. The simulations were started from a random configuration of 120 N_2 molecules, 360 H_2 molecules, and 0 NH_3 molecules.

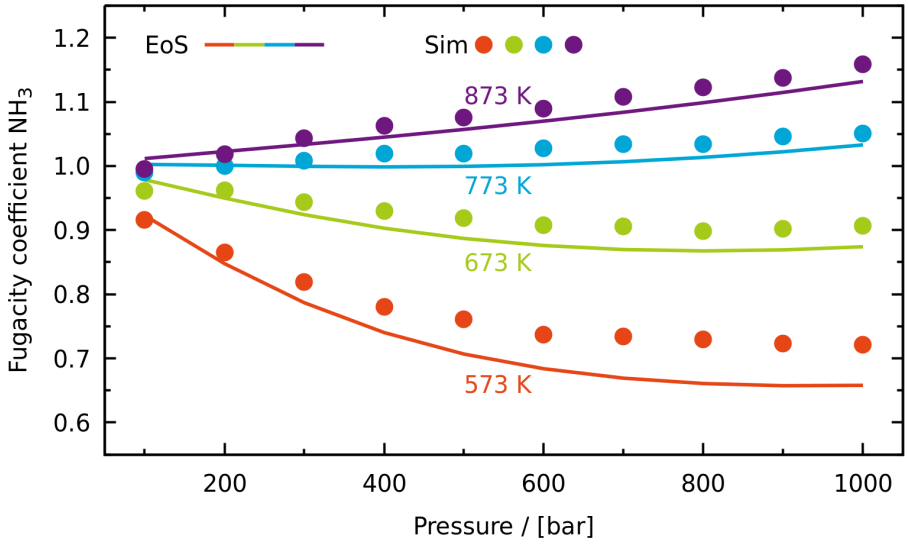

Figure 4.2: Fugacity coefficients of ammonia at equilibrium obtained with the serial CFC method in the Reaction Ensemble as a function of pressure for different temperatures. Comparison of the Peng-Robinson Equation of State [87] and simulations using the serial CFC method. The simulations were started from a random configuration of 120 N_2 molecules, 360 H_2 molecules, and 0 NH_3 molecules.

4.4. Conclusions

In this chapter, we compared the serial CFC method with the parallel CFC method and conventional method for the Reaction Ensemble. Systems of Lennard-Jones particles were studied at different pressures. Furthermore, equilibrium compositions obtained for the ammonia synthesis reaction using the serial CFC method are compared with experimental results and compositions obtained from equation of state modeling. The equilibrium compositions obtained with the serial CFC method are in excellent agreement with those obtained from the conventional method and parallel CFC method in the Reaction Ensemble. For the ammonia synthesis reaction, excellent agreement between the results obtained from the simulations and experimental results was found for the equilibrium compositions. For systems at high pressures, the acceptance probability of the reaction trial move is improved by factor 2 to 3 (depending on the system under study) compared to the parallel CFC method. The serial CFC method has the following advantages: (1) one directly obtains chemical potentials of all reactants and products. These chemical potentials can directly be used as an independent check to ensure that chemical equilibrium is achieved; (2) independent biasing is applied to the fractional molecules of reactants and products, therefore, the efficiency of the algorithm is increased; (3) changes in the maximum scaling parameter of intermolecular interactions can be chosen differently for reactants and products. The serial CFC method can be easily extended to molecules with intramolecular degrees of freedom. The trial moves can be performed by inserting fractional molecules at random positions with random orientations. The internal configuration of the molecule can be generated randomly or using the Rosenbluth scheme [15]. For ergodic sampling, trial moves that attempt to change the internal configuration of flexible molecules should be added to the method [15]. The serial CFC method could also be used for reactions involving ions. One can calculate the potential energy of a periodic system with a net charge by placing a dummy charge at the center of charges. Although it is difficult to interpret computed partial molar properties of ions (such as the chemical potential or the partial molar volume) [43], by using the serial CFC method one can still benefit from other advantages of the method such as efficient reaction trial moves.

5

Partial Molar Properties in the *NPT* Ensemble

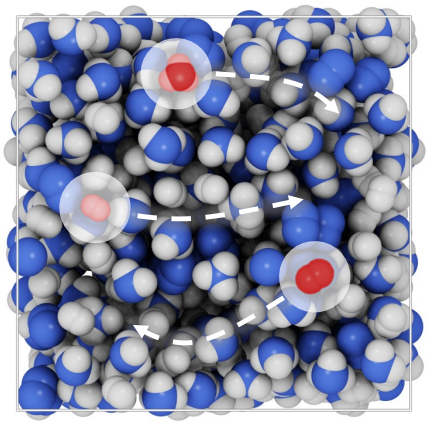

Schematic illustration of a mixture of N_2, H_2 and NH_3 in the *NPT* ensemble. Fractional molecules are used as 'probes' to compute the partial molar properties of the different compounds.

This chapter is based on the paper:

A. Rahbari, R. Hens, I. K. Nikolaidis, A. Poursaeidesfahani, M. Ramdin, I. G. Economou, O. A. Moultos, D. Dubbeldam, and T. J. H. Vlugt, *Computation of Partial Molar Properties using Continuous Fractional Component Monte Carlo*, Molecular Physics, **116**, 3331-3344 (2018) [28].

5.1. Introduction

In this chapter, we combine the original idea of Frenkel et al. [30, 31], and the Continuous Fractional Component (CFC) method to compute partial molar properties by gradual insertion and removal of molecules as described in Chapter 2. This method avoids the drawbacks of the Widom Test Particle Insertion (WTPI) method at high densities. As a test case, partial molar properties in the *NPT* ensemble and the expanded CFC*NPT* ensemble are computed for a 50%-50% binary color mixture of Lennard-Jones particles. Since the WTPI method works efficiently for this mixture, the results are used to verify the CFC method. Next, we apply the CFC method to simulations for an industrial relevant case: the Haber-Bosch process for ammonia production [171]. The reason to select this system as a realistic case study is that ammonia is a useful chemical commodity and has received lots of attention both in academia and industry [169, 170, 172–176]. It is also a promising alternative medium for energy storage and transportation [177–180]. Industrial ammonia synthesis is carried out using the Haber-Bosch process with heterogeneous iron or ruthenium catalysts at high temperatures (623 K to 873 K) and pressures between 20 MPa and 40 MPa [181–183]. In industrial applications, the ammonia synthesis and many other gas phase reactions are mostly modeled with cubic Equations of State (EoS) because of their simplicity [184–186]. Ammonia is a molecule that forms hydrogen bonds, but this phenomenon cannot be modeled using a standard cubic EoS [187]. Moreover, limitations of using a cubic EoS in studying thermodynamic properties of mixtures at high pressures are well-known [3, 188, 189]. Therefore, due to the hydrogen bonding of ammonia, and the elevated pressures at which the ammonia synthesis reaction takes place, it is of interest to study the pressure dependency of partial molar properties of the mixture using physically based models i.e. molecular simulation and PC-SAFT [190–192]), and compare the results to those obtained from a cubic EoS. In this work, partial molar properties for mixtures of N_2, H_2 and NH_3 at reaction equilibrium, based on the Haber-Bosch reaction [171, 172], are computed at $T = 573$ K and pressures ranging from 10 MPa to 80 MPa [62, 169, 173, 193]. This chapter is organized as follows. The simulation details and an overview of the systems considered are summarized in Sec. 5.2. The results of the simulations are presented in Sec. 5.3. It is shown that the computed partial molar properties for a binary Lennard-Jones color mixture obtained using the different methods are identical. Partial molar properties for mixtures of N_2, H_2 and NH_3 at reaction equilibrium are computed as a function of pressure. Based on these results, the reaction enthalpy of the Haber-Bosch process is computed using Monte Carlo simulations. It is shown that the results obtained from the simulations are in good agreement with results from the PC-SAFT EoS [190–192]. The results obtained from the Peng-Robinson EoS [87] deviate from those obtained from the simulations and PC-SAFT EoS at high pressures. This leads to a relative difference of up to 8% in calculated reaction enthalpies at 80 MPa. The conclusions of this chapter are summarized in Sec. 5.4.

5.2. Simulation Details

As a proof of principle of the CFC method in the *NPT* Ensemble (Sec. 2.2), Monte Carlo simulations were performed to compute the partial molar properties of a binary Lennard-Jones color mixture (composition: 50%-50%), both in the conventional *NPT* ensemble using the WTPI method and in the CFC*NPT* ensemble. The binary color mixture contained 200 Lennard-Jones particles. All simulations were carried out at a temperature of $T = 2$ and pressures ranging from $P = 0.1$ to $P = 9$, leading to average densities between $\langle\rho\rangle = 0.052$ and $\langle\rho\rangle = 0.880$. Note that the values are in reduced units i.e. σ and ϵ were set as units of length and energy, respectively. Interactions were truncated and shifted at 2.5σ. In the conventional *NPT* ensemble, $6{\cdot}10^6$ production cycles were carried out. Each cycle consists of N Monte Carlo steps (N being the total number of particles in the system). At each step, a trial move was selected with the following probabilities: 99% translations and 1% volume changes. For sampling the partial molar properties of each component, 10 trial insertions per cycle were performed.

In the CFC*NPT* ensemble simulations, $5{\cdot}10^7$ production cycles were carried out for the same binary mixture at the same temperature and pressures. Each trial move was selected with the following probabilities: 33% translations, 33% λ changes, 33% hybrid trial move (Sec. 2.2.1), and 1% volume changes. In the hybrid trial move, the switching points are: $\lambda_{\mathrm{h},0} = \lambda_{\mathrm{h},1} = 0.3$ (Sec. 2.5.2).

The equilibrium compositions of a mixture of N_2, H_2 and NH_3 at 573 K and pressures from 10 MPa to 80 MPa were obtained by performing Monte Carlo simulations in the Reaction Ensemble as described in Chapter 4. The obtained equilibrium compositions were in excellent agreement with experimental data [169, 170, 173]. All molecules are treated as rigid, and a combination of Lennard-Jones and electrostatic interactions is used to describe the interactions between molecules. The force field parameters and geometries of N_2, H_2 and NH_3 [89, 168, 169] can be found in Tables A.3 and A.4 of the Appendix. The Lennard-Jones interactions are truncated and analytic tail corrections are used [15]. The Wolf method (Sec. 2.5.5) was used for the calculation of the electrostatic interactions [27, 68, 194].The equilibrium compositions were used as a starting point for the simulations of the mixture of N_2, H_2 and NH_3 in the *NPT* and CFC*NPT* Ensembles. Simulation details corresponding to each method are summarized below.

CFC*NPT* ensemble

With this method, simulations were performed of a mixture of N_2, H_2 and NH_3 at 573 K and pressures between 10 and 80 MPa in the CFC*NPT* ensemble. To compute partial molar properties of each component, simulations were performed in which one fractional molecule of that component was added to the system. This was done for all pressures. A complete overview of all the starting compositions can be found in the Supporting Information of Ref. [28]. In each simulation, $2{\cdot}10^5$ equilibration cycles were performed to compute the weight function $W(\lambda)$ using the Wang-Landau algorithm [74, 195]. Each cycle consists of N Monte Carlo steps (N being the total number of molecules in the system). Starting with equilibrated configurations and weight functions, $3.2{\cdot}10^6$ production cycles were carried out.

Trial moves were selected with the following probabilities: 35% translations, 30% rotations, 17% λ-changes, and 17% hybrid trial moves (Sec. 2.2.1), and 1% volume changes. In the hybrid trial move, the switching points are: $\lambda_{\mathrm{h},0} = \lambda_{\mathrm{h},1} = 0.3$ (Sec. 2.5.2).

Numerical Differentiation

With this method, simulations in the *NPT* ensemble were performed of a mixture of N_2, H_2 and NH_3 to obtain the partial molar properties of each component at 573 K and pressures between 10 MPa and 80 MPa. At each pressure, simulations of the mixture were performed by changing the number of the molecules of component i with respect to that of the stoichiometric mixture (N_i) [28], while keeping the number of the other molecules in mixture constant [39]. Seven compositions were used with N_i, $N_i \pm 1$, $N_i \pm 3$ and $N_i \pm 5$ molecules around the equilibrium composition. Simulations in the *NPT* ensemble were performed for every composition and pressure to compute the total enthalpy (H) and the volume (V) of the mixture as a function of N_i. First order polynomials were fitted to H and V as a function of N_i. The slopes of these lines were calculated to obtain the partial molar excess enthalpy and the partial molar volume. Each simulation was carried out with $2{\cdot}10^5$ equilibration cycles and $5{\cdot}10^5$ production cycles. Each cycle consists of N Monte Carlo steps (N being the total number of molecules in the system). Trial moves were selected with the following probabilities: 49.5% translations, 49.5% rotations, and 1% volume changes.

5.3. Results

In Fig. 5.1 the acceptance probability for reinsertions and identity changes is shown as a function of λ for the system of Lennard-Jones particles at different densities ($\langle\rho\rangle = 0.052$, $\langle\rho\rangle = 0.433$, and $\langle\rho\rangle = 0.880$). The acceptance probability of reinsertions of fractional molecules goes to 100% when λ is close to 0. This is the case for all densities, which is caused by the weak interactions of the fractional molecule at low values of λ. For the system at the highest density ($\langle\rho\rangle = 0.880$) and $\lambda > 0.3$, reinsertions are mostly rejected. This is caused by overlaps between the reinserted fractional molecule and the whole molecules. In sharp contrast to reinsertions, identity changes are most likely to be accepted when λ is close to 1. This is expected as a fractional molecule behaves almost as a whole molecule when λ is close to 1. Therefore, the energy difference associated with an identity change is small. For the system with the highest density, identity changes are mostly rejected when $\lambda < 0.3$. A whole molecule within an equilibrated system already has favorable interactions with the surrounding molecules. For small values of λ, exchanging a whole molecule with the fractional molecule results in formation of a cavity which has an unfavorable energy. As a result, the energy difference associated with the attempted identity change is high for λ close to 0. It can be concluded that defining switching points (Sec. 2.5.2) will ensure a higher acceptance probability for the hybrid trial move. It is found that the same value for the switching points can be used in the simulations for the mixture of N_2, H_2 and NH_3. For the validation of

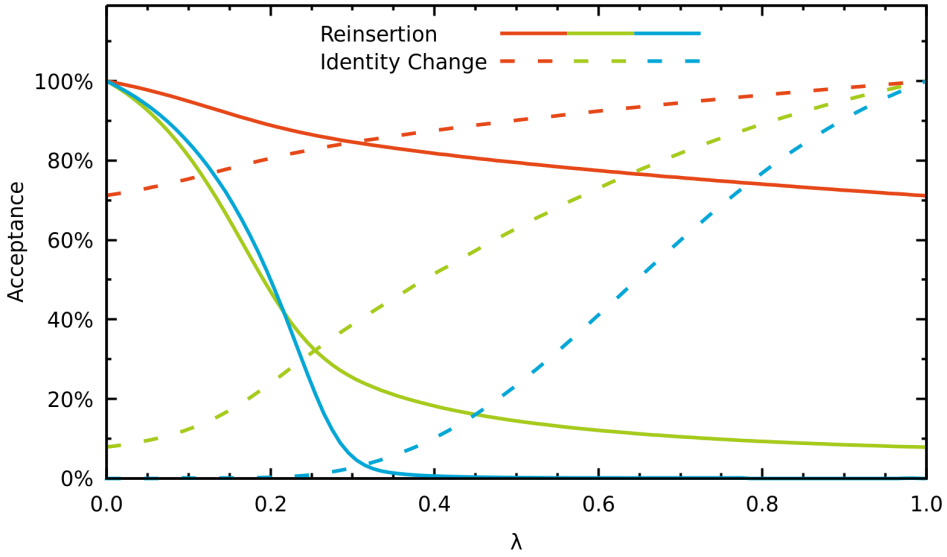

Figure 5.1: Acceptance probabilities for reinsertion and identity change of the fractional molecule in a binary Lennard-Jones color mixture (50%-50%) consisting of 200 molecules at $T = 2$ and different pressures (reduced units). Red (dashed) line: $P = 0.1$ ($\langle\rho\rangle = 0.052$), green (dashed) line: P=1 ($\langle\rho\rangle = 0.433$), and blue (dashed) line, $P = 9$ ($\langle\rho\rangle = 0.880$).

the expressions for partial molar excess enthalpy and partial molar volume (Eq. 2.8 and Eq. 2.9), we perform simulations in the the CFC*NPT* ensemble and in the *NPT* ensemble (as proposed by Frenkel et al. [30, 31]). Results for the partial molar excess enthalpy and partial molar volume are shown in Fig. 5.2. At low pressures (low densities) and the error bars are small. The partial molar excess enthalpy approaches 0 at low pressures which indicates (and confirms) ideal gas behavior. There is a clear distinction between the computed partial molar excess enthalpies at higher pressures (high densities) using the two methods. The performance of the method proposed by Frenkel et al. [30, 31] strongly depends on the sampling efficiency of the WTPI method, and it is well known that this method becomes less efficient at high densities [52, 54]. Indeed, the values of partial molar excess enthalpies computed using the WTPI method show strong fluctuations as the pressure increases, and the error bars are significantly larger compared to those obtained from simulations in the CFC*NPT* ensemble. The simulations in the CFC*NPT* ensemble provide better statistics for computing the partial molar excess enthalpies as the density of the system increases, and the magnitude of the error bars remains almost the same for the whole pressure range. Similarly, comparison of the partial molar volumes shows that computation using the WTPI method at high pressures results in large uncertainties. Average partial molar volumes computed using simulations in the CFC*NPT* ensemble have smaller error bars at high pressures. In Fig. 5.3, the partial molar excess enthalpy and the partial molar volume of NH_3 are plot-

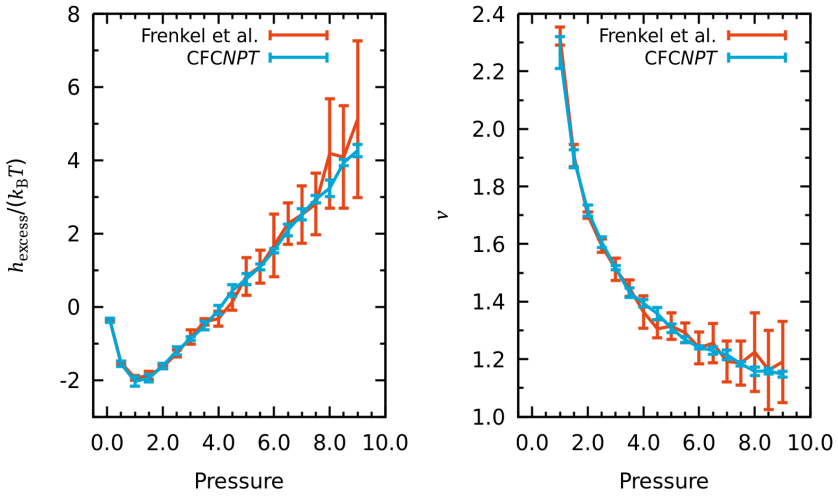

Figure 5.2: Partial molar excess enthalpy and partial molar volume as a function of pressure for a binary Lennard-Jones color mixture (50%-50%) consisting of 200 molecules at $T = 2$. Red line: values obtained with the method proposed by Frenkel et al. [30, 31], blue line: values obtained with the CFC method. Values are in reduced units.

ted as a function of pressure. Results from four different methods are compared: Peng-Robinson EoS [87], the PC-SAFT EoS [190, 191, 196–198], the Numerical Differentiation method [39], and simulations in the CFC*NPT* ensemble. It is clear from Fig. 5.3 that the results for the partial molar excess enthalpy and partial molar volume of the simulations in the CFC*NPT* ensemble are in excellent agreement with those obtained from the Numerical Differentiation method. This is used as a check for validating the CFC method for systems other than the simple system of Lennard-Jones particles. We would like to point out that the partial molar excess enthalpies of NH_3 are negative and decrease with increasing pressure. In Fig. 5.4 and Fig. 5.5, the partial molar excess enthalpy and the partial molar volume of N_2 and H_2, respectively, are plotted as a function of pressure. In contrast to NH_3, the values of the partial molar excess enthalpies are positive and increase with increasing pressure. Overall, good agreement between the different methods is observed.

The reaction enthalpy of the Haber-Bosch process can be computed using:

$$\Delta\bar{h}\,(P,T) = 2\bar{h}_{\mathrm{NH_3}}\,(P,T) - \bar{h}_{\mathrm{N_2}}\,(P,T) - 3\bar{h}_{\mathrm{H_2}}\,(P,T) \tag{5.1}$$

where, for component i:

$$\bar{h}_i\,(P,T) = \bar{h}_i^{\circ} + \left[\bar{h}_i\,(P_{\mathrm{ref}},T) - \bar{h}_i\,(P_{\mathrm{ref}},T_{\mathrm{ref}})\right] + \left[\bar{h}_i^{\mathrm{excess}}\,(P,T) - \bar{h}_i^{\mathrm{excess}}\,(P_{\mathrm{ref}},T)\right] \tag{5.2}$$

where P_{ref} and T_{ref} are the standard reference state pressure and temperature: 1 bar and 298 K. $\bar{h}_i^{\circ}$ is the enthalpy of formation at the reference state $(P_{\mathrm{ref}}, T_{\mathrm{ref}})$ and can

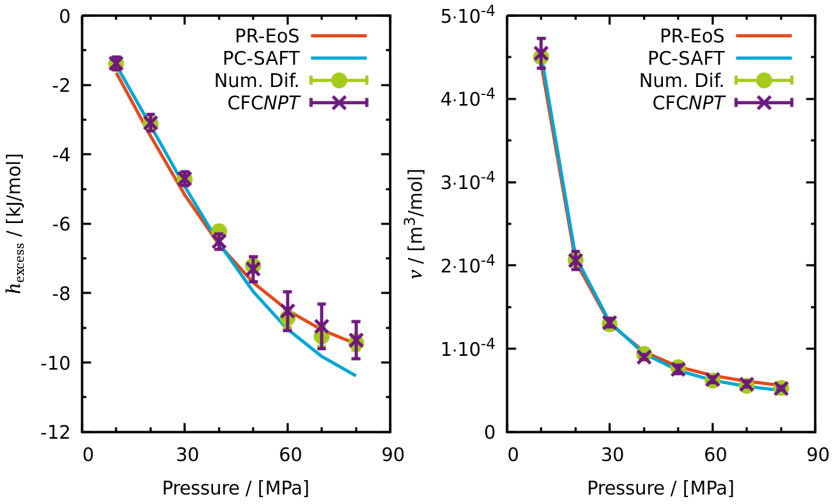

Figure 5.3: Computed partial molar excess enthalpies and partial molar volumes as a function of pressure for NH_3 in a stoichiometric mixture of N_2, H_2 and NH_3 at 573 K. The equilibrium compositions of the mixtures are obtained from simulations of the Haber-Bosch reaction using the Reaction Ensemble (Chapter 4). Red line: Peng-Robinson equation of state, blue line: PC-SAFT equation of state, green symbol: Numerical Differentiation, and purple: simulations in the CFC*NPT* ensemble (Eq. 2.8 and Eq. 2.9). The error bars for the Numerical Differentiation and CFC*NPT* ensemble simulations indicate one standard deviation from the mean.

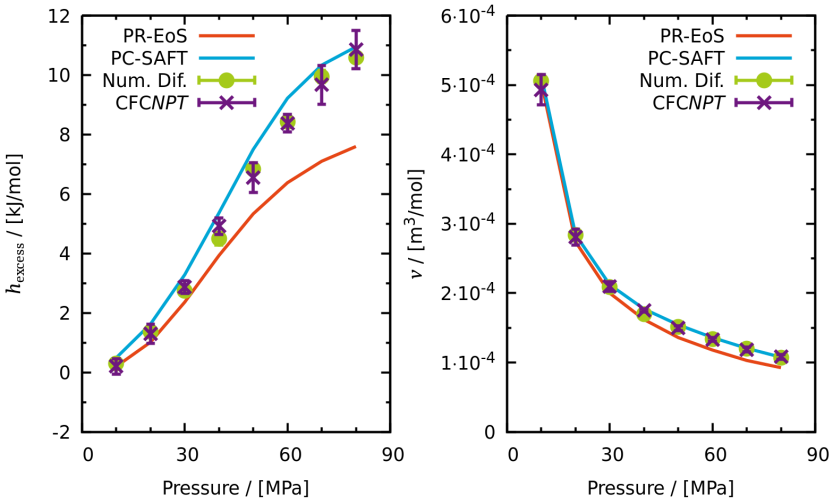

Figure 5.4: Computed partial molar excess enthalpies and partial molar volumes as a function of pressure for N_2 in a stoichiometric mixture of N_2, H_2 and NH_3 at 573 K. The equilibrium compositions of the mixtures are obtained from simulations of the Haber-Bosch reaction using the Reaction Ensemble (Chapter 4). Red line: Peng-Robinson equation of state, blue line: PC-SAFT equation of state, green symbol: Numerical Differentiation, and purple: simulations in the CFC*NPT* ensemble (Eq. 2.8 and Eq. 2.9). The error bars for the Numerical Differentiation and CFC*NPT* ensemble simulations indicate one standard deviation from the mean.

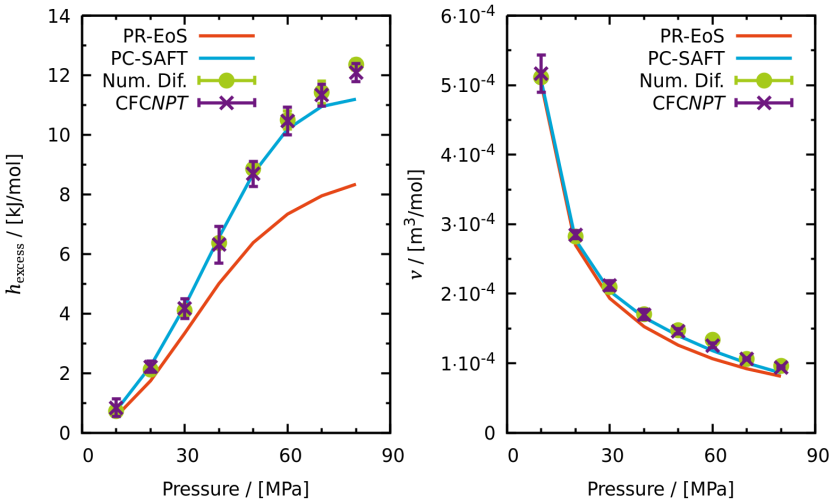

Figure 5.5: Computed partial molar excess enthalpies and partial molar volumes as a function of pressure for H_2 in a stoichiometric mixture of N_2, H_2 and NH_3 at 573 K. The equilibrium compositions of the mixtures are obtained from simulations of the Haber-Bosch reaction using the Reaction Ensemble (Chapter 4). Red line: Peng-Robinson equation of state, blue line: PC-SAFT equation of state, green symbol: Numerical Differentiation, and purple: simulations in the CFC*NPT* ensemble (Eq. 2.8 and Eq. 2.9). The error bars for the Numerical Differentiation and CFC*NPT* ensemble simulations indicate one standard deviation from the mean.

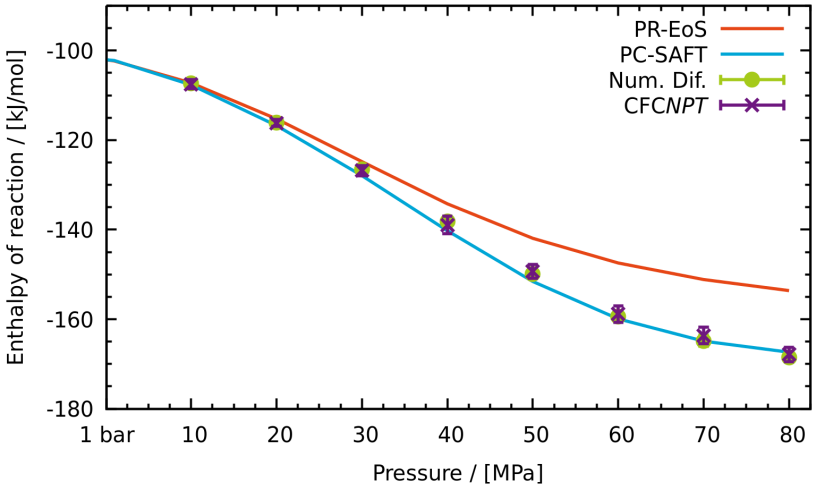

Figure 5.6: Reaction enthalpy of the Haber-Bosch process per mole of N_2 as a function of pressure at 573 K. The equilibrium compositions of the mixtures are obtained from simulations of the Haber-Bosch reaction using the Reaction Ensemble (Chapter 4). Red line: Peng-Robinson equation of state, blue line: PC-SAFT equation of state, green symbol: Numerical Differentiation, and purple: simulations in the CFC*NPT* ensemble (Eq. 2.8). The error bars for the Numerical Differentiation and CFC*NPT* ensemble simulations indicate one standard deviation from the mean.

be obtained from literature [142, 199, 200]. The second term on the right-hand side of Eq. 5.2 is associated with the enthalpy difference between the state points (P_{ref}, T) and $(P_{\text{ref}}, T_{\text{ref}})$. The last term on the right-hand side of Eq. 5.2 is associated with the excess enthalpy difference between the state points (P, T) and (P_{ref}, T) and accounts for the deviation of the ideal gas behavior. Using the values obtained for the partial molar excess enthalpies of the different components in the stoichiometric mixture of N_2, H_2 and NH_3, we can compute the reaction enthalpy as a function of pressure. In Fig. 5.6 the reaction enthalpy of the ammonia synthesis reaction at 573 K is shown as a function of pressure. At the standard reference pressure ($P_{\text{ref}} = 1$bar) the reaction enthalpy is 102.07 kJ per mole of N_2 [28]. Excellent agreement is observed between the PC-SAFT equation of state and the results from Monte Carlo simulations in the CFC*NPT* ensemble for pressures up to 80 MPa. The Peng-Robinson equation of state deviates from the other methods as pressure increases (up to 8% at 80 MPa). This is associated with the well-known limitations of a cubic equation of state. At high pressures, volumetric estimates, fugacity coefficients and other related derivative thermodynamic properties calculated using the PR-EoS are known to be inaccurate [3, 184, 188, 189].

From Fig. 5.6 it is clear that the contribution of the partial molar excess enthalpy to the reaction enthalpy become significant at high pressures for the Haber-Bosch process. Not including the contribution of the partial molar excess enthalpies results in differences of 24% to 64% relative to the reaction enthalpy at the reference pressure for pressures ranging from 30 MPa to 80 MPa. From Fig. 4.1 (Chapter 4) one can observe that at chemical equilibrium, the mole fraction of NH_3 increases with increasing pressure. As NH_3 molecules show association behavior [187], this results in favorable NH_3-NH_3 interactions. This is reflected by the negative partial molar excess enthalpy of NH_3 at high pressures (Fig. 5.3). In sharp contrast to NH_3, the N_2-N_2 and H_2-H_2 interactions become less favorable at high pressures as indicated by a positive partial molar excess enthalpy (Fig. 5.4 and Fig. 5.5). The combined result of this behavior of the partial molar excess enthalpies is that the reaction enthalpy becomes more exothermic with increasing pressure.

5.4. Conclusions

In this chapter, we studied the applicability of the CFC method to compute partial molar excess enthalpies and partial molar volumes in the *NPT* ensemble (Chapter 2). To compute the partial molar properties of component i in a mixture, the *NPT* ensemble is expanded with a fractional molecule of type i. Computation of partial molar properties in the CFC*NPT* ensemble does not have the drawbacks of Widom-like test particle methods, since particle insertions and removals take place in a gradual manner. As a proof of principle, this method is compared to the original method by Frenkel et al. [30, 31] for a binary color mixture of Lennard-Jones particles at different conditions. Partial molar properties obtained using both methods are in excellent agreement. The CFC method is also applied to an industrially relevant system: stoichiometric mixtures of N_2, H_2 and NH_3. We also compared the CFC method with Numerical Differentiation where excellent agreement is found between the results. It is shown that the contribution of the partial molar enthalpies

in calculating the reaction enthalpy of the Haber-Bosch process is significant at high pressures (up to 64% at a pressure of 80 MPa, relative to the reaction enthalpy at a pressure of 1 bar). It is observed that at high pressures, the contribution of the partial molar excess enthalpies is not negligible for this process. This means that that the Haber-Bosch process becomes more exothermic with increasing pressure.

6

Combining the Gibbs Ensemble and Reaction Ensemble

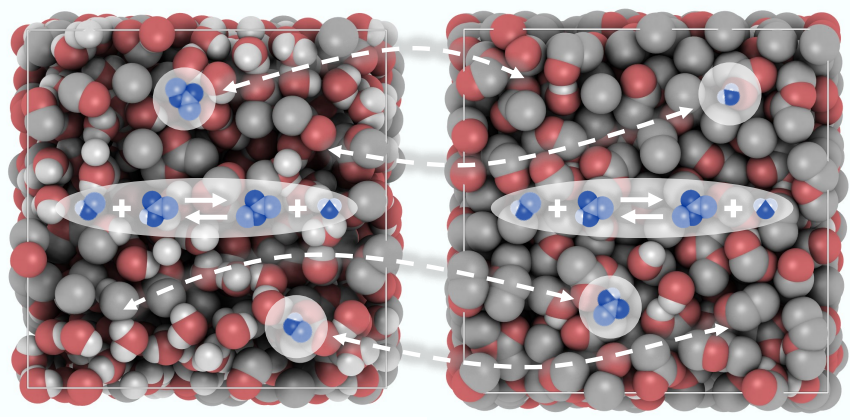

Schematic illustration of the esterification of methanol with acetid acid. Fractional molecules are used to facilitate the phase separation of the mixture and to facilitate the chemical reaction.

This chapter is based on the paper:

R. Hens, A. Rahbari, S. Caro-Ortiz, N. Dawass, M. Erdős, A. Poursaeidesfahani, H. S. Salehi, A. T. Celebi, M. Ramdin, O. A. Moultos, D. Dubbeldam, and T. J. H. Vlugt, *Brick-CFCMC: Open Source Software for Monte Carlo Simulations of Phase and Reaction Equilibria using the Continuous Fractional Component Method*, Journal of Chemical Information and Modeling, **60**, 2678-2682 (2020) [25].

6.1. Introduction

In this dissertation, Monte Carlo simulations were performed using the software package Brick (Sec. 2.5). Brick is open source and can be downloaded from `https://gitlab.com/ETh_TU_Delft/Brick-CFCMC`. To demonstrate some features of Brick, we simulate the esterification of acetic acid with methanol in the liquid phase [201, 202]:

$$CH_3OH + CH_3COOH \rightleftarrows CH_3COOCH_3 + H_2O$$

6.2. Simulation Details

In the esterification of acetic acid with methanol, two phases form due to the polar nature of acetic acid, methanol, and water and the nonpolar methyl acetate. Chemical reaction equilibria can be simulated using the Reaction Ensemble, where molecules are converted from reactants into products (and vice versa) using Monte Carlo trial moves such that the reaction equilibrium is obtained [21, 26, 62, 64]. Phase equilibria can be simulated in the Gibbs Ensemble, where molecules are being transferred between two simulation boxes such that the phase equilibrium is obtained [20, 37]. The Gibbs Ensemble is therefore combined with the Reaction Ensemble for simulating the esterification. This is illustrated in Fig. 6.1. Simulations in this combined ensemble were performed starting from an initial configuration of 900 molecules.

The cutoff radius for Lennard-Jones and electrostatic interactions is 14 Å. Analytic tail corrections for the Lennard-Jones interactions are used (Sec. 2.5.4), and the Ewald method is used for electrostatic interactions (Sec. 2.5.5). The force field parameters and geometries of the molecules can be found in Tables A.5, A.6, A.7 and A.8 of the Appendix. Partition functions of the isolated molecule were obtained from the Gibbs free energy of formation [204] and are listed in Table 6.1. We consider the system at $T = 343$ K and $P = 1$ bar. For equilibrating the system, $5{\cdot}10^5$ cycles were used, where each cycle consists of N trial moves (N being the total number of molecules in the system). We study two cases: (1) all molecules are rigid; (2) all molecules (except water) are flexible (i.e. bond bending and torsion are taken into account). The trial moves are randomly selected with the following probabilities: 25% translations, 25% rotations, 1% volume changes, 25% λ changes, 16% Gibbs Ensemble swap/identity changes and, 8% Reaction Ensemble swap/identity changes for the case where molecules are treated as rigid. When flexibility of the molecules is taken into account, the trial moves are selected with the following probabilities: 20% translations, 20% rotations, 14% bond bending changes, 7% torsion rotations, 1% volume changes, 20% λ changes, 12% Gibbs Ensemble swap/identity changes and, 6% Reaction Ensemble swap/identity changes. For more details about the trial moves we refer the reader to the Supporting Information of Ref. [25]. The Gibbs Ensemble swap and identity change trial moves facilitate the particle transfer between the two simulation boxes [37]. The Reaction Ensemble swap and identity change trial moves facilitate the conversion of reactants into products (and vice versa) in each simulation box [26]. In the first 10^5 cycles, the Wang-Landau scheme was used to obtain weight functions for the frac-

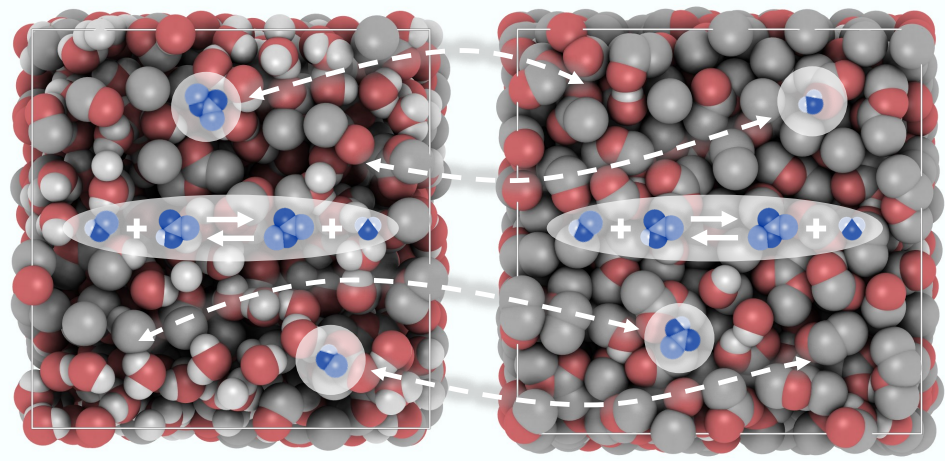

Figure 6.1: Schematic representation of the combination of the Gibbs Ensemble with the Reaction Ensemble for the esterification of methanol with acetic acid, $CH_3OH + CH_3COOH \rightleftarrows CH_3COOCH_3 + H_2O$. A total of 900 molecules is distributed over the two simulation boxes. Four fractional molecules, one for each component, are added to the system to facilitate molecule transfers between the two simulation boxes. These fractional molecules can be in either simulation box and can change from one to the other simulation box by the Gibbs Ensemble swap and identity change trial moves [37]. Fractional molecules of either reactants or products are added to each simulation box to facilitate the chemical reaction. These fractional molecules remain in the same simulation box during the simulation and can be converted from reactants into products (or vice versa) by the Reaction Ensemble swap and identity change trial moves [26]. This means that in total, at all times during the simulation, we have eight fractional molecules (four for achieving phase equilibrium and two in each simulation box to achieve reaction equilibrium). This is less than 1% of the total number of molecules so that the fractional molecules do not affect the simulation results [73]. Figure created with iRASPA [203].

tional molecules. Then, every 10^5 cycles an iterative scheme was used in which the probability distribution of λ was used to improve the weight function further. After equilibrating, 10^5 production cycles were performed to obtain average properties of the system such as the equilibrium composition. Additional simulations were run in the *NPT* ensemble at this equilibrium composition to obtain the chemical potentials using probe molecules of the four species involved in the reaction.

6.3. Results

The equilibrium composition obtained from the simulations in the combined Gibbs Ensemble and Reaction Ensemble are listed in Table 6.2. We observe a clear phase separation. One phase contains mostly water while the other phase contains mostly methyl acetate. We will refer to these two phases as the water-rich phase and ester-rich phase, respectively. The chemical potential per mole can be written as the sum of three parts [26, 28] by multiplying Eq. 2.7 with Avogadro's number N_A:

$$\mu_i = -RT \ln\left(\frac{q_i V_0}{\Lambda_i^3}\right) + RT \ln\left(\frac{\langle \rho_i \rangle}{\rho_0}\right) - RT \ln\left(\frac{p\,(\lambda_i = 1)}{p\,(\lambda_i = 0)}\right) \tag{6.1}$$

Table 6.1: Partition functions of the isolated molecule (excluding the translational part) divided by the thermal wavelength, and chemical potentials of different molecules at $T = 343$ K calculated from Gibbs free energies of formation (calculated with Outotec HSC Chemistry Software [204]) $\mu_i^\circ = -RT \ln\left(q_i V_0/\Lambda_i^3\right)$ with the reference volume $V_0 = 1$ Å^3.

Molecule	q_i/Λ_i^3/[Å^{-3}]	μ_i°/kJ·mol^{-1}]
CH_3OH	$1.37 \cdot 10^{19}$	-125.67
CH_3COOH	$3.07 \cdot 10^{52}$	-344.66
CH_3COOCH_3	$7.46 \cdot 10^{42}$	-281.53
H_2O	$6.73 \cdot 10^{29}$	-195.87

where R is the gas constant, T is the temperature, q_i is the partition function, excluding the translational part, of an isolated molecule of component i, V_0 is an arbitrary reference volume (here set to 1 Å^3), Λ_i is the thermal wavelength, $\langle \rho_i \rangle$ is the average number density, ρ_0 is an arbitrary reference number density (here set to 1 Å^{-3}), and $p\,(\lambda_i = 1)$ and $p\,(\lambda_i = 0)$ are the probabilities that the fractional parameter λ_i takes the values 1 and 0, respectively. As mentioned earlier in Chapter 2, the first term on the right-hand side of Eq. 6.1 only depends on the temperature and is denoted by μ_i°. The second term on the right-hand side depends on the number density (and is together with the first term referred to as the ideal gas contribution to the chemical potential). The third term on the right-hand side is the excess chemical potential. Chemical potentials that were obtained from simulations in the *NPT* ensemble are listed in Table 6.2. We observe that for each component the chemical potentials in both phases are equal. This shows that the system is at phase equilibrium. To verify that the system achieved reaction equilibrium, we add the chemical potentials (Eq. 6.1) of the reactants (CH_3OH+CH_3COOH) and of the products (CH_3COOCH_3+H_2O) in both phases (Table 6.3). Since these sums are equal in both phases, we conclude that we achieved reaction equilibrium in each simulation box, phase equilibrium between the simulation boxes, and that there is almost no difference between treating the molecules as rigid or flexible in the simulations.

The thermodynamic activities are defined as [205]:

$$a_i = \gamma_i x_i = \exp\left[\frac{\mu_i - \mu_i^{\mathrm{ref}}}{RT}\right] = \frac{\langle \rho_i \rangle}{\langle \rho_i^{\mathrm{ref}} \rangle} \exp\left[\frac{\mu_{\mathrm{ex},i} - \mu_{\mathrm{ex},i}^{\mathrm{ref}}}{RT}\right] \tag{6.2}$$

where a_i is the thermodynamic activity of component i, γ_i is the activity coefficient, x_i is the mole fraction, μ_i is the chemical potential (Eq. 6.1), ρ_i is the number density, and $\mu_{\mathrm{ex},i}$ is the excess chemical potential. The quantities μ_i^{ref}, ρ_i^{ref}, and $\mu_{\mathrm{ex},i}^{\mathrm{ref}}$ are the reference chemical potential, number density and excess chemical potential, defined as that of the pure component i at the same temperature and pressure as the mixture. Additional simulations were performed in the *NPT* ensemble to obtain the reference chemical potentials. All computed reference chemical potentials can be found in the Supporting Information of Ref. [25]. The mole fractions and

Table 6.2: Compositions and chemical potentials at reaction and phase equilibrium of the esterification of methanol with acetic acid at T = 343 K and P = 1 bar. Results for a system where all molecules are rigid and a system where molecule are flexible (i.e. bond bending and torsion are taken into account). The superscripts I and II indicate the water-rich and ester-rich phases, respectively, x_i is the mole fraction of component i, μ_i is the chemical potential (Eq. 6.1), $\mu_i^\circ = -RT \ln\left(q_i V_0 / \Lambda_i^3\right)$ is the contribution to the chemical potential due to the internal degrees of freedom (Table 6.1) with the reference volume V_0 = 1 Å^3, and a_i is the thermodynamic activity (Eq. 6.2). The number between brackets indicate the uncertainty (one standard deviation) in the last digit.

	Component	x_i^{I}	x_i^{II}	$\mu_i^{\mathrm{I}} - \mu_i^\circ$/[kJ·mol^{-1}]	$\mu_i^{\mathrm{II}} - \mu_i^\circ$/[kJ·mol^{-1}]	a_i
Rigid	CH_3OH	0.135(9)	0.072(6)	-36.0(8)	-35.8(5)	0.15(2)
	CH_3COOH	0.06(2)	0.151(7)	-38.1(9)	-38.7(7)	0.21(5)
	CH_3COOCH_3	0.14(2)	0.67(2)	-29.6(10)	-30.3(5)	0.9(2)
	H_2O	0.67(2)	0.11(2)	-37.0(4)	-36.6(7)	1.4(2)
Flexible	CH_3OH	0.150(7)	0.073(8)	-35.7(8)	-36.2(6)	0.14(3)
	CH_3COOH	0.06(2)	0.17(2)	-39.0(10)	-39.1(6)	0.17(5)
	CH_3COOCH_3	0.120(9)	0.69(3)	-30.1(8)	-30.1(8)	0.9(2)
	H_2O	0.66(2)	0.08(3)	-37.1(4)	-37.9(5)	1.1(2)

Table 6.3: Sum of chemical potentials of reactants (CH_3OH+CH_3COOH) and products (CH_3COOCH_3+H_2O) at reaction and phase equilibrium of the esterification of methanol with acetic acid at T = 343 K and P = 1 bar. Results for a system where all molecules are rigid and a system where molecule are flexible (i.e. bond bending and torsion are taken into account). The number between brackets indicate the uncertainty (one standard deviation) in the last digit.

	Phase	$\sum_{\text{Reactants}} \nu_i \mu_i$/[kJ·mol^{-1}]	$\sum_{\text{Products}} \nu_i \mu_i$/[kJ·mol^{-1}]
Rigid	water-rich	-544(2)	-544(2)
	ester-rich	-545(2)	-544(2)
Flexible	water-rich	-545(2)	-545(2)
	ester-rich	-546(2)	-545(2)

chemical potentials at equilibrium are listed in Table 6.2. The thermodynamic activities can be calculated from the chemical potentials (Eq. 6.2), and from there the equilibrium constant of the reaction can be computed:

$$\begin{aligned}\ln K &= \ln\left(\frac{a_{CH_3COOCH_3}\cdot a_{H_2O}}{a_{CH_3OH}\cdot a_{CH_3COOH}}\right)\\ &= \frac{1}{RT}\Big[\left(\mu_{CH_3COOCH_3}-\mu^{ref}_{CH_3COOCH_3}\right)+\left(\mu_{H_2O}-\mu^{ref}_{H_2O}\right)\\ &\qquad -\left(\mu_{CH_3OH}-\mu^{ref}_{CH_3OH}\right)-\left(\mu_{CH_3COOCH_3}-\mu^{ref}_{CH_3COOCH_3}\right)\Big].\end{aligned} \tag{6.3}$$

We obtain $\ln K = 3.8 \pm 0.4$ for the system with rigid molecules, and $\ln K = 3.7 \pm 0.5$ for the system with flexibility taken into account. The uncertainty is defined as the standard deviation. The computed equilibrium constants are in good agreement with experimental data [206] where values for $\ln K$ are found to be in the range from 3.25 to 3.41. In comparison, the equilibrium constant would be $\ln K_{IG} = 2.48$ if the system was treated as an ideal gas, showing that the medium has a large effect on the reaction equilibrium.

6.4. Conclusions

For the esterification of methanol with acetic acid we calculated the equilibrium composition, chemical potentials, thermodynamic activities and activity coefficients. For comparison we distinguished two cases: the system where molecules are treated as rigid and the system where flexibility is taken into account. We conclude that there is no significant difference in treating the molecules as rigid or flexible for this system.

Conclusions

In this work, we have worked on improvements of the Continuous Fractional Component (CFC) method for Monte Carlo simulations. We developed a software package, Brick-CFCMC (Brick) for molecular simulation in various ensembles using the CFC method. Phase and reaction equilibria, chemical potentials and partial molar properties can be calculated directly from single simulations.

The Wolf method was found to be a suitable and computationally cheaper method than the Ewald method for the calculation of electrostatic interactions. Using Brick, accurate vapor-liquid equilibrium curves are obtained from simulations in the Gibbs Ensemble as well as critical densities and temperatures. Furthermore, a procedure for choosing the correct parameters for the Wolf method was obtained. The CFC method has been developed further for simulations in the Reaction Ensemble. The new (serial) formulation of the CFC method has been compared to the previous (parallel) formulation and the conventional method in Monte Carlo simulations. For different systems of Lennard-Jones particles, the serial CFC method proves to be more efficient and one can directly check for chemical equilibrium. Simulations of the ammonia synthesis reaction (Haber-Bosch process) show the suitability of the serial CFC method for an industrial relevant case. Also for the *NVT* and *NPT* ensembles the CFC method has been developed further to compute partial molar enthalpies and partial molar volumes directly from single simulations. For the Haber-Bosch process, partial molar properties have been accurately calculated using the CFC method in the *NPT* ensemble. Simulations of the esterification of acetic acid with methanol in the combined Gibbs Ensemble and Reaction Ensemble show the formation of two phases in this system. Equilibrium compositions, chemical potentials, activity coefficients and the equilibrium constant have been successfully calculated using Brick and the CFC method.

Brick has been proven to be a reliable software package for molecular simulations of phase and reaction equilibria. In future work, more (complex) interaction potentials could be added to the package such as bond stretching, improper dihedrals and polarizability. Furthermore, combining the Configurational-Bias Monte Carlo scheme with the CFC method may increase the efficiency of these simulations more.

Appendix

Table A.1: Force field parameters of hydrogen sulfide [109], methanol [110], and carbon dioxide [89]. CH_3 is described as united atom and M is a dummy site.

Molecule	Site	ε/k_B/[K]	σ/[Å]	q/e
H_2S	S	122.0	3.60	0
	H	50.0	2.50	0.21
	M	0	0	-0.42
CH_3OH	CH_3	110.45	3.6499	0.1546
	O	97.775	3.1659	-0.6544
	H	0	0	0.4998
CO_2	C	27.0	2.800	0.700
	O	79.0	3.050	-0.350

Table A.2: Geometries of hydrogen sulfide [109], methanol [110], and carbon dioxide [89].

Molecule	Type	Sites	Length/angle
H_2S	bond	S-H	1.34 Å
	bond	S-M	0.30 Å
	angle	H-S-H	92°
	angle	H-S-M	46°
CH_3OH	bond	CH_3-O	1.43 Å
	bond	O-H	0.945 Å
	angle	CH_3-O-H	108.5°
CO_2	bond	C-O	1.16 Å
	angle	O-C-O	180°

Table A.3: Force field parameters of nitrogen [89], hydrogen [169], and ammonia [168]. H_2 is described as united atom and M is a dummy site.

Molecule	Site	ε/k_B/[K]	σ/[Å]	q/e
N_2	N	36.0	3.31	-0.482
	M	0	0	0.964
H_2	H_2	38.0	2.915	0
NH_3	N	185.0	3.42	0
	H	0	0	0.41
	M	0	0	-1.23

Table A.4: Geometries of of nitrogen [89], and ammonia [168].

Molecule	Type	Sites	Length/angle
N_2	bond	N-N	1.10 Å
	bond	N-M	0.55 Å
	angle	N-M-N	180°
NH_3	bond	N-H	1.012 Å
	bond	N-M	0.080 Å
	angle	H-N-H	106.7°
	angle	H-N-M	67.9°

Table A.5: Force field parameters of methanol [90], acetic acid [207], methyl acetate [208], and water [209, 210]. CH_3 is described as united atom and M is a dummy site.

Molecule	Atom/site	ϵ/k_B/[K]	σ/[Å]	q/[e]
CH_3OH	CH_3	98.0	3.75	0.265
	O	93.0	3.02	-0.700
	H	0	0	0.435
CH_3COOH	CH_3	98.0	3.75	0.120
	C	41.0	3.90	0.420
	O(=C)	79.0	3.05	-0.450
	O(-H)	93.0	3.02	-0.460
	H	0	0	0.370
CH_3COOCH_3	CH_3(-C)	98.0	3.75	0.050
	C	41.0	3.90	0.550
	O(=C)	79.0	3.05	-0.450
	O	55.0	2.80	-0.400
	CH_3(-O)	98.0	3.75	0.050
H_2O	H	0	0	0.52422
	O	81.899	3.16435	0
	M	0	0	-1.04844

Table A.6: Bond lengths in methanol [90], acetic acid [207], methyl acetate [208], and water [209, 210].

Molecule	Bond	Length/[Å]
CH_3OH	CH_3-O	1.43
	O-H	0.945
CH_3COOH	CH_3-C	1.520
	C=O	1.214
	C-O	1.364
	O-H	0.970
CH_3COOCH_3	CH_3-C	1.520
	C=O	1.2
	C-O	1.344
	O-CH_3	1.41
H_2O	O-H	0.9572
	O-M	0.15

Table A.7: Force field parameters for bond bendings in methanol [90], acetic acid [207], methyl acetate [208], and water [209, 210]. Bond bending is described by the following interaction potential: $U_{\text{bending}} = \frac{k_\theta}{2}(\theta - \theta_0)^2$.

Molecule	Bending	k_θ/k_B/[K]	θ_0
CH_3OH	CH_3-O-H	55400	108.5°
CH_3COOH	CH_3-C=O	40300	126°
	CH_3-C-O	35300	111°
	O=C-O	40300	123°
	C-O-H	17600	107°
CH_3COOCH_3	CH_3-C=O	62500	125°
	CH_3-C-O	70600	110°
	O=C-O	62500	125°
	C-O-CH_3	62500	115°
H_2O	H-O-H	Rigid	104.52°
	H-O-M	Rigid	52.26°

Table A.8: Force field parameters for torsions in acetic acid [207] and methyl acetate [208]. Torsion is described by the following interaction potential: $U_{\text{torsion}} = \sum_{i=0}^{3} c_i \cos^i(\phi)$.

Molecule	Torsion	c_0/k_B/[K]	c_1/k_B/[K]	c_2/k_B/[K]	c_3/k_B/[K]
CH_3COOH	O=C-O-H	2192.4	-630.0	-1562.4	0
	CH_3-C-O-H	2192.4	630.0	-1562.4	0
CH_3COOCH_3	O=C-O-CH_3	10874.6	-2654.2	-4118.0	613.6
	CH_3-C-O-CH_3	6551.3	1566.1	-4196.0	789.2

References

[1] R. A. Alberty, *Thermodynamics of Biochemical Reactions*, 1st ed. (John Wiley & Sons, New Jersey, USA, 2005).

[2] T. Engel and P. J. Reid, *Thermodynamics, Statistical Thermodynamics, & Kinetics*, 3rd ed. (Prentice Hall Upper Saddle River, Upper Saddle River, NJ, USA, 2010).

[3] B. E. Poling, J. M. Prausnitz, and J. P. O'Connell, *The Properties of Gases and Liquids*, Vol. 5 (Mcgraw-hill, New York, 2001).

[4] A. Podgoršek, J. Jacquemin, A. Pádua, and M. Costa Gomes, *Mixing Enthalpy for Binary Mixtures Containing Ionic Liquids,* Chem. Rev. **116**, 6075 (2016).

[5] D. Almantariotis, O. Fandiño, J.-Y. Coxam, and M. C. Gomes, *Direct Measurement of the Heat of Solution and Solubility of Carbon Dioxide in 1-Hexyl-3-Methylimidazolium Bis[trifluoromethylsulfonyl]amide and 1-Octyl-3-Methylimidazolium Bis[trifluoromethylsulfonyl]amide,* Int. J. Greenhouse Gas Control **10**, 329 (2012).

[6] M. B. Shiflett, B. A. Elliott, S. R. Lustig, S. Sabesan, M. S. Kelkar, and A. Yokozeki, *Phase Behavior of CO_2 in Room-Temperature Ionic Liquid 1-Ethyl-3-Ethylimidazolium Acetate,* ChemPhysChem **13**, 1806 (2012).

[7] D. S. Firaha, O. Hollóczki, and B. Kirchner, *Computer-Aided Design of Ionic Liquids as CO_2 Absorbents,* Angew. Chem. Int. Ed. **54**, 7805 (2015).

[8] B. Zhang, A. C. T. van Duin, and J. K. Johnson, *Development of a ReaxFF Reactive Force Field for Tetrabutylphosphonium Glycinate/CO_2 Mixtures,* J. Phys. Chem. B **118**, 12008 (2014).

[9] S. P. Šerbanović, B. D. Djordjević, and D. K. Grozdanić, *Excess Molar Volume Prediction for Some Hydrocarbons and Related Mixtures by Means of Simple Cubic Equations of State,* Fluid Phase Equilib. **57**, 47 (1990).

[10] S. P. Balaji, S. Gangarapu, M. Ramdin, A. Torres-Knoop, H. Zuilhof, E. L. V. Goetheer, D. Dubbeldam, and T. J. H. Vlugt, *Simulating the Reactions of CO_2 in Aqueous Monoethanolamine Solution by Reaction Ensemble Monte Carlo Using the Continuous Fractional Component Method,* J. Chem. Theory Comput. **11**, 2661 (2015).

[11] B. L. Eggimann, A. J. Sunnarborg, H. D. Stern, A. P. Bliss, and J. I. Siepmann, *An Online Parameter and Property Database for the TraPPE Force Field,* Mol. Sim. **40**, 101 (2014).

[12] W. L. Jorgensen and J. Tirado-Rives, *The OPLS [optimized Potentials for Liquid Simulations] Potential Functions for Proteins, Energy Minimizations for Crystals of Cyclic Peptides and Crambin,* J. Am. Chem. Soc. **110**, 1657 (1988).

[13] W. D. Cornell, P. Cieplak, C. I. Bayly, I. R. Gould, K. M. Merz, D. M. Ferguson, D. C. Spellmeyer, T. Fox, J. W. Caldwell, and P. A. Kollman, *A Second Generation Force Field for the Simulation of Proteins, Nucleic Acids, and Organic Molecules,* J. Am. Chem. Soc. **117**, 5179 (1995).

[14] T. A. Halgren, *Merck Molecular Force Field. I. Basis, Form, Scope, Parameterization, and Performance of MMFF94,* J. Comput. Chem. **17**, 490 (1996).

[15] D. Frenkel and B. Smit, *Understanding Molecular Simulation: From Algorithms to Applications*, 2nd ed. (Academic Press, 525 B Street, Suite 1900, San Diego, California 92101-4495, United States of America, 2002).

[16] M. P. Allen and D. J. Tildesley, *Computer Simulation of Liquids*, 2nd ed. (Oxford University Press, Great Clarendon Street, Oxford, OX2 6DP, United Kingdom, 2017).

[17] R. Bowley and M. Sánchez, *Introductory Statistical Mechanics* (Oxford University Press, Great Clarendon Street, Oxford OX2 6DP, United Kingdom, 1999).

[18] N. Metropolis, A. W. Rosenbluth, M. N. Rosenbluth, A. H. Teller, and E. Teller, *Equation of State Calculations by Fast Computing Machines,* J. Chem. Phys. **21**, 1087 (1953).

[19] A. Z. Panagiotopoulos, *Direct Determination of Phase Coexistence Properties of Fluids by Monte Carlo Simulation in a New Ensemble,* Mol. Phys. **61**, 813 (1987).

[20] A. Z. Panagiotopoulos, N. Quirke, M. Stapleton, and D. J. Tildesley, *Phase Equilibria by Simulation in the Gibbs Ensemble,* Mol. Phys. **63**, 527 (1988).

[21] J. K. Johnson, A. Z. Panagiotopoulos, and K. E. Gubbins, *Reactive Canonical Monte Carlo: A New Simulation Technique for Reacting or Associating Fluids,* Mol. Phys. **81**, 717 (1994).

[22] W. Smith and B. Triska, *The Reaction Ensemble Method for the Computer Simulation of Chemical and Phase Equilibria. I. Theory and Basic Examples,* J. Chem. Phys. **100**, 3019 (1994).

[23] D. J. Adams, *Chemical Potential of Hard-Sphere Fluids by Monte Carlo Methods,* Mol. Phys. **28**, 1241 (1974).

[24] D. J. Adams, *Grand Canonical Ensemble Monte Carlo for a Lennard-Jones Fluid,* Mol. Phys. **29**, 307 (1975).

[25] R. Hens, A. Rahbari, S. Caro-Ortiz, N. Dawass, M. Erdős, A. Poursaeidesfahani, H. S. Salehi, A. T. Celebi, M. Ramdin, O. A. Moultos, D. Dubbeldam, and T. J. H. Vlugt, *Brick-CFCMC: Open Source Software for Monte Carlo Simulations of Phase and Reaction Equilibria Using the Continuous Fractional Component Method,* J. Chem. Inf. Model. **60**, 2678 (2020).

[26] A. Poursaeidesfahani, R. Hens, A. Rahbari, M. Ramdin, D. Dubbeldam, and T. J. H. Vlugt, *Efficient Application of Continuous Fractional Component Monte Carlo in the Reaction Ensemble,* J. Chem. Theory Comput. **13**, 4452 (2017).

[27] R. Hens and T. J. H. Vlugt, *Molecular Simulation of Vapor–Liquid Equilibria Using the Wolf Method for Electrostatic Interactions,* J. Chem. Eng. Data **63**, 1096 (2018).

[28] A. Rahbari, R. Hens, I. K. Nikolaidis, A. Poursaeidesfahani, M. Ramdin, I. G. Economou, O. A. Moultos, D. Dubbeldam, and T. J. H. Vlugt, *Computation of Partial Molar Properties using Continuous Fractional Component Monte Carlo,* Mol. Phys. **116**, 3331 (2018).

[29] M. Michelsen and J. M. Mollerup, *Thermodynamic Models: Fundamental & Computational Aspects*, 2nd ed. (Tie-Line Publications, Holte, Denmark, 2007).

[30] P. Sindzingre, G. Ciccotti, C. Massobrio, and D. Frenkel, *Partial Enthalpies and Related Quantities in Mixtures from Computer Simulation,* Chem. Phys. Lett. **136**, 35 (1987).

[31] P. Sindzingre, C. Massobrio, G. Ciccotti, and D. Frenkel, *Calculation of Partial Enthalpies of an Argon-Krypton Mixture by NPT Molecular Dynamics,* Chem. Phys. **129**, 213 (1989).

[32] I. M. Abdulagatov, A. R. Bazaev, E. A. Bazaev, S. P. Khokhlachev, M. B. Saidakhmedova, and A. E. Ramazanova, *Excess, Partial, and Molar Volumes of N-Alkanes in Near-Critical and Supercritical Water,* J. Solution Chem. **27**, 731 (1998).

[33] I. M. Abdulagatov, A. R. Bazaev, E. A. Bazaev, M. B. Saidakhmedova, and A. E. Ramazanova, *Volumetric Properties of Near-Critical and Supercritical Water + Pentane Mixtures: Molar, Excess, Partial, and Apparent Volumes,* J. Chem. Eng. Data **43**, 451 (1998).

[34] H. Liu and J. P. O'Connell, *On the Measurement of Solute Partial Molar Volumes in Near-Critical Fluids with Supercritical Fluid Chromatography,* Ind. Eng. Chem. Res. **37**, 3323 (1998).

[35] R. Chang and J. L. Sengers, *Behavior of Dilute Mixtures Near the Solvent's Critical Point,* J. Phys. Chem. **90**, 5921 (1986).

[36] M. B. Shiflett and E. J. Maginn, *The Solubility of Gases in Ionic Liquids,* AIChE J. **63**, 4722 (2017).

[37] A. Poursaeidesfahani, A. Torres-Knoop, D. Dubbeldam, and T. J. H. Vlugt, *Direct Free Energy Calculation in the Continuous Fractional Component Gibbs Ensemble,* J. Chem. Theory Comput. **12**, 1481 (2016).

[38] B. Smit and D. Frenkel, *Calculation of the Chemical Potential in the Gibbs Ensemble,* Mol. Phys. **68**, 951 (1989).

[39] S. K. Schnell, R. Skorpa, D. Bedeaux, S. Kjelstrup, T. J. H. Vlugt, and J.-M. Simon, *Partial Molar Enthalpies and Reaction Enthalpies from Equilibrium Molecular Dynamics Simulation,* J. Chem. Phys. **141**, 144501 (2014).

[40] S. I. Sandler, *Chemical, Biochemical, and Engineering Thermodynamics*, 4th ed. (John Wiley & Sons, Hoboken, N.J., USA, 2006).

[41] S. M. Walas, *Phase Equilibria in Chemical Engineering*, 1st ed. (Butterworth Publishers, 80 Montvale Avenue, Stoneham, MA 02180, United States of America, 1985).

[42] J. G. Kirkwood and F. P. Buff, *The Statistical Mechanical Theory of Solutions. I,* J. Chem. Phys. **19**, 774 (1951).

[43] S. K. Schnell, P. Englebienne, J.-M. Simon, P. Krüger, S. P. Balaji, S. Kjelstrup, D. Bedeaux, A. Bardow, and T. J. H. Vlugt, *How to Apply the Kirkwood-Buff Theory to Individual Species in Salt Solutions,* Chem. Phys. Lett. **582**, 154 (2013).

[44] P. Krüger, S. K. Schnell, D. Bedeaux, S. Kjelstrup, T. J. H. Vlugt, and J.-M. Simon, *Kirkwood-Buff Integrals for Finite Volumes,* J. Phys. Chem. Lett. **4**, 235 (2012).

[45] P. Krüger and T. J. H. Vlugt, *Size and Shape Dependence of Finite-Volume Kirkwood-Buff Integrals,* Phys. Rev. E **97**, 051301 (2018).

[46] N. Dawass, P. Krüger, J.-M. Simon, and T. J. H. Vlugt, *Kirkwood–Buff Integrals of Finite Systems: Shape Effects,* Mol. Phys. **116**, 1573 (2018).

[47] N. Dawass, P. Krüger, S. K. Schnell, O. A. Moultos, I. G. Economou, T. J. H. Vlugt, and J.-M. Simon, *Kirkwood-Buff Integrals Using Molecular Simulation: Estimation of Surface Effects,* Nanomaterials **10**, 771 (2020).

[48] A. Y. Ben-Naim, *Statistical Thermodynamics for Chemists and Biochemists*, 1st ed. (Springer Science & Business Media, New York, USA, 1992).

[49] B. Widom, *Structure of Interfaces from Uniformity of the Chemical Potential,* J. Stat. Phys. **19**, 563 (1978).

[50] K. B. Daly, J. B. Benziger, P. G. Debenedetti, and A. Z. Panagiotopoulos, *Massively Parallel Chemical Potential Calculation on Graphics Processing Units,* Comput. Phys. Commun. **183**, 2054 (2012).

[51] C. H. Bennett, *Efficient Estimation of Free Energy Differences from Monte Carlo Data,* J. Comput. Phys. **22**, 245 (1976).

[52] D. A. Kofke and P. T. Cummings, *Quantitative Comparison and Optimization of Methods for Evaluating the Chemical Potential by Molecular Simulation,* Mol. Phys. **92**, 973 (1997).

[53] I. Nezbeda and J. Kolafa, *A New Version of the Insertion Particle Method for Determining the Chemical Potential by Monte Carlo Simulation,* Mol. Sim. **5**, 391 (1991).

[54] A. Rahbari, A. Poursaeidesfahani, A. Torres-Knoop, D. Dubbeldam, and T. J. H. Vlugt, *Chemical Potentials of Water, Methanol, Carbon Dioxide and Hydrogen Sulphide at Low Temperatures Using Continuous Fractional Component Gibbs Ensemble Monte Carlo,* Mol. Sim. **44**, 405 (2018).

[55] T. R. Josephson, R. Singh, M. S. Minkara, E. O. Fetisov, and J. I. Siepmann, *Partial Molar Properties from Molecular Simulation Using Multiple Linear Regression,* Mol. Phys. **117**, 3589 (2019).

[56] A. Rahbari, T. R. Josephson, Y. Sun, O. A. Moultos, D. Dubbeldam, J. I. Siepmann, and T. J. H. Vlugt, *Multiple Linear Regression and Thermodynamic Fluctuations are Equivalent for Computing Thermodynamic Derivatives,* Manuscript submitted.

[57] W. Shi and E. J. Maginn, *Continuous Fractional Component Monte Carlo: An Adaptive Biasing Method for Open System Atomistic Simulations,* J. Chem. Theory Comput. **3**, 1451 (2007).

[58] W. Shi and E. J. Maginn, *Improvement in Molecule Exchange Efficiency in Gibbs Ensemble Monte Carlo: Development and Implementation of the Continuous Fractional Component Move,* J. Comput. Chem. **29**, 2520 (2008).

[59] B. Widom, *Some Topics in the Theory of Fluids,* J. Chem. Phys. **39**, 2808 (1963).

[60] B. Widom, *Potential-Distribution Theory and the Statistical Mechanics of Fluids,* J. Phys. Chem. **86**, 869 (1982).

[61] D. A. McQuarrie and J. D. Simon, *Physical Chemistry: A Molecular Approach*, 1st ed. (University Science Books, Sausalito, California, 1997).

[62] H. C. Turner, J. K. Brennan, M. Lisal, W. R. Smith, K. J. Johnson, and K. E. Gubbins, *Simulation of Chemical Reaction Equilibria by the Reaction Ensemble Monte Carlo Method: A Review,* Mol. Sim. **34**, 119 (2008).

[63] N. Hansen, S. Jakobtorweihen, and F. J. Keil, *Reactive Monte Carlo and Grand-Canonical Monte Carlo Simulations of the Propene Metathesis Reaction System,* J. Chem. Phys. **122**, 164705 (2005).

[64] T. W. Rosch and E. J. Maginn, *Reaction Ensemble Monte Carlo Simulation of Complex Molecular Systems,* J. Chem. Theory Comput. **7**, 269 (2011).

[65] A. Poursaeidesfahani, A. Rahbari, A. Torres-Knoop, D. Dubbeldam, and T. J. H. Vlugt, *Computation of Thermodynamic Properties in the Continuous Fractional Component Monte Carlo Gibbs Ensemble,* Mol. Sim. **43**, 189 (2017).

[66] A. Torres-Knoop, A. Poursaeidesfahani, T. J. H. Vlugt, and D. Dubbeldam, *Behavior of the Enthalpy of Adsorption in Nanoporous Materials Close to Saturation Conditions,* J. Chem. Theory Comput. **13**, 3326 (2017).

[67] P. P. Ewald, *Die Berechnung Optischer und Elektrostatischer Gitterpotentiale,* Ann. Phys. **369**, 253 (1921).

[68] D. Wolf, P. Keblinski, S. R. Phillpot, and J. Eggebrecht, *Exact Method for the Simulation of Coulombic Systems by Spherically Truncated, Pairwise r^{-1} Summation,* J. Chem. Phys. **110**, 8254 (1999).

[69] P. Rossky, J. Doll, and H. Friedman, *Brownian Dynamics as Smart Monte Carlo Simulation,* J. Chem. Phys. **69**, 4628 (1978).

[70] D. Dubbeldam, A. Torres-Knoop, and K. S. Walton, *On the Inner Workings of Monte Carlo Codes,* Mol. Sim. **39**, 1253 (2013).

[71] D. Dubbeldam, S. Calero, D. E. Ellis, and R. Q. Snurr, *RASPA: Molecular Simulation Software for Adsorption and Diffusion in Flexible Nanoporous Materials,* Mol. Sim. **42**, 81 (2016).

[72] M. Ramdin, S. P. Balaji, J. M. Vicent-Luna, J. J. Gutirrez-Sevillano, S. Calero, T. W. de Loos, and T. J. H. Vlugt, *Solubility of the Precombustion Gases CO_2, CH_4, CO, H_2, N_2, and H_2S in the Ionic Liquid [bmim][Tf2N] from Monte Carlo Simulations,* J. Phys. Chem. C **118**, 23599 (2014).

[73] A. Rahbari, R. Hens, D. Dubbeldam, and T. J. H. Vlugt, *Improving the Accuracy of Computing Chemical Potentials in CFCMC Simulations,* Mol. Phys. **117**, 3493 (2019).

[74] F. Wang and D. P. Landau, *Efficient, Multiple-Range Random Walk Algorithm to Calculate the Density of States,* Phys. Rev. Lett. **86**, 2050 (2001).

[75] C. J. Fennell and J. D. Gezelter, *Is the Ewald Summation Still Necessary? Pairwise Alternatives to the Accepted Standard for Long-Range Electrostatics,* J. Chem. Phys. **124**, 234104 (2006).

[76] R. D. Skeel, *An Alternative Construction of the Ewald Sum,* Mol. Phys. **114**, 3166 (2016).

[77] T. J. H. Vlugt, E. García-Pérez, D. Dubbeldam, S. Ban, and S. Calero, *Computing the Heat of Adsorption Using Molecular Simulations: The Effect of Strong Coulombic Interactions,* J. Chem. Theory Comput. **4**, 1107 (2008).

[78] A. Rahbari, R. Hens, S. H. Jamali, M. Ramdin, D. Dubbeldam, and T. J. H. Vlugt, *Effect of Truncating Electrostatic Interactions on Predicting Thermodynamic Properties of Water-Methanol Systems,* Mol. Sim. **45**, 336 (2019).

[79] L. N. Naden, T. T. Pham, and M. R. Shirts, *Linear Basis Function Approach to Efficient Alchemical Free Energy Calculations. 1. Removal of Uncharged Atomic Sites,* J. Chem. Theory Comput. **10**, 1128 (2014).

[80] T. T. Pham and M. R. Shirts, *Identifying Low Variance Pathways for Free Energy Calculations of Molecular Transformations in Solution Phase,* J. Chem. Phys. **135**, 034114 (2011).

[81] S. Duane, A. Kennedy, B. J. Pendleton, and D. Roweth, *Hybrid Monte Carlo,* Phys. Lett. B **195**, 216 (1987).

[82] L. Verlet, *Computer "Experiments" on Classical Fluids. I. Thermodynamical Properties of Lennard-Jones Molecules,* Phys. Rev. **159**, 98 (1967).

[83] E. Hairer, C. Lubich, and G. Wanner, *Geometric Numerical Integration Illustrated by the Störmer-Verlet Method,* Acta Numer. **12**, 399 (2003).

[84] M. Tuckerman, B. J. Berne, and G. J. Martyna, *Reversible Multiple Time Scale Molecular Dynamics,* J. Chem. Phys. **97**, 1990 (1992).

[85] I. Matito-Martos, A. Rahbari, A. Martin-Calvo, D. Dubbeldam, T. J. H. Vlugt, and S. Calero, *Adsorption Equilibrium of Nitrogen Dioxide in Porous Materials,* Phys. Chem. Chem. Phys. **20**, 4189 (2018).

[86] M. J. Frisch, G. W. Trucks, H. B. Schlegel, G. E. Scuseria, M. A. Robb, J. R. Cheeseman, G. Scalmani, V. Barone, G. A. Petersson, H. Nakatsuji, X. Li, M. Caricato, A. Marenich, J. Bloino, B. G. Janesko, R. Gomperts, B. Mennucci, H. P. Hratchian, J. V. Ortiz, A. F. Izmaylov, J. L. Sonnenberg, D. Williams-Young, F. Ding, F. L. F. Egidi, J. Goings, B. Peng, A. Petrone, T. Henderson, D. Ranasinghe, V. G. Zakrzewski, J. Gao, N. Rega, G. Zheng, W. Liang, M. Hada, M. Ehara, K. Toyota, R. Fukuda, J. Hasegawa, M. Ishida, T. Nakajima, Y. Honda, O. Kitao, H. Nakai, T. Vreven, K. Throssell, J. A. Montgomery, Jr., J. E. Peralta, F. Ogliaro, M. Bearpark, J. J. Heyd, E. Brothers, K. N. Kudin, V. N. Staroverov, T. Keith, R. Kobayashi, J. Normand, K. Raghavachari, A. Rendell, J. C. Burant, S. S. Iyengar, J. Tomasi, M. Cossi, J. M. Millam, M. Klene, C. Adamo, R. Cammi, J. W. Ochterski, R. L. Martin, K. Morokuma, O. Farkas, J. B. Foresman, and D. J. Fox, Gaussian 16. 2016, Gaussian Inc. Wallingford CT.

[87] D.-Y. Peng and D. B. Robinson, *A New Two-Constant Equation of State,* Ind. Eng. Chem. Fundam. **15**, 59 (1976).

[88] J. Seader, E. Henley, and D. Roper, *Seperation Process Principles*, 3rd ed. (John Wiley & Sons, Inc., United Stated of America, 2011).

[89] J. J. Potoff and J. I. Siepmann, *Vapor-Liquid Equilibria of Mixtures Containing Alkanes, Carbon Dioxide, and Nitrogen,* AIChE J. **47**, 1676 (2001).

[90] B. Chen, J. J. Potoff, and J. I. Siepmann, *Monte Carlo Calculations for Alcohols and Their Mixtures with Alkanes. Transferable Potentials for Phase Equilibria. 5. United-Atom Description of Primary, Secondary, and Tertiary Alcohols,* J. Phys. Chem. B **105**, 3093 (2001).

[91] B. R. Brooks, R. E. Bruccoleri, B. D. Olafson, D. J. States, S. Swaminathan, and M. Karplus, *CHARMM: A Program for Macromolecular Energy, Minimization, and Dynamics Calculations,* J. Comput. Chem. **4**, 187 (1983).

[92] M. J. McGrath, J. I. Siepmann, I.-F. W. Kuo, and C. J. Mundy, *Vapor-liquid Equilibria of Water from First Principles: Comparison of Density Functionals and Basis Sets,* Mol. Phys. **104**, 3619 (2006).

[93] J.-W. Handgraaf, E. J. Meijer, and M.-P. Gaigeot, *Density-Functional Theory-Based Molecular Simulation Study of Liquid Methanol,* J. Chem. Phys. **121**, 10111 (2004).

[94] A. Warshel, M. Kato, and A. V. Pisliakov, *Polarizable Force Fields: History, Test Cases, and Prospects,* J. Chem. Theory Comput. **3**, 2034 (2007).

[95] M. G. Martin, B. Chen, and J. I. Siepmann, *A Novel Monte Carlo Algorithm for Polarizable Force Fields: Application to a Fluctuating Charge Model for Water,* J. Chem. Phys. **108**, 3383 (1998).

[96] O. Borodin, *Polarizable Force Field Development and Molecular Dynamics Simulations of Ionic Liquids,* J. Phys. Chem. B **113**, 11463 (2009).

[97] J. W. Perram, H. G. Petersen, and S. W. D. Leeuw, *An Algorithm for the Simulation of Condensed Matter Which Grows As the 3/2 Power of the Number of Particles,* Mol. Phys. **65**, 875 (1988).

[98] C. Sagui and T. A. Darden, *Molecular Dynamics Simulations of Biomolecules: Long-Range Electrostatic Effects,* Annu. Rev. Biophys. Biomol. Struct. **28**, 155 (1999).

[99] L. Onsager, *Electric Moments of Molecules in Liquids,* J. Am. Chem. Soc. **58**, 1486 (1936).

[100] J. Barker and R. Watts, *Monte Carlo Studies of the Dielectric Properties of Water-like Models,* Mol. Phys. **26**, 789 (1973).

[101] J. Eastwood, R. Hockney, and D. Lawrence, *P3M3DP - the Three-Dimensional Periodic Particle-Particle/particle-Mesh Program,* Comput. Phys. Commun. **19**, 215 (1980).

[102] P. Demontis, S. Spanu, and G. B. Suffritti, *Application of the Wolf Method for the Evaluation of Coulombic Interactions to Complex Condensed Matter Systems: Aluminosilicates and Water,* J. Chem. Phys. **114**, 7980 (2001).

[103] D. Zahn, B. Schilling, and S. M. Kast, *Enhancement of the Wolf Damped Coulomb Potential: Static, Dynamic, and Dielectric Properties of Liquid Water from Molecular Simulation,* J. Phys. Chem. B **106**, 10725 (2002).

[104] P. X. Viveros-Méndez and A. Gil-Villegas, *Computer Simulation of Sedimentation of Ionic Systems Using the Wolf Method,* J. Chem. Phys. **136**, 154507 (2012).

[105] B. W. McCann and O. Acevedo, *Pairwise Alternatives to Ewald Summation for Calculating Long-Range Electrostatics in Ionic Liquids,* J. Chem. Theory Comput. **9**, 944 (2013).

[106] N. B. Wilding, *Critical-Point and Coexistence-Curve Properties of the Lennard-Jones Fluid: A Finite-Size Scaling Study,* Phys. Rev. E **52**, 602 (1995).

[107] K. Kiyohara, K. E. Gubbins, and A. Z. Panagiotopoulos, *Phase Coexistence Properties of Polarizable Stockmayer Fluids,* J. Chem. Phys. **106**, 3338 (1997).

[108] M. Dinpajooh, P. Bai, D. A. Allan, and J. I. Siepmann, *Accurate and Precise Determination of Critical Properties from Gibbs Ensemble Monte Carlo Simulations,* J. Chem. Phys. **143**, 114113 (2015).

[109] M. S. Shah, M. Tsapatsis, and J. I. Siepmann, *Development of the Transferable Potentials for Phase Equilibria Model for Hydrogen Sulfide,* J. Phys. Chem. B **119**, 7041 (2015).

[110] D. Gonzalez-Salgado and C. Vega, *A New Intermolecular Potential for Simulations of Methanol: The OPLS/2016 Model,* J. Chem. Phys. **145**, 034508 (2016).

[111] R. D. Goodwin, *Methanol Thermodynamic Properties from 176 to 673 K at Pressures to 700 bar,* J. Phys. Chem. Ref. Data **16**, 799 (1987).

[112] E. W. Lemmon, M. O. McLinden, and D. G. Friend, *NIST Chemistry WebBook, NIST Standard Reference Database Number 69*, edited by P. J. Linstrom and W. G. Mallard (National Institute of Standards and Technology, Gaithersburg MD, 20899) Chap. Thermophysical Properties of Fluid Systems.

[113] W. Duschek, R. Kleinrahm, and W. Wagner, *Measurement and Correlation of the (pressure, Density, Temperature) Relation of Carbon Dioxide II. Saturated-Liquid and Saturated-Vapour Densities and the Vapour Pressure Along the Entire Coexistence Curve,* J. Chem. Therm. **22**, 841 (1990).

[114] R. D. Goodwin, *Hydrogen Sulfide Provisional Thermophysical Properties from 188 to 700 K at Pressures to 75 MPa,* (1983).

[115] Y. Suehiro, M. Nakajima, K. Yamada, and M. Uematsu, *Critical Parameters of XCO_2 + (1-X)CHF_3 for X= (1.0000, 0.7496, 0.5013, and 0.2522),* J. Chem. Therm. **28**, 1153 (1996).

[116] J. Dykyj, J. Svoboda, R. C. Wilhoit, M. Frenkel, and K. R. Hall, *Vapor Pressure and Antoine Constants for Hydrocarbons, and S, Se, Te, and Halogen Containing Organic Compounds*, edited by K. R. Hall (Springer-Verlag Berlin Heidelberg, Tiergartenstrasse 17, D-69121 Heidelberg, Germany, 1999).

[117] J. F. Izquierdo, F. Cunill, M. Vila, J. Tejero, and M. Iborra, *Equilibrium Constants for Methyl Tert-butyl Ether Liquid-Phase Synthesis,* J. Chem. Eng. Data **37**, 339 (1992).

[118] R. M. Stephenson and S. Malanowski, *Handbook of the Thermodynamics of Organic Compounds* (Springer Netherlands, Dordrecht, 1987).

[119] M. Ross, *A High-Density Fluid-Perturbation Theory Based on an Inverse 12th-Power Hard-Sphere Reference System,* J. Chem. Phys. **71**, 1567 (1979).

[120] D. W. Brenner, *Empirical Potential for Hydrocarbons for Use in Simulating the Chemical Vapor Deposition of Diamond Films,* Phys. Rev. B **42**, 9458 (1990).

[121] R. Car and M. Parrinello, *Unified Approach for Molecular Dynamics and Density-Functional Theory,* Phys. Rev. Lett. **55**, 2471 (1985).

[122] K. Laasonen, M. Sprik, M. Parrinello, and R. Car, *"Ab initio" Liquid Water,* J. Chem. Phys. **99**, 9080 (1993).

[123] M. Iannuzzi, A. Laio, and M. Parrinello, *Efficient Exploration of Reactive Potential Energy Surfaces Using Car-Parrinello Molecular Dynamics,* Phys. Rev. Lett. **90**, 238302 (2003).

[124] A. C. van Duin, S. Dasgupta, F. Lorant, and W. A. Goddard, *ReaxFF: A Reactive Force Field for Hydrocarbons,* J. Phys. Chem. A **105**, 9396 (2001).

[125] K. Chenoweth, A. C. van Duin, and W. A. Goddard, *ReaxFF Reactive Force Field for Molecular Dynamics Simulations of Hydrocarbon Oxidation,* J. Phys. Chem. A **112**, 1040 (2008).

[126] A. Laio and F. L. Gervasio, *Metadynamics: A Method to Simulate Rare Events and Reconstruct the Free Energy in Biophysics, Chemistry and Material Science,* Rep. Prog. Phys. **71**, 126601 (2008).

[127] G. Bussi, A. Laio, and M. Parrinello, *Equilibrium Free Energies from Nonequilibrium Metadynamics,* Phys. Rev. Lett. **96**, 090601 (2006).

[128] A. Barducci, M. Bonomi, and M. Parrinello, *Metadynamics,* Wiley Interdiscip. Rev. Comput. Mol. Sci. **1**, 826 (2011).

[129] C. Dellago, P. G. Bolhuis, F. S. Csajka, and D. Chandler, *Transition Path Sampling and the Calculation of Rate Constants,* J. Chem. Phys. **108**, 1964 (1998).

[130] P. G. Bolhuis, C. Dellago, and D. Chandler, *Sampling Ensembles of Deterministic Transition Pathways,* Faraday Discuss. **110**, 421 (1998).

[131] T. J. H. Vlugt, C. Dellago, and B. Smit, *Diffusion of Isobutane in Silicalite Studied by Transition Path Sampling,* J. Chem. Phys. **113**, 8791 (2000).

[132] P. G. Bolhuis, D. Chandler, C. Dellago, and P. L. Geissler, *Transition Path Sampling: Throwing Ropes over Rough Mountain Passes, in the Dark,* Annu. Rev. Phys. Chem. **53**, 291 (2002).

[133] J. Rogal and P. G. Bolhuis, *Multiple State Transition Path Sampling,* J. Chem. Phys. **129**, 12B609 (2008).

[134] T. S. van Erp and P. G. Bolhuis, *Elaborating Transition Interface Sampling Methods,* J. Comput. Phys. **205**, 157 (2005).

[135] D. Moroni, T. S. van Erp, and P. G. Bolhuis, *Investigating Rare Events by Transition Interface Sampling,* Physica A **340**, 395 (2004).

[136] D. Moroni, P. G. Bolhuis, and T. S. van Erp, *Rate Constants for Diffusive Processes by Partial Path Sampling,* J. Chem. Phys. **120**, 4055 (2004).

[137] D. Moroni, T. S. van Erp, and P. G. Bolhuis, *Simultaneous Computation of Free Energies and Kinetics of Rare Events,* Phys. Rev. E **71**, 056709 (2005).

[138] S. C. Glotzer, D. Stauffer, and N. Jan, *Monte Carlo Simulations of Phase Separation in Chemically Reactive Binary Mixtures,* Phys. Rev. Lett. **72**, 4109 (1994).

[139] J. K. Johnson, *Reactive Canonical Monte Carlo,* Adv. Chem. Phys. **105**, 461 (1999).

[140] S. Jakobtorweihen, N. Hansen, and F. Keil, *Combining Reactive and Configurational-Bias Monte Carlo: Confinement Influence on the Propene Metathesis Reaction System in Various Zeolites,* J. Chem. Phys. **125**, 224709 (2006).

[141] P. Ungerer, J. Collell, and M. Yiannourakou, *Molecular Modeling of the Volumetric and Thermodynamic Properties of Kerogen: Influence of Organic Type and Maturity,* Energy Fuels **29**, 91 (2014).

[142] M. W. Chase, *NIST-JANAF Themochemical Tables* (American Institute of Physics for the National Institute of Standards and Technology, New York, 1998).

[143] E. O. Fetisov, I.-F. W. Kuo, C. Knight, J. VandeVondele, T. van Voorhis, and J. I. Siepmann, *First-Principles Monte Carlo Simulations of Reaction Equilibria in Compressed Vapors,* ACS Cent. Sci. **2**, 409 (2016).

[144] M. M. Ghahremanpour, P. J. van Maaren, J. C. Ditz, R. Lindh, and D. van der Spoel, *Large-Scale Calculations of Gas Phase Thermochemistry: Enthalpy of Formation, Standard Entropy, and Heat Capacity,* J. Chem. Phys. **145**, 114305 (2016).

[145] P. Bai and J. I. Siepmann, *Assessment and Optimization of Configurational-Bias Monte Carlo Particle Swap Strategies for Simulations of Water in the Gibbs Ensemble,* J. Chem. Theory Comput. **13**, 431 (2017).

[146] J. I. Siepmann, *A Method for the Direct Calculation of Chemical Potentials for Dense Chain Systems,* Mol. Phys. **70**, 1145 (1990).

[147] J. I. Siepmann, S. Karaborni, and B. Smit, *Vapor-Liquid Equilibria of Model Alkanes,* J. Am. Chem. Soc. **115**, 6454 (1993).

[148] S. Consta, T. J. H. Vlugt, J. Wichers Hoeth, B. Smit, and D. Frenkel, *Recoil Growth Algorithm for Chain Molecules with Continuous Interactions,* Mol. Phys. **97**, 1243 (1999).

[149] J. Houdayer, *The Wormhole Move: A New Algorithm for Polymer Simulations,* J. Chem. Phys. **116**, 1783 (2002).

[150] A. Poursaeidesfahani, A. Torres-Knoop, M. Rigutto, N. Nair, D. Dubbeldam, and T. J. H. Vlugt, *Computation of the Heat and Entropy of Adsorption in Proximity of Inflection Points,* J. Phys. Chem. C **120**, 1727 (2016).

[151] N. Combe, T. J. H. Vlugt, P. R. ten Wolde, and D. Frenkel, *Dynamic Pruned-Enriched Rosenbluth Method,* Mol. Phys. **101**, 1675 (2003).

[152] N. Boon, *Efficient Configurational-Bias Monte-Carlo Simulations of Chain Molecules with "Swarms" of Trial Configurations,* J. Chem. Phys. **149**, 064109 (2018).

[153] F. A. Escobedo and J. J. de Pablo, *Monte Carlo Simulation of the Chemical Potential of Polymers in an Expanded Ensemble,* J. Chem. Phys. **103**, 2703 (1995).

[154] A. P. Lyubartsev, A. A. Martsinovski, S. V. Shevkunov, and P. N. Vorontsov-Velyaminov, *New Approach to Monte Carlo Calculation of the Free Energy: Method of Expanded Ensembles,* J. Chem. Phys. **96**, 1776 (1992).

[155] K. S. Rane, S. Murali, and J. R. Errington, *Monte Carlo Simulation Methods for Computing Liquid-Vapor Saturation Properties of Model Systems,* J. Chem. Theory Comput. **9**, 2552 (2013).

[156] M. Ramdin, S. P. Balaji, A. Torres-Knoop, D. Dubbeldam, T. W. de Loos, and T. J. H. Vlugt, *Solubility of Natural Gas Species in Ionic Liquids and Commercial Solvents: Experiments and Monte Carlo Simulations,* J. Chem. Eng. Data **60**, 3039 (2015).

[157] W. Shi and E. J. Maginn, *Atomistic Simulation of the Absorption of Carbon Dioxide and Water in the Ionic Liquid 1-N-Hexyl-3-Methylimidazolium Bis(trifluoromethylsulfonyl)imide ([hmim][Tf2N],* J. Phys. Chem. B **112**, 2045 (2008).

[158] E. J. Maginn, *Atomistic Simulation of the Thermodynamic and Transport Properties of Ionic Liquids,* Acc. Chem. Res. **40**, 1200 (2007).

[159] M. S. Kelkar, W. Shi, and E. J. Maginn, *Determining the Accuracy of Classical Force Fields for Ionic Liquids: Atomistic Simulation of the Thermodynamic and Transport Properties of 1-Ethyl-3-Methylimidazolium Ethylsulfate ([emim][$EtSO_4$]) and Its Mixtures with Water,* Ind. Eng. Chem. Res. **47**, 9115 (2008).

[160] X. Zhang, F. Huo, Z. Liu, W. Wang, W. Shi, and E. J. Maginn, *Absorption of CO_2 in the Ionic Liquid 1-N-Hexyl-3-Methylimidazolium Tris(pentafluoroethyl)trifluorophosphate ([hmim][FEP]): A Molecular View by Computer Simulations,* J. Phys. Chem. B **113**, 7591 (2009).

[161] Q. Chen, S. P. Balaji, M. Ramdin, J. J. Gutiarrez-Sevillano, A. Bardow, E. L. V. Goetheer, and T. J. H. Vlugt, *Validation of the CO_2/N_2O Analogy Using Molecular Simulation,* Ind. Eng. Chem. Res. **53**, 18081 (2014).

[162] W. Shi, N. S. Siefert, and B. D. Morreale, *Molecular Simulations of CO_2, H_2, H_2O, and H_2S Gas Absorption into Hydrophobic Poly(dimethylsiloxane) (PDMS) Solvent: Solubility and Surface Tension,* J. Phys. Chem. C **119**, 19253 (2015).

[163] A. Torres-Knoop, S. P. Balaji, T. J. H. Vlugt, and D. Dubbeldam, *A Comparison of Advanced Monte Carlo Methods for Open Systems: CFCMC vs CBMC,* J. Chem. Theory Comput. **10**, 942 (2014).

[164] S. H. Jamali, M. Ramdin, T. M. Becker, A. Torres-Knoop, D. Dubbeldam, W. Buijs, and T. J. H. Vlugt, *Solubility of Sulfur Compounds in Commercial Physical Solvents and an Ionic Liquid from Monte Carlo Simulations,* Fluid Phase Equilib. **433**, 50 (2017).

[165] M. Ramdin, S. P. Balaji, J. M. Vicent-Luna, A. Torres-Knoop, Q. Chen, D. Dubbeldam, S. Calero, T. W. de Loos, and T. J. H. Vlugt, *Computing Bubble-Points of CO_2/CH_4 Gas Mixtures in Ionic Liquids from Monte Carlo Simulations,* Fluid Phase Equilib. **418**, 100 (2016).

[166] M. Ramdin, Q. Chen, S. P. Balaji, J. M. Vicent-Luna, A. Torres-Knoop, D. Dubbeldam, S. Calero, T. W. de Loos, and T. J. H. Vlugt, *Solubilities of CO_2, CH_4, C_2H_6, and SO_2 in Ionic Liquids and Selexol from Monte Carlo Simulations,* J. Comput. Sci. **15**, 74 (2016).

[167] D. N. Theodorou, *Progress and Outlook in Monte Carlo Simulations,* Ind. Eng. Chem. Res. **49**, 3047 (2010).

[168] L. Zhang and J. I. Siepmann, *Development of the TraPPE Force Field for Ammonia,* Collect. Czech. Chem. Commun. **75**, 577 (2010).

[169] C. H. Turner, J. K. Johnson, and K. E. Gubbins, *Effect of Confinement on Chemical Reaction Equilibria: The Reactions $2NO \leftrightarrows (NO)_2$ and $N_2+3H_2 \leftrightarrows 2NH_3$ in Carbon Micropores,* J. Chem. Phys. **114**, 1851 (2001).

[170] L. J. Gillespie and J. A. Beattie, *The Thermodynamic Treatment of Chemical Equilibria in Systems Composed of Real Gases. I. an Approximate Equation for the Mass Action Function Applied to the Existing Data on the Haber Equilibrium,* Phys. Rev. **36**, 743 (1930).

[171] J. W. Erisman, M. A. Sutton, J. Galloway, Z. Klimont, and W. Winiwarter, *How a Century of Ammonia Synthesis Changed the World,* Nat. Geosci. **1**, 636 (2008).

[172] L. J. Winchester and B. F. Dodge, *The Chemical Equilibrium of the Ammonia Synthesis Reaction at High Temperatures and Extreme Pressures,* AIChE J. **2**, 431 (1956).

[173] M. Lísal, M. Bendová, and W. R. Smith, *Monte Carlo Adiabatic Simulation of Equilibrium Reacting Systems: The Ammonia Synthesis Reaction,* Fluid Phase Equilib. **235**, 50 (2005).

[174] X. Peng, W. Wang, and S. Huang, *Monte Carlo Simulation for Chemical Reaction Equilibrium of Ammonia Synthesis in MCM-41 Pores and Pillared Clays,* Fluid Phase Equilib. **231**, 138 (2005).

[175] J. R. Jennings, *Catalytic Ammonia Synthesis: Fundamentals and Practice*, 1st ed. (Plenum Press, New York, USA, 1991).

[176] H. Xiao, A. Valera-Medina, R. Marsh, and P. J. Bowen, *Numerical Study Assessing Various Ammonia/methane Reaction Models for Use Under Gas Turbine Conditions,* Fuel **196**, 344 (2017).

[177] H. Nozari and A. Karabeyoğlu, *Numerical Study of Combustion Characteristics of Ammonia As a Renewable Fuel and Establishment of Reduced Reaction Mechanisms,* Fuel **159**, 223 (2015).

[178] H. Xiao, M. Howard, A. Valera-Medina, S. Dooley, and P. J. Bowen, *Study on Reduced Chemical Mechanisms of Ammonia/Methane Combustion Under Gas Turbine Conditions,* Energy Fuels **30**, 8701 (2016).

[179] C. Zamfirescu and I. Dincer, *Using Ammonia As a Sustainable Fuel,* J. Power Sources **185**, 459 (2008).

[180] C. Zamfirescu and I. Dincer, *Ammonia As a Green Fuel and Hydrogen Source for Vehicular Applications,* Fuel Process. Technol. **90**, 729 (2009).

[181] M. Kitano, Y. Inoue, Y. Yamazaki, F. Hayashi, S. Kanbara, S. Matsuishi, T. Yokoyama, S.-W. Kim, M. Hara, and H. Hosono, *Ammonia Synthesis Using a Stable Electride As an Electron Donor and Reversible Hydrogen Store,* Nat. Chem. **4**, 934 (2012).

[182] C. J. van der Ham, M. T. Koper, and D. G. Hetterscheid, *Challenges in Reduction of Dinitrogen by Proton and Electron Transfer,* Chem. Soc. Rev. **43**, 5183 (2014).

[183] X. Guo, Y. Zhu, and T. Ma, *Lowering Reaction Temperature: Electrochemical Ammonia Synthesis by Coupling Various Electrolytes and Catalysts,* J. Energy Chem. **26**, 1107 (2017).

[184] J. O. Valderrama, *The State of the Cubic Equations of State,* Ind. Eng. Chem. Res. **42**, 1603 (2003).

[185] G. H. Graaf and J. G. M. Winkelman, *Chemical Equilibria in Methanol Synthesis Including the Water-Gas Shift Reaction: A Critical Reassessment,* Ind. Eng. Chem. Res. **55**, 5854 (2016).

[186] G. H. Graaf, P. J. J. M. Sijtsema, E. J. Stamhuis, and G. E. H. Joosten, *Chemical Equilibria in Methanol Synthesis,* Chem. Eng. Sci. **41**, 2883 (1986).

[187] G. M. Kontogeorgis and G. K. Folas, *Thermodynamic Models for Industrial Applications: From Classical and Advanced Mixing Rules to Association Theories*, 1st ed. (John Wiley & Sons, Wiltshire, Great Britain, 2009).

[188] K. G. Harstad, R. S. Miller, and J. Bellan, *Efficient High-Pressure State Equations,* AIChE J. **43**, 1605 (1997).

[189] B. S. Jhaveri and G. K. Youngren, *Three-Parameter Modification of the Peng-Robinson Equation of State to Improve Volumetric Predictions,* SPE reservoir engineering **3**, 1033 (1988).

[190] J. Gross and G. Sadowski, *Perturbed-Chain SAFT: An Equation of State Based on a Perturbation Theory for Chain Molecules,* Ind. Eng. Chem. Res. **40**, 1244 (2001).

[191] N. I. Diamantonis and I. G. Economou, *Evaluation of Statistical Associating Fluid Theory (SAFT) and Perturbed Chain-SAFT Equations of State for the Calculation of Thermodynamic Derivative Properties of Fluids Related to Carbon Capture and Sequestration,* Energy Fuels **25**, 3334 (2011).

[192] N. I. Diamantonis, G. C. Boulougouris, E. Mansoor, D. M. Tsangaris, and I. G. Economou, *Evaluation of Cubic, SAFT, and PC-SAFT Equations of State for the Vapor–Liquid Equilibrium Modeling of CO_2 Mixtures with Other Gases,* Ind. Eng. Chem. Res. **52**, 3933 (2013).

[193] W. R. Smith and M. Lísal, *Direct Monte Carlo Simulation Methods for Nonreacting and Reacting Systems at Fixed Total Internal Energy or Enthalpy,* Phys. Rev. E **66**, 011104 (2002).

[194] D. Wolf, *Reconstruction of NaCl Surfaces from a Dipolar Solution to the Madelung Problem,* Phys. Rev. Lett. **68**, 3315 (1992).

[195] P. Poulain, F. Calvo, R. Antoine, M. Broyer, and P. Dugourd, *Performances of Wang-Landau Algorithms for Continuous Systems,* Phys. Rev. E **73**, 056704 (2006).

[196] J. Gross and G. Sadowski, *Application of the Perturbed-Chain SAFT Equation of State to Associating Systems,* Ind. Eng. Chem. Res. **41**, 5510 (2002).

[197] J. A. Barker and D. Henderson, *Perturbation Theory and Equation of State for Fluids: The Square-Well Potential,* J. Chem. Phys. **47**, 2856 (1967).

[198] K. Mejbri and A. Bellagi, *Modelling of the Thermodynamic Properties of the Water–ammonia Mixture by Three Different Approaches,* Int. J. Ref. **29**, 211 (2006).

[199] M. J. Moran and H. N. Shapiro, *Fundamentals of Engineering Thermodynamics*, 5th ed. (John Wiley & Sons, West Sussex, England, 2006).

[200] M. W. Chase, J. Curnutt, H. Prophet, R. McDonald, and A. Syverud, *JANAF Thermochemical Tables, 1975 Supplement,* J. Phys. Chem. Ref. Data **4**, 1 (1975).

[201] R. Rönnback, T. Salmi, A. Vuori, H. Haario, J. Lehtonen, A. Sundqvist, and E. Tirronen, *Development of a Kinetic Model for the Esterification of Acetic Acid with Methanol in the Presence of a Homogeneous Acid Catalyst,* Chem. Eng. Sci. **52**, 3369 (1997).

[202] W. Song, G. Venimadhavan, J. M. Manning, M. F. Malone, and M. F. Doherty, *Measurement of Residue Curve Maps and Heterogeneous Kinetics in Methyl Acetate Synthesis,* Ind. Eng. Chem. Res. **37**, 1917 (1998).

[203] D. Dubbeldam, S. Calero, and T. J. H. Vlugt, *iRASPA: GPU-Accelerated Visualization Software for Materials Scientists,* Mol. Sim. **44**, 653 (2018).

[204] Outotec, *HSC Chemistry Software 9,* `https://www.outotec.com/products-and-services/technologies/digital-solutions/hsc-chemistry/` (visited on 2/20/2020).

[205] T. Renner, *Quantities, Units and Symbols in Physical Chemistry*, edited by E. R. Cohen, T. Cvitas, J. G. Frey, B. Holström, K. Kuchitsu, R. Marquardt, I. Mills, F. Pavese, M. Quack, J. Stohner, H. L. Strauss, M. Takami, and A. J. Thor (The Royal Society of Chemistry, 2007) pp. P001–232.

[206] T. Pöpken, L. Götze, and J. Gmehling, *Reaction Kinetics and Chemical Equilibrium of Homogeneously and Heterogeneously Catalyzed Acetic Acid Esterification with Methanol and Methyl Acetate Hydrolysis,* Ind. Eng. Chem. Res. **39**, 2601 (2000).

[207] G. Kamath, F. Cao, and J. J. Potoff, *An Improved Force Field for the Prediction of the Vapor-Liquid Equilibria for Carboxylic Acids,* J. Phys. Chem. B **108**, 14130 (2004).

[208] G. Kamath, J. Robinson, and J. J. Potoff, *Application of TraPPE-UA Force Field for Determination of Vapor-Liquid Equilibria of Carboxylate Esters,* Fluid Phase Equilib. **240**, 46 (2006).

[209] W. L. Jorgensen, J. Chandrasekhar, J. D. Madura, R. W. Impey, and M. L. Klein, *Comparison of Simple Potential Functions for Simulating Liquid Water,* J. Chem. Phys. **79**, 926 (1983).

[210] H. W. Horn, W. C. Swope, J. W. Pitera, J. D. Madura, T. J. Dick, G. L. Hura, and T. Head-Gordon, *Development of an Improved Four-Site Water Model for Biomolecular Simulations: TIP4P-Ew,* J. Chem. Phys. **120**, 9665 (2004).

Summary

In the past decades, molecular simulation has become an important tool for studying phase and reaction equilibria. In this dissertation, we work on improvements of the *Continuous Fractional Component* (CFC) method in Monte Carlo simulations. We also develop a software package for molecular simulations that uses this method. In Chapter 2, we briefly introduce partial molar properties that we want to compute from molecular simulations. The CFC method is introduced and we explain how it can be modified to calculate properties in the *NPT* ensemble. After that, we focus on the Reaction Ensemble and modify the CFC method such that it becomes suitable for the calculation of chemical potentials and fugacity coefficients. We shortly point out the applicability of the CFC method in the Gibbs Ensemble and the software, Brick-CFCMC, that was developed and used for this research. In Chapter 3, we study the vapor-liquid equilibria of hydrogen sulfide, methanol and carbon dioxide. We use the CFC method for simulations in the Gibbs Ensemble and the Wolf method for calculations of the electrostatic interactions. The Wolf method is a computationally cheaper method than the commonly used Ewald method but has the same accuracy, provided that it is parametrized correctly. In Chapter 4, we test our new formulation of the CFC method in the Reaction Ensemble. For different systems of Lennard-Jones particles, we compare the efficiency with the previous variant of the CFC method and the conventional method. Our formulation of the CFC method is more efficient and can directly check if the system has reached equilibrium. We continue our study by using this method for simulations of the Haber-Bosch process for the production of ammonia from nitrogen and hydrogen. In Chapter 5, we use the CFC method for computation of partial molar enthalpies and partial molar volumes. We start with simple systems of Lennard-Jones particles and compare with a different method (similar to Widom's method for obtaining chemical potentials). We calculate partial molar properties of nitrogen, hydrogen and ammonia in the stoichiometric compositions that were obtained in Chapter 4. From these results, we obtain the enthalpy of reaction. In Chapter 6, we combine the Gibbs Ensemble with the Reaction Ensemble for simulations of the esterification of methanol with acetic acid. We obtain a clear phase separation and calculate equilibrium compositions, chemical potentials, activity coefficients, and equilibrium constants. We distinguish two cases: one where the molecules are treated as rigid objects, and one where the molecules are flexible. No significant difference is observed between the results for the different cases. The simulations in Chapter 3 till Chapter 6 were performed with the software that was written as part of this research. This has lead to the software package Brick-CFCMC and is available (open source) from: `https://gitlab.com/ETh_TU_Delft/Brick-CFCMC`.

Samenvatting

De laatste decennia zijn moleculaire simulaties een belangrijk middel geworden voor het bestuderen van fase- en reactie-evenwichten. In dit proefschrift werken we aan het verbeteren van de *Continuous Fractional Component* (CFC) methode in Monte Carlo simulaties. Tegelijkertijd ontwikkelen we een software pakket voor moleculaire simulaties die gebruik maken van deze methode. In Hoofdstuk 2 presenteren we een korte beschrijving van de *partial molar properties* die we willen berekenen met behulp van moleculaire simulaties. We geven een korte uitleg over hoe de CFC methode gebruikt kan worden om deze eigenschappen te berekenen in het *NPT* ensemble. Daarna bekijken we het Reactie Ensemble en maken we de CFC methode geschikt voor het berekenen van chemische potentialen en fugaciteitscoëfficiënten. We staan kort stil bij CFC in het Gibbs Ensemble en het softwarepakket, Brick-CFCMC, dat in dit onderzoek is ontwikkeld en gebruikt. In Hoofdstuk 3 bestuderen we de gas-vloeistofevenwichten van waterstofsulfide, methanol en koolstofdioxide. We gebruiken de CFC methode voor simulaties in het Gibbs Ensemble en de Wolf methode voor de berekening van electrostatische interacties. De Wolf methode kan een hoop rekentijd besparen vergeleken met de vaak gebruikte Ewald methode. In Hoofdstuk 4 testen we onze nieuwe variant van de CFC methode in het Reactie Ensemble. Voor verschillende systemen van Lennard-Jones-deeltjes vergelijken we de efficiëntie met de oude variant van de CFC methode en de meer algemene methode die gebruikt wordt. Onze variant is efficiënter en kan direct gebruikt worden om te controleren of het systeem een reactie-evenwicht bereikt heeft. Vervolgens gebruiken we deze methode ook voor simulaties van het Haber-Boschproces, voor de productie van ammoniak uit stikstof en waterstof. In Hoofdstuk 5 gebruiken we de CFC methode voor het berekenen van *partial molar enthalpies* en *partial molar volumes*. We beginnen met simpele systemen van Lennard-Jones-deeltjes en vergelijken de resultaten met een andere methode (vergelijkbaar met Widom's methode voor het berekenen van chemische potentialen). Vervolgens berekenen we de *partial molar properties* voor stikstof, waterstof en ammoniak in de evenwichtmengsels uit de simulaties van Hoofdstuk 4. Met deze resultaten berekenen we tenslotte de reactie-enthalpie. In Hoofdstuk 6 combineren we het Gibbs Ensemble met het Reactie Ensemble voor simulaties van de verestering van methanol met azijnzuur. We zien een duidelijke fasescheiding en berekenen evenwichtscomposities, chemische potentialen, activiteitscoëfficiënten en de evenwichtsconstante. Twee gevallen worden bestudeerd: één systeem waarin alle moleculen star zijn en één systeem waarin de moleculen flexibel zijn. We vinden geen grote verschillen tussen deze twee gevallen. De simulaties in Hoofdstuk 3 tot en met Hoofdstuk 6 zijn uitgevoerd met het softwarepakket dat als onderdeel van dit onderzoek is ontwikkeld. Dit heeft geleid tot het pakket Brick-CFCMC en dit is beschikbaar (open source) via: `https://gitlab.com/ETh_TU_Delft/Brick-CFCMC`.

Curriculum Vitæ

Remco Hens

04-04-1992 Born in Tilburg, The Netherlands.

Education

2010–2013 BSc. in Physics and Astronomy
Radboud University, Nijmegen, The Netherlands

2010–2014 BSc. in Mathematics
Radboud University, Nijmegen, The Netherlands

2013–2015 MSc. in Physics and Astronomy
Radboud University, Nijmegen, The Netherlands

2016–2020 PhD in Molecular Simulation
Delft University of Technology, Delft, The Netherlands
Thesis: Molecular Simulation of Phase and Reaction Equilibria: Software and Algorithm Development
Promotor: Prof. dr. ir. T. J. H. Vlugt

List of Publications

Publications included in this thesis:

1. **R. Hens**, A. Rahbari, S. Caro-Ortiz, N. Dawass, M. Erdős, A. Poursaeidesfahani, H. S. Salehi, A. T. Celebi, M. Ramdin, O. A. Moultos, D. Dubbeldam, and T. J. H. Vlugt *Brick-CFCMC: Open Source Software for Monte Carlo Simulations of Phase and Reaction Equilibria using the Continuous Fractional Component Method*, Journal of Chemical Information and Modeling, **60**, 2678-2682 (2020).

2. A. Rahbari, **R. Hens**, I. K. Nikolaidis, A. Poursaeidesfahani, M. Ramdin, I. G. Economou, O. A. Moultos, D. Dubbeldam, and T. J. H. Vlugt, *Computation of Partial Molar Properties using Continuous Fractional Component Monte Carlo*, Molecular Physics, **116**, 3331-3344 (2018).

3. **R. Hens** and T. J. H. Vlugt, *Molecular Simulation of Vapor-Liquid Equilibria using the Wolf Method for Electrostatic Interactions*, Journal of Chemical and Engineering Data, **63**, 1096-1102 (2018).

4. A. Poursaeidesfahani, **R. Hens**, A. Rahbari, M. Ramdin, D. Dubbeldam, and T. J. H. Vlugt, *Efficient Application of Continuous Fractional Component Monte Carlo in the Reaction Ensemble*, Journal of Chemical Theory and Computation, **13**, 4452-4466 (2017).

Publications not included in this thesis:

1. H. S. Salehi, **R. Hens**, O. A. Moultos, T. J. H. Vlugt, *Computation of Gas Solubilities in Choline Chloride Urea and Choline Chloride Ethylene Glycol Deep Eutectic Solvents Using Monte Carlo Simulations*, Journal of Molecular Liquids, in press, doi: 10.1016/j.molliq.2020.113729.

2. A. Rahbari, **R. Hens**, O. A. Moultos, D. Dubbeldam, T. J. H. Vlugt, *Multiple Free Energy Calculations from Single State Point Continuous Fractional Component Monte Carlo Simulation using Umbrella Sampling*, Journal of Chemical Theory and Computation, **16**, 1757-1767 (2020).

3. S. Caro-Ortiz, **R. Hens**, E. Zuidema, M. Rigutto, D. Dubbeldam, T. J. H. Vlugt, *Corrigendum to "Molecular Simulation of the Vapor-Liquid Equilibria of Xylene Mixtures: Force field Performance, and Wolf vs. Ewald for Electrostatic Interactions" [Fluid Phase Equilib.] 485 (2019) 239–247*, Fluid Phase Equilibria, **506**, 112370 (2020).

4. A. Rahbari, **R. Hens**, D. Dubbeldam, T. J. H. Vlugt, *Improving the Accuracy of Computing Chemical Potentials in CFCMC Simulations*, Molecular Physics, **117**, 3493-3508 (2019).

5. A. Rahbari, **R. Hens**, S.H. Jamali, M. Ramdin, D. Dubbeldam, T. J. H. Vlugt, *Effect of Truncating Electrostatic Interactions on Predicting Thermodynamic Properties of Water-Methanol Systems*, Molecular Simulation, **45**, 336-350 (2019).

6. S. Caro-Ortiz, **R. Hens**, E. Zuidema, M. Rigutto, D. Dubbeldam, T. J. H. Vlugt, *Molecular Simulation of the Vapor-Liquid Equilibria of Xylene Mixtures: Force Field Performance, and Wolf vs. Ewald for Electrostatic Interactions*, Fluid Phase Equilibria, **485**, 239-247 (2019).

7. A. Rahbari, J. Brenkman, **R. Hens**, M. Ramdin, L. J. P. van den Broeke, R. Schoon, R. Henkes, O. A. Moultos, T. J. H. Vlugt, *Solubility of Water in Hydrogen at High Pressure: a Molecular Simulation Study*, Journal of Chemical and Engineering Data, **64**, 4103-4115 (2019).

8. **R. Hens**, A. Fasolino, *An Asymmetric Dimer in a Periodic Potential: a Minimal Model for Friction of Graphene Flakes*, European Physical Journal B, **89**, 167 (2016).

Acknowledgements

Now that my dissertation is finished, I would like to thank everyone who has been involved in the work. First of all, I thank my promotor. Thijs, I could not have wished for a better supervisor than you. You taught me a lot about doing research, molecular simulations and programming. You also offered me time to develop myself as a teacher and helped me prepare for my career after my PhD. Thank you for your guidance, motivation and all the opportunities you offered me to present my work in amazing places I probably never would have visited otherwise.

The four years of my PhD project have flown by, mainly because I was surrounded by kind and helpful people. I consider myself to be very lucky that many colleagues are now also some of my best friends. Julia, you always supported me and were always available to share some thoughts. Thank you for all the pleasant and interesting talks and discussions we had, and introducing me to git. Sebastián, your jokes made our office a fun work place. Thank you for your support and the good times during our trips, conferences, and RASPA workshops. Tim, whenever you were around, computers and RASPA always started to behave nicely. Thanks for all your help and also the good times on trips and conferences. Metin, you made me feel welcome when I started my PhD and helped me with starting up. Thanks for your support and interesting discussions. Christos, talking with you always motivated me. Thank you for showing so much interest in my work. Mahinder, you were always there to answer my questions, thank you for that, and in particular, for the help at the start of my PhD. Dion, thank you for all your help with any programming related questions and teaching me a lot about computer clusters. Reza, thanks for all the important and thorough work done that has lead to the development of Brick-CFCMC. Mariëtte, thanks for all our interesting discussions and introducing me to the experimental field of chemical engineering. Máté, thanks for sharing ideas, discussing thoughts and helping me to solve problems. Max, thank you for always willing to give useful feedback on my writing, figures and presentations. Alper, thanks for the interesting discussions, testing Brick-CFCMC and giving useful feedback. Noura, Hirad and Mert, thank you for your help with the development of Brick-CFCMC. Your feedback and suggestions have led to many improvements. Ali and Seyed, thank you for teaching me a lot about molecular simulations, especially at the start of my project. Otto and David, thank you for your contributions to Brick-CFCMC and the paper accompanying it.

Thanks to all the other people (that have been) working in the Engineering Thermodynamics group: Carlos, Brian, Martijn, Hongxia, Karsten, Meng, Vilborg and Xuan, for making the group so interesting and nice to work in. I would also like to thank everyone else at the Process & Energy department and the TU Delft, who, one way or another, have supported me during my PhD research.

There are other people, who might not have been involved in my research itself

but have supported me in other ways, to whom I am grateful. I would like to thank the supervisor of my Master thesis project, Annalisa, for giving me the push and self-confidence I needed to start a PhD. Thank you, Daphne and Lucie, for the interest in my work, (moral) support and the incredible trip we made through Australia. This trip was a very welcome break from work when I was halfway my PhD research. Rowena, thank you for your interest and support too, and the interesting talks about education.

Last, but definitely not least, I want to thank my parents and sister. You have always been my greatest supporters even though it was sometimes difficult for me to explain what my research exactly was about. I am very grateful and happy with the stable foundation and support that you offer in my life.